SOLAR POWERED ELECTROCOAGULATION PROCESSES FOR PB(II) REMOVAL USING NOVEL ELECTRODE MATERIALS AND CONFIGURATIONS

FARIHAHUSNAH BINTI HUSSIN

FACULTY OF ENGINEERING
UNIVERSITY OF MALAYA
KUALA LUMPUR

2018

SOLAR POWERED ELECTROCOAGULATION PROCESSES FOR PB(II) REMOVAL USING NOVEL ELECTRODE MATERIALS AND CONFIGURATIONS

FARIHAHUSNAH BINTI HUSSIN

THESIS SUBMITTED IN FULFILMENT OF THE REQUIREMENTS FOR THE DEGREE OF DOCTOR OF PHILOSOPHY

FACULTY OF ENGINEERING
UNIVERSITY OF MALAYA
KUALA LUMPUR

2018

UNIVERSITY OF MALAYA

ORIGINAL LITERARY WORK DECLARATION

Name of Candidate: **Farihahusnah Binti Hussin**

Matric No: **KHA130134**

Name of Degree: **Doctor of Philosophy**

Title of Project Paper/Research Report/Dissertation/Thesis ("this Work"):

SOLAR POWERED ELECTROCOAGULATION PROCESSES FOR PB (II) REMOVAL USING NOVEL ELECTRODE MATERIALS AND CONFIGURATIONS

Field of Study: **Purification and Separation Processes**

I do solemnly and sincerely declare that:

(1) I am the sole author/writer of this Work;
(2) This Work is original;
(3) Any use of any work in which copyright exists was done by way of fair dealing and for permitted purposes and any excerpt or extract from, or reference to or reproduction of any copyright work has been disclosed expressly and sufficiently and the title of the Work and its authorship have been acknowledged in this Work;
(4) I do not have any actual knowledge nor do I ought reasonably to know that the making of this work constitutes an infringement of any copyright work;
(5) I hereby assign all and every rights in the copyright to this Work to the University of Malaya ("UM"), who henceforth shall be owner of the copyright in this Work and that any reproduction or use in any form or by any means whatsoever is prohibited without the written consent of UM having been first had and obtained;
(6) I am fully aware that if in the course of making this Work I have infringed any copyright whether intentionally or otherwise, I may be subject to legal action or any other action as may be determined by UM.

Candidate's Signature Date:

Subscribed and solemnly declared before,

Witness's Signature Date:

Name:

Designation:

SOLAR POWERED ELECTROCOAGULATION PROCESSES FOR PB(II) REMOVAL USING NOVEL ELECTRODE MATERIALS AND CONFIGURATIONS

ABSTRACT

Electrocoagulation is a process used to remove heavy metals from diluted wastewater streams using anode materials such as aluminium, iron and copper. One of the disadvantages of conventional electrocoagulation systems is the high operating costs associated with the high energy consumption of these systems. However, nowadays, it is possible to develop a solar photovoltaic electrocoagulation system with the advent of renewable energy technologies. This study is divided into four parts. In Part 1, a new material (perforated zinc) was proposed for the anode of the solar photovoltaic electrocoagulation system to remove lead (Pb(II)) ions from aqueous solutions. The effects of the type of electrode material, electrode geometry, energy consumption and sludge production on removal of Pb(II) were also investigated in this study. Part 2 of this study evaluates the effect of operating parameters such as electrode distance, pH, current density and initial concentration on Pb(II) removal efficiency of solar photovoltaic electrocoagulation. The results showed that the perforated zinc electrode gives superior performance with a Pb(II) removal efficiency of 99.9% after 10 min of treatment at a current density of 1.13 mA/cm^2. Morphological and elemental analyses were carried out on the electrode surface and the formed sludge in which the results confirmed that a lower amount of sludge was produced during the removal of Pb(II) from the simulated wastewater using the solar photovoltaic electrocoagulation system under optimal conditions. Part 3 of this study involves the assessment on the feasibility of oil palm shell activated carbon (OPSAC) as an adsorbent for removal of Pb(II) ions from aqueous solutions. Batch experiments were conducted by varying the initial Pb(II) concentration,

pH, treatment time, temperature and adsorbent dosage for the adsorption process. The structure and surface texture of the prepared materials were characterised using FESEM, EDAX and BET surface area analysis. The results indicated that the adsorption process achieved equilibrium after 30 min of treatment. In addition, the adsorption of Pb(II) is strongly dependent on pH, whereby the highest Pb(II) removal was attained at pH 6. The Pb(II) removal efficiency increases with an increase in the OPSAC dosage of up to 4 g/L and the highest Pb(II) removal efficiency achieved was 99.1%. The results suggest that the adsorption data are well-described by the Langmuir isotherm model, whereby the maximum adsorption capacity is 58.05 mg/g. In addition, the adsorption kinetics are best described by the pseudo second-order model. In Part 4 of this study, an integration system of electrocoagulation-activated carbon adsorption process was carried out to remove Pb(II) ions from aqueous solutions. The optimum results obtained from the electrocoagulation and adsorption studies were used to investigate the performance of this integration treatment by varying the pH, initial Pb(II) ion concentration and OPSAC dosage.

Keywords: electrocoagulation, solar photovoltaic, perforated zinc, lead

PROSES ELEKTROKOAGULASI BERKUASA SURIA UNTUK PENYINGKIRAN PB(II) MENGGUNAKAN BAHAN ELEKTROD BARU DAN KONFIGURASI

ABSTRAK

Elektrokoagulasi merupakan suatu proses untuk menyingkirkan logam berat dari saliran air sisa, di mana aluminium, besi dan kuprum lazimnya digunakan sebagai anod. Salah satu kelemahan sistem elektrokoagulasi konvensional adalah kos operasinya yang tinggi kerana sistem seperti ini menggunakan tenaga yang tinggi. Kini, pembangunan sistem elektrokoagulasi berasaskan tenaga suria bukan sesuatu yang mustahil berikutan kemajuan teknologi tenaga yang boleh diperbaharui yang semakin berkembang. Kajian ini terdiri daripada empat bahagian. Dalam Bahagian 1, zink tertebuk telah dicadangkan sebagai anod dalam sistem elektrokoagulasi berasaskan tenaga suria bagi menyingkirkan ion Pb(II) daripada larutan akueus. Kesan jenis bahan elektrod, geometri elektrod, penggunaan tenaga dan penghasilan enap cemar terhadap penyingkiran ion Pb(II) juga turut dikaji. Bahagian 2 kajian ini menilai kesan parameter operasi seperti jarak elektrod, pH, ketumpatan arus and kepekatan awal dalam kecekapan penyingkiran ion Pb(II) pada elektrokoagulasi fotovolta suria. Hasil kajian menunjukkan bahawa elektrod zink tertebuk memberikan prestasi yang cukup memberangsangkan selepas rawatan selama 10 min pada ketumpatan arus 1.13 mA/cm^2, di mana kecekapan penyingkiran ion Pb(II) mencapai 99.9%. Analisis morfologi dan analisis unsur telah dijalankan ke atas permukaan elektrod dan enap cemar yang terhasil. Keputusan kajian yang diperolehi daripada simulasi air sisa mengesahkan bahawa sistem elektrokoagulasi berasaskan tenaga suria dapat mengurangkan enap cemar yang terhasil semasa penyingkiran ion Pb(II) dalam keadaan proses optimum. Bahagian 3 kajian ini melibatkan penilaian berkenaan kebolehlaksanaan karbon teraktif berasaskan tempurung kelapa sawit

(OPSAC) sebagai penjerap bagi menyingkirkan ion Pb(II) dari larutan akueus. Ujikaji berkelompok telah dijalankan di mana kepekatan asal Pb(II), pH, masa rawatan, suhu dan dos penjerap dipilih sebagai pemboleh ubah tak bersandar untuk proses penjerapan. Struktur dan tekstur permukaan bahan dikaji dengan menggunakan FESEM, EDAX dan analisis luas permukaan BET. Hasil kajian menunjukkan bahawa proses penjerapan mencapai tahap keseimbangan selepas 30 min. Hasil kajian juga menunjukkan bahawa penjerapan ion Pb(II) bergantung pada pH, di mana pH 6 memberikan penyingkiran ion Pb(II) tertinggi. Secara umumnya, kecekapan penyingkiran ion Pb(II) meningkat selaras dengan peningkatan dos OPSAC sehingga 4 g/L, di mana kecekapan penyingkiran ion Pb(II) yang dicapai adalah 99.1%. Berdasarkan keputusan kajian, model isoterma Langmuir merupakan model yang paling sesuai untuk menjelaskan data penjerapan, di mana kapasiti penjerapan maksimum adalah 58.05 mg/g. Sementara itu, didapati bahawa model tertib kedua pseudo adalah model yang paling sesuai untuk mewakili kinetik penjerapan. Dalam Bahagian 4 kajian ini, suatu proses elektrokoagulasi-penjerapan hibrid dengan menggunakan OPSAC sebagai penjerap telah dijalankan untuk menyingkirkan ion Pb(II) dari larutan akueus. Keputusan optimum yang diperolehi daripada kajian elektrokoagulasi dan penjerapan sebelum ini digunakan untuk menilai prestasi proses hibrid ini. pH, kepekatan asal ion Pb(II) dan dos OPSAC dipilih sebagai pemboleh ubah tak bersandar.

Kata kunci: elektrokoagulasi, fotovolta suria, zink tertebuk, plumbum

ACKNOWLEDGEMENTS

First and the foremost, all praise be to Allah SWT for giving me the strength, courage, patience, and perseverance to overcome all the obstacles throughout my PhD journey and complete this thesis.

I would like to express my heartfelt appreciation to my supervisor, Prof Mohamed Kheireddine Aroua, for his invaluable guidance, patience, encouragement, and support, which enabled me to complete this research successfully. I am greatly indebted to him for his insightful comments and constructive criticisms which helped me to solve many problems regarding my research and finally, complete this thesis. I am also greatly indebted to University of Malaya for providing me the financial support to pursue my PhD under the University of Malaya Scholarship Scheme.

I specially thank the laboratory staff, Mr. Kamaruddin, Mr. Azaruddin, Mr. Rizman, and Ms. Fazizah, for providing me with the technical assistance throughout my research. In addition, I am grateful to my friends for their friendship, assistance, and moral support throughout the course of my PhD. The long hours in the Thermodynamics Laboratory were enjoyable with all of them around.

Last but not least, I would like to express my sincere appreciation to my parents, Hussin A. Manaf and Dasimah Yaacob, and my siblings for their endless love, prayers, and support. I am blessed to have such wonderful parents and I would not have been able to complete my study without them.

TABLE OF CONTENTS

LIST OF FIGURES

LIST OF TABLES

LIST OF SYMBOLS AND ABBREVIATIONS

AC	:	Activated carbon
Al	:	Aluminium
Co	:	Initial concentration
CC	:	Chemical coagulation
EC	:	Electrocoagulation
EF	:	Electroflotation
EO		Electrooxidation
Fe	:	Iron
I	:	Current density (mA/cm^2)
M	:	Molecular mass (g/mol)
OPSAC	:	Oil palm shell activated carbon
Pb	:	Lead
PV	:	Photovoltaic
S/V	:	Surface area to volume ratio
SVI	:	Sludge volume index
t	:	Time (min)
U	:	Voltage (V)
V	:	Volume (m^3)
Zn	:	Zinc

LIST OF APPENDICES

CHAPTER 1: INTRODUCTION

1.1 Background

Water pollution is a serious issue which needs an immediate solution because of its adverse effects on the environment. The emission of heavy metal ions into water reservoirs from factories are main contributors of water pollution. In general, metals are used to manufacture a broad range of products and despite the important role of metals in various processes, a certain proportion of these metals are dragged out and account for a significant amount of wastes in effluent streams (Maarof et al., 2017; Siahkamari et al., 2017). For this reason, it is crucial to reduce heavy metal concentrations to within permissible limits before industrial wastewater is discharged to the environment. Promoting environmental awareness, establishing strict regulations, and enforcing environment legislations, and developing new technologies to treat industrial wastewater are among the initiatives that can be done to mitigate water pollution due to heavy metals.

Among the various types of heavy metals, lead (Pb(II)) is one of the most toxic substances and it has been extensively documented as a highly toxic heavy metal (Cechinel et al., 2014; Jayaram et al., 2009). In fact, Pb(II) was ranked second in the list of prioritised hazardous substances by the Agency for Toxic Substances and Disease Registry in 2015 (ATSDR, 2014; Hussin et al., 2017). Pb(II) is typically used in the production of batteries (Mansoorian et al., 2014), paints, pigments, glass (Günay et al., 2007), fertilisers (Singh et al., 2008a), cables, alloys, steel and plastics (Abdel-Aty et al., 2013) as well as in electroplating processes (El-Korashy et al., 2016). Industrial wastewater usually contains high concentrations of Pb(II) within a range of 1–20 mg/L (Wang et al., 2010; Zhou, 2015), 20–140 mg/L (Fales, 1948), 0.02-42 mg/L (Wang et al., 2010) and 1–25 mg/L (Nwachukwu et al., 2015) resulting from battery production, electroplating, metal

finishing and paint/pigment manufacturing processes, respectively. The high Pb(II) content of industrial wastewater is detrimental to humans since it can cause damage to the brain, liver, kidneys and reproductive system (Hernández-Morales et al., 2012). According to the World Health Organization (WHO), Pb(II) exposure is the cause of approximately 143 million deaths in developing countries every year (WHO, 2016). For these reasons, it is mandatory to reduce Pb(II) concentrations to within permissible levels before industrial wastewater is discharged to the environment. A few organisations have set the maximum allowable limit for Pb(II) in wastewater effluents. The U.S. Environmental Protection Agency (USEPA), European Union, UK, South Korea, and Japan specifies that the maximum allowable limit for Pb(II) is 0.1 mg/L (Balaria & Schiewer, 2008; Bhattacharjee et al., 2003). According to the Department of Environment Malaysia, the maximum permissible limits for Pb(II) in sewage and industrial effluents are 0.1 and 0.5 mg/L for upstream and downstream discharge, respectively (IWK, 2016).

There are several techniques used to remove Pb(II) from industrial wastewater such as chemical precipitation, chemical coagulation, electrocoagulation, ion exchange, adsorption and membrane separation (Escobar et al., 2006; Liu et al., 2013). The main challenge in industrial wastewater treatment is to achieve a good trade-off between treatment efficiency and operating costs. Among these techniques, electrocoagulation and adsorption techniques have received much attention from the scientific community in the past decade. This is indeed expected because the electrocoagulation technique offers the following advantages: simplicity of operation, (2) rapid sedimentation, (3) low production of sludge, and (4) environmental compatibility (Kamaraj et al., 2015). In addition, there is possibility that electrocoagulation systems can be powered by renewable energy-based systems such as solar photovoltaic panels, which will transform solar energy into direct current electricity. Solar PV panels are favourable compared with

conventional electrical power supplies because these panels make use of clean, renewable energy. Furthermore, solar PV panels reduce energy consumption because the electricity can be stored in backup batteries and these panels require relatively low maintenance costs. Solar PV panels can be used in a wide range of applications which include providing electricity to remote communities (Sharma et al., 2011). Besides electrocoagulation process, adsorption has been found as an effective method to eliminate heavy metal ions. Adsorption of lead ions using activated carbon has been extensively explored by numerous researchers (Abdelhafez & Li, 2016; Adebisi et al., 2017; Anwar et al., 2010; Garba et al., 2016; Goel et al., 2005; Largitte et al., 2016; Momčilović et al., 2011; Ren et al., 2016; Soliman et al., 2016; Yang et al., 2009). This process is a promising effective technique to remove lead because of its low cost and high effectiveness, and more importantly, the process does not produce secondary pollutants.

Electrocoagulation and adsorption processes are typically carried out independently. At present, there are some water and wastewater treatment systems based on integrated processes such as flotation-electrocoagulation, chemical coagulation-electrocoagulation, membrane-electrocoagulation, and oxidation-electrocoagulation systems (Aziz et al., 2016; Chen & Deng, 2012; Emamjomeh & Sivakumar, 2009; Lee & Gagnon, 2016). However, to the best of the author's knowledge, no attempts have been made to integrate electrocoagulation and adsorption processes for Pb(II) removal. It is believed that the benefits of these processes can be leveraged by integrating them into a single system, which will significantly boost the Pb(II) removal efficiency compared with a single process.

1.2 Problem statement

It is known that electrode material is one of the crucial factors which affect the Pb(II) removal efficiency of the electrocoagulation process. Hence, it is imperative to select the appropriate anode material in order to enhance the efficiency of the electrocoagulation process. Various anode materials have been tested extensively for Pb(II) removal by electrocoagulation such as iron (Fe), aluminium (Al) and copper (Cu). The anode material is chosen based on several factors such as its electrochemical potential, current efficiency, service life, resistivity to the environment, and cost of the material. Among the anode materials mentioned above, Fe and Al are commonly used for sacrificial anodes due to the low electronegativities of these materials. In addition, these materials are capable of oxidising metal into hydrated metal cations during the electrocoagulation process (Cicek, 2017). However, the main drawbacks of Fe electrode are its low electrochemical potential, low current efficiency and poor settleability. In contrast, Al electrode has low corrosion resistance and it can be used in low resistivity environments. Cu electrode, on the other hand, has low electrochemical potential, and low current efficiency (Cicek, 2017). Al and Fe plane electrodes are typically used for electrocoagulation treatment and therefore, there is a critical need to explore novel anode materials with favourable properties and excellent Pb(II) removal efficiency. In this study, perforated zinc (Zn) is proposed as the anode material, which is a new electrode material for the removal of Pb(II) by electrocoagulation process. Zn is an appealing choice for electrocoagulation treatment systems because of its high current efficiency, long service life and low overpotential for anodic dissolution. This material is also can be used in high resistivity environments.

High energy consumption and long treatment time are drawbacks of electrocoagulation systems and therefore, much effort has been made in recent years to study and improve the electrocoagulation technique in order to simplify the process and ensure ease of implementation, boost its efficiency for Pb(II) removal, and ensure environmental compatibility of the system. In addition, the use of conventional electrical power supplies for water and wastewater treatment systems is inappropriate in remote areas, especially in rural communities with restricted access to the electricity grid. Furthermore, conventional power systems are not economically feasible because of their high capital investments and operating costs. For these reasons, solar PV systems have gained much attention in order to address the issues associated with conventional power systems. In this regard, it is imperative to explore the potential of solar PV systems for water and wastewater treatment, especially to remove heavy metals.

In general, electrocoagulation and adsorption processes are conducted separately. It is not economically viable to implement these systems on an industrial scale because these systems are incapable of removing substantial amounts of heavy metal ions present in water or wastewater. Therefore, an in-depth understanding of these processes will greatly facilitate the innovation and development of an efficient, economical, and sustainable system for water treatment plants while maintain compliance with standard regulations for Pb(II) removal. The benefits of an integrated electrocoagulation-adsorption system include ease of operation, high efficiency, short reaction time, low sludge production, and low energy consumption (Aziz et al., 2016). This system exploits the benefits offered by the individual treatment processes, which forms the motivation of this study. In order to achieve this goal, it is essential to understand the factors that affect electrocoagulation and adsorption processes, as well as predict the optimum process conditions.

1.3 Objectives of the study

The main objectives of this study are as follows:

1. To evaluate the performance of Zn as a new anode material for Pb(II) removal and compare its performance with those of conventional anode materials (Al, Fe and Cu).
2. To investigate the feasibility of a solar PV electrocoagulation system for Pb(II) removal.
3. To study the effects of important process parameters on the removal of Pb(II) by adsorption on palm shell activated carbon.
4. To evaluate the performance of a novel process integrating the solar electrocoagulation with adsorption for the removal of Pb(II).

1.4 Scope of the study

This study is divided into four stages. The first stage involves selecting a new electrode material for the electrocoagulation process with emphasis on the anode materials, anode configurations, current efficiency, sludge index, and electrode morphology. A solar PV electrocoagulation system is used to assess the capability of the new anode material in removing Pb(II) from aqueous solutions. The second stage is focused on investigating the effects of operating parameters (namely, electrode distance, pH, current density and initial concentration) on the Pb(II) removal efficiency of the solar PV electrocoagulation treatment system. In the third stage of this study, the feasibility of oil palm shell activated carbon (OPSAC) as an adsorbent to remove Pb(II) ions from aqueous solutions are

studied. In the fourth stage of this study, the results obtained from both electrocoagulation and adsorption processes are used to develop the integrated electrocoagulation-adsorption treatment system. A response surface methodology (RSM) is used to optimise the process parameters of the integrated electrocoagulation-adsorption treatment system in order to enhance the Pb(II) removal efficiency.

1.5 Outline of the thesis

This report consists of five chapters, namely, Introduction, Literature Review, Research Methodology, Results and Discussion, and Conclusions.

Chapter 1: Introduction

The background of this study including the motivation, objectives and scope of this study are presented in this chapter.

Chapter 2: Literature review

Past studies relevant to this work are reviewed and presented in this chapter, with emphasis on the electrocoagulation process, adsorption process and its mechanism as well as solar PV systems. The fundamentals of solar photovoltaic energy as well as the development of solar PV technologies, their applications and impact on the society and economy are also presented in this chapter.

Chapter 3: Research methodology

The experimental set-up and procedure adopted in this study are described in detail in this chapter. This chapter begins with a description of the experimental rig, followed by a

description of the solar PV electrocoagulation treatment, adsorption process and integration process.

Chapter 4: Results and discussion

The key findings obtained in this study are presented and discussed in this chapter.

Chapter 5: Conclusions and recommendations

The conclusions drawn based on the findings of this study are presented in this chapter. The recommendations for future work are also given in this chapter, which serve as a guideline for other researchers who are interested to explore this work further in the future.

CHAPTER 2: LITERATURE REVIEW

2.1 Lead

Lead is an element that can be obtained naturally from the environment. It is particularly useful in various manufacturing industries. However, no specific biological role has been reported on the lead element, and it can be poisonous to humans and mammals. It can accumulate in the body and cause serious health problems (Alloway, 1995). The Agency for Toxic Substances and Disease Registry (ATSDR) and U.S. Environmental Protection Agency (USEPA) are the two federal public agencies that play important roles to protect people and environment from hazardous substances disease. The ATSDR has consolidated a comprehensive list as a guidance and information on the toxicological profile for each substance. Based on the list, lead is one of the most toxic heavy metals and is ranked as the second most hazardous substance (ATSDR, 2014). Therefore, this guideline is beneficial for researchers to develop new technologies for reduction of lead discharge in which such technology can be applied in the industrial waste treatment plant.

2.2 Properties of lead

Lead is categorised as a member in group 14 (IVA) of the periodic table of elements (Alloway, 1995). Lead has various unique properties such as high softness, high flexibility, ductility, low melting point and resistance to corrosion, which are valuable properties for a wide range of different industrial applications (Flora et al., 2012). The relative atomic mass of lead is 207.2 g/mol and its density is 11.34 g/cm^3 at 20^{o}C. Lead is a blue-grey coloured metal which melts at 327^{o}C and boils at 1749^{o}C (Alloway, 1995; Sharma et al., 2010). There are three common oxidation states of lead: Pb (0), Pb (II) and Pb (IV). Lead mainly exists as Pb (II) in the environment. Pb (IV) only occurs under

extremely oxidising conditions, and inorganic Pb (IV) compounds usually do not exist under ordinary environmental conditions. Likewise, Pb (0) is found in nature, but its occurrence is rare. The approximate relative abundance of the four lead isotopes are: ^{208}Pb (51-53%), ^{206}Pb (23.5-27%), ^{207}Pb (20.5-23%), and ^{204}Pb (1.35-1.5%). Lead has attractive chemical and physical properties (Abadin et al., 2007). Hence, it is used extensively in various global industrial applications.

2.3 Effects of lead

Lead exposure can cause various health effects to human body. For instance, lead can cause problems in the central nervous system and the peripheral nervous system (Bellinger, 2004). These adverse effects are more prominently experienced by the fetus, pregnant women, and young children. In addition, it also has several neurological effects with major symptoms such as a headache, loss of memory, dullness, poor span of attention and hallucinations. These neurological effects were more significant in children than adults as children has immature immune systems which makes them more susceptible to disease. Moreover, long-term lead exposure can cause additional side effects including delirium, lack of coordination, paralysis, and coma (Needleman, 2004). Children who are exposure to high concentration of lead may suffer growth retardation, hindered cognitive development, acute memory loss and hearing loss (Flora et al., 2006). Lead also has side effects on female and male reproductive systems. These include abnormal spermatogenesis, premature membrane rupture, abnormal prostatic function, pregnancy hypertension and premature delivery (Flora et al., 2006).

2.4 Standard and regulations of lead

Exposure to lead is comparatively higher in some parts of the world, particularly in underdeveloped countries. Besides, rapid growth in industrialisation has contributed to water pollution that comes from wastewater streams containing lead ions. In the recent years, a few small-scale industries were major contributors to the overall wastewater generated. The dangerous aspect of this issue is there is no sufficient control over wastewater discharge and treatment in the small-scale industry by the government agencies. Most of the time, wastewater is discharged directly into rivers and natural water streams without being treated. Public awareness of environmental issues and strict regulations are essential. Therefore, wastewater regulations were established to minimise human and environmental exposure to hazardous chemicals. The maximum allowable limit for Pb(II) in wastewater is 0.1 mg/L in the European Union, UK, South Korea and Japan (Balaria & Schiewer, 2008; Bhattacharjee et al., 2003; Reddy et al., 2010; Wako, 2012). Besides, the maximum acceptable concentrations of lead in sewage and industrial effluents are 0.1 and 0.5 mg/L for upstream and downstream discharges respectively, according to the Malaysia regulations (IWK, 2016). Furthermore, in Malaysia, landfill criteria for disposing scheduled waste was introduced by Kualiti Alam Sdn Bhd (a body approved by the government to handle waste treatment and disposal). The maximum limit of lead concentration for landfill disposal is 5mg/L (Alam, 2005).

2.5 Lead removal methods

Over the past few decades, numerous conventional technologies have been devised to removal lead ions from aqueous solutions, including chemical precipitation, coagulation-flocculation, reverse osmosis, adsorption, ion exchange and membrane filtration

(Vasudevan & Lakshmi, 2011a). Numerous researchers reported that these treatment methods are effective for lead ions removal from aqueous solution (Adebisi et al., 2017; Al-Rashdi et al., 2011; Kavak, 2013; Levy, 1992; Maher et al., 2014; Matlock et al., 2002; Mohammadi et al., 2014; Pang et al., 2009; Pang et al., 2011; Rahman et al., 2017; Singh et al., 2008b; Vergili et al., 2017). Several recent studies on the removal and recovery of lead ions are listed in Table 2.1.

Table 2.1: A summary of recent studies on the removal and recovery of lead

Wastewater/ Pollutant	Method of treatments	Removal efficiency (%)	References
Battery recycling	Chemical precipitation	99.4	(Matlock et al., 2002)
Aqueous solution	Chemical precipitation	99.42	(Kavak, 2013)
Aqueous solution	Coagulation-Flocculation	98.0	(Pang et al., 2009)
Aqueous solution	Coagulation-Flocculation	99.0	(Pang et al., 2011)
Drinking water	Reverse Osmosis	99.0	(Levy, 1992)
Wastewater	Adsorption (Tamarind wood)	97.95	(Singh et al., 2008b)
Wastewater	Adsorption (Lemon peel)	95	(Mohammadi et al., 2014)
Aqueous solution	Adsorption (Palm oil mill effluent)	>90	(Adebisi et al., 2017)
Wastewater	Ion exchange	>98	(Rahman et al., 2017)
Battery industry	Ion exchange	>90	(Vergili et al., 2017)
Drinking water	Membrane technology	86	(Maher et al., 2014)
Wastewater	Membrane technology	84	(Al-Rashdi et al., 2011)

Nevertheless, most of the above-mentioned methods have some drawbacks such as high energy consumption, high operational costs, ineffective removal of high heavy metal ion concentration and the need to use a large amount of chemicals. On the other hand, many

studies have reported that the electrochemical and adsorption processes showed high competency in removing of lead ions at a maximum level (Li et al., 2017; Vasudevan & Oturan, 2014; Wei et al., 2012; ZhangJiang et al., 2013). These two processes have received significant attention from researchers in the past decade. Therefore, these reviews focused extensively on the application of electrochemical (concentrated on the electrocoagulation process) and adsorption processes for the removal of lead ions. For electrocoagulation process, the discussions emphasise on the theoretical part of electrocoagulation process, the design of electrocoagulation reactor, effects of operating parameters and new technology for lead ions removal. Meanwhile, for adsorption process, the discussions cover the types of adsorbent, recent studies on the application of adsorption process to remove lead ions and main operating parameters that affect adsorption capacity. Finally, the application of the integration process was also discussed.

2.6 Electrochemical

Electrochemical technology provides ways for maximum recovery and removal of metals from wastewater (Bebelis et al., 2013; Maarof et al., 2017). The growing demand for industrial metals makes this treatment method suitable and extremely attractive. Thus, this technology can technically offer an excellent way to treat wastewater that is contaminated with lead ions. The potential of using electrochemical technology with respect to wastewater treatment has notably increased at a global level. In recent decades, electrochemical technologies have been widely applied in various fields of research such as organic and inorganic biosensing electrochemical (Singh et al., 2017), metal and alloy electrocoating (Romano & Olivier, 2015), heavy metal recovery (Park et al., 2015), dye removal (Nandi & Patel, 2017), sensors (Xia et al., 2017) and etc. Several electrochemical treatment methods like electroflotation, electrocoagulation, electrooxidation,

electrodeposition, electrodialysis, electrodeionisation and electrosorption were employed to remove heavy metal ions from aqueous solution (Maarof et al., 2017). The summary of recent research on the electrochemical treatments are given in Table 2.2.

Table 2.2: A summary of recent research on the electrochemical treatments

Wastewater/ Pollutant	Method of treatments	Removal/Recovery efficiency (%)	References
Aqueous solution	Electrodialysis	91	(Abou-Shady et al., 2012)
Wastewater	Electrodeposition	>80	(Gonzalez et al., 2016)
Aqueous solution	Electrooxidation	99.6	(Liu et al., 2013)
Aqueous solution	Electrodialysis	90	(Hamane et al., 2015)
Aqueous solution	Electrodeposition	-	(Najafi et al., 2009)
Aqueous solution	Electrodeionisation	-	(Lingfang et al., 2014)
Aqueous solution	Electrosorption	-	(Wei et al., 2016)
Aqueous solution	Electrosorption	-	(Yang & Shi, 2015)
Aqueous solution	Electrocoagulation	99.9	(Hussin et al., 2017)
Battery industry	Electrocoagulation	97.3	(Mansoorian et al., 2014)
Aqueous solution	Electrocoagulation	99.3	(Kamaraj et al., 2015)
Aqueous solution	Electrocoagulation	99.4	(Ferniza-García et al., 2017)
Wastewater	Electroflotation	97	(de Oliveira da Mota et al., 2015)
Wastewater	Electroflotation	-	(Rajeshwar & Ibanez, 1997)

However, among all the various technologies available, electrocoagulation is one of the best solutions for lead ions removal. Electrocoagulation has many advantages such as being excellent in destabilising small colloidal particles, producing less sludge, fitting in for installation in a limited space available and keeping operational cost low (Chen et al., 2002). Although this treatment method shows several benefits, there is a need for more in-depth studies to minimise the shortcomings of the existing processes such as low

conductivity of electrodes, high energy consumption, poor electrode reliability and impracticable implementation in the rural area (Maarof et al., 2017). Thus, next section only focuses on the electrocoagulation process for lead ions removal as less comprehensive studies on this field of research can be obtained from the literature.

2.7 Theoretical background on electrocoagulation process

The basic principle of electrocoagulation is based on electrolysis process. The principle of electrolysis was first discovered by Michael Faraday in 1820 (Chen et al., 2005). The term electrolysis is a process that refers to the use of electricity to chemically break down a chemical compound. This process requires an electrolyte (e.g., soluble salts, acids or bases) which gives the ions a possibility to be transferred between two electrodes (anode and cathode). The two electrodes are connected to an electric circuit. When applying a direct current, the negative ions would move to the anode, and positive ions would travel to the cathode. During the process, the cations will be reduced to form neutral metal atoms, and the anions will be oxidised to form oxygen gas at the anode electrode (Sahu et al., 2014a).

In general, electrocoagulation process involves numerous phenomena of chemical and physical that utilise sacrificial electrodes in supplying ions in the water stream. Metal is broken down from the anode to create metal ions, which promptly hydrolyse to polymeric metal hydroxide. These polymeric hydroxides are incredible agents of coagulation (Vasudevan & Lakshmi, 2011b). In the electrocoagulation process, several reactions occur at both the anode and the cathode. The basic schematic of the electrocoagulation system unit is shown in Figure 2.1 (Moussa et al., 2017).

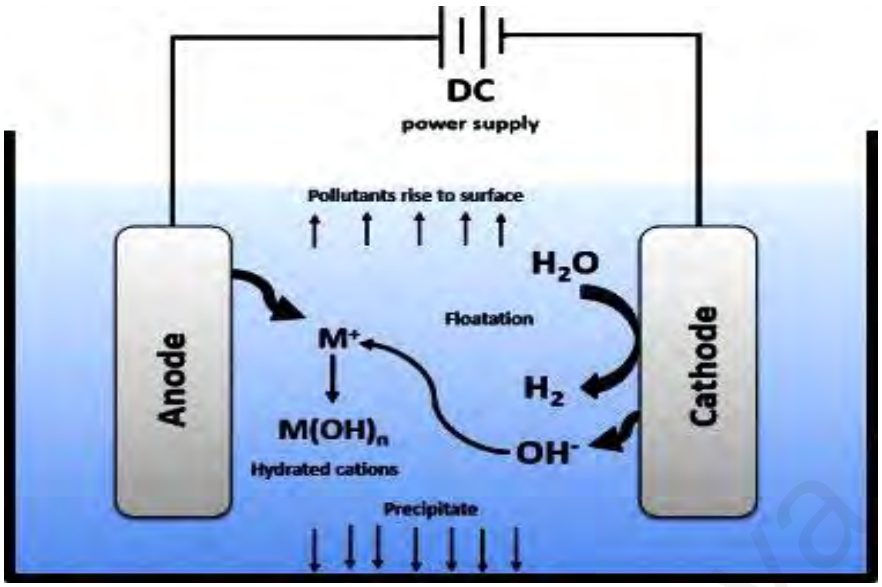

Figure 2.1: Schematic diagram of the electrocoagulation mechanism
(adopted from (Moussa et al., 2017)

In the electrocoagulation process, heavy metals are mainly removed by two main mechanisms (Garcia-Segura et al., 2017; MollahMorkovsky et al., 2004):

1) surface complexation
2) electrostatic attraction

For the surface complexation mechanism, the pollutant could act as a ligand to chemically bind metal hydroxide ($Fe(OH)_n$, $Al(OH)_n$ or $Zn(OH)_n$). Then, the metal hydroxide forms a coagulant precipitate, allowing the separation of the pollutants from the wastewater or aqueous solution (Garcia-Segura et al., 2017; Naje et al., 2017).

The second mechanism related to electrostatic attraction between the heavy metal contaminant and the coagulant floc. Coagulation forms when the metal ionic species adsorb on the surface of these hydroxide particles and neutralise their surface charge, and

finally large flocs will produce by metal hydroxide precipitate causes pollutant is rapidly removed (de Mello Ferreira et al., 2013).

The metal hydroxide flocs generally have large surface areas which could make the active surface for a quick adsorption of compounds and trapping of colloidal particles. Then, these flocs are removed simply from aqueous solution by sedimentation and flotation (Daneshvar et al., 2006; Garcia-Segura et al., 2017). The mechanism of electrocoagulation process is shown in Figure 2.2.

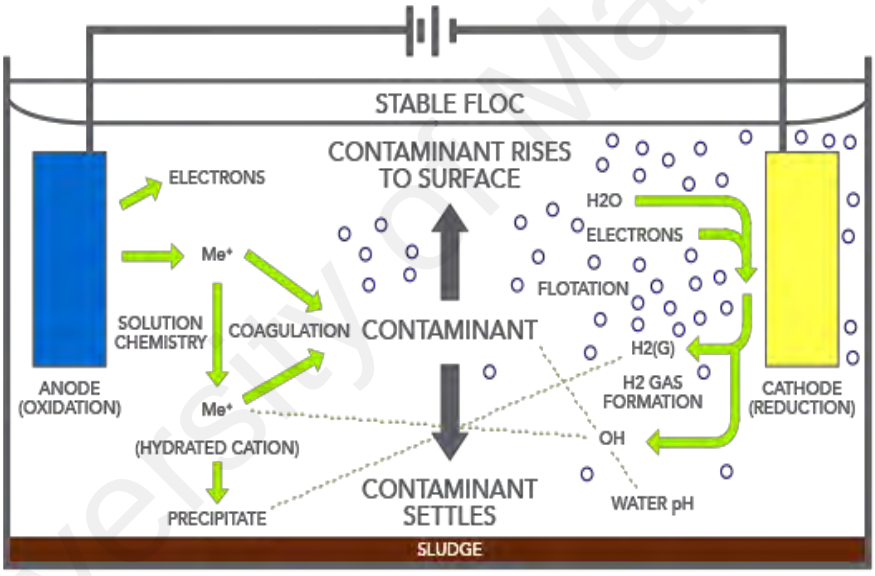

Figure 2.2: Mechanism of electrocoagulation process
(adopted from (An et al., 2017; CRS, 2017))

In the electrocoagulation process, the summary of the pollutants and particle suspension's destabilisation mechanism, and the breaking of emulsions are provided below (Comninellis & Chen, 2009):

1. The diffused double layer close to the charged particles is compressed via the interaction of the ions which are made through the oxidation at the sacrificial anode.

2. The ionic species that exists in wastewater undergoes charge counterbalancing by counter ions that are twisted through the sacrificial anode's electrochemical disintegration. The electrostatic interparticle is reduced by the counter ions to the extent that the Van der Waals attraction exists, and therefore leading to coagulation.

3. A sludge blanket is produced via the floc that is formed through coagulation. The colloidal species in the aqueous phase is bridged and capitulated by the sludge blanket. The active surfaces to adsorb the contaminants are formed through the solid oxides, hydroxides, and oxyhydroxides.

2.8 Main reactions

Metals such as iron, aluminium or zinc are categorised as an active electrode material and are suitable to be used as the anode for electrocoagulation process due to their strong affinities for dispersed particles and by generating coagulation through counter ions (Sahu et al., 2014b). The following chemical reactions that take place during the electrocoagulation process are shown below. When a direct current is passed through anode material (zinc for instance), it will dissolve to Zn^{2+} ions. OH^- ions will be released during the cathodic reaction at the side of the cathode, resulting an increase in pH of the solution. Furthermore, vigorous H_2 bubbles production will be observed according to equations (2.1-2.4) (Ferniza-García et al., 2017; Naje et al., 2017):

General reaction : $$M(s) \rightarrow M^{n+}(aq) + ne^- \quad (2.1)$$

At the anode : $$Zn \rightarrow Zn^{2+} + 2e^- \quad (2.2)$$

At the cathode : $$2H_2O_{(l)} + 2e^- \rightarrow H_{2(g)} + 2OH^-$$ (2.3)

Overall reaction : $$Zn^{2+}_{(aq)} + 2H_2O_{(l)} \rightarrow Zn(OH)_2 + 2H^+_{(aq)}$$ (2.4)

2.9 Fundamental laws of the electrocoagulation process

There are some criteria that should be considered in the design of the electrocoagulation reactor such as the overpotential of electrodes, the mass transfer overpotential and the ohmic potential drop. Electrode potential explains the reactions occur on the surface of the electrode. The efficiency of the removal of heavy metals from electrocoagulation system is affected by the geometry of the electrodes and the optimum conditions of the process (Naje et al., 2017). The applied overpotential is thus written as Equation 2.5 (Essadki, 2012):

$$\eta AP = \eta Mt + \eta k + \eta IR \quad (2.5)$$

Where ηAP is the applied overpotential, ηMt the concentration overvoltage, ηk the kinetic overpotential and ηIR the overpotential that happens due to solution ohmic drop.

Concentration overpotential, also called as diffusion over potential or mass transfer, is because of the change in analyte concentration happening near the electrode surface as a result of electrode reaction. The over potential occurs because of the changes in electro active species concentration among the bulk solution and the electrode surface. This condition occurs when the electrochemical reaction is adequately fast to transfer the concentration of surface of electro active species under that of the mass solution. Over potential is unimportantly at the point when response rate constant is significantly smaller

than the mass transfer coefficient of the concentration. By concentration of over potential can be decreased by increasing the masses of the metal particles transported from the anode surface to the greater part of the solution, and by improving the solution's turbulence (Naje et al., 2017). At a higher velocity by passing the solution of electrolyte from anode to cathode mechanically it can also be overcome. It can be reduced by eliminating this gradient by ensuring that the amounts of cations being transported from the surface of anode to the bulk solution is increased. This can be done, for example, by increasing the mixture between the electrodes. Kinetic over potential, which is also known as activation potential, begins from the barrier of activation energy to electron transfer reactions. Meanwhile, the IR-drop could be lowered down with a greater ease by reducing the distance of inter electrode and increasing enhancing the electrodes' cross sectional area and the solution's specific conductivity (Emamjomeh & Sivakumar, 2009; Kabdaşlı et al., 2012; MollahMorkovsky et al., 2004; Mollah et al., 2001; Nasrullah et al., 2014). To achieve the maximum efficiency, there are some important factors that should be considered (Table 2.3):

Table 2.3: Factors influencing the performance of the electrocoagulation process

Important factors	Performance criteria	Recommendations
Ohmic potential drop (IR-drop)	IR-drop between the electrodes should be minimised	Decreasing the inter electrode distance
O_2 and H_2 gas at the electrode surfaces	The O_2 and H_2 gas bubble accumulation that nucleates at the surfaces of the electrode should be minimised	Use appropriate electrode geometry and increased cross-sectional area of electrodes
Mass transfer	Mass transfer impediment through the spaces between the electrodes should be lowest	Increase the mixing rate between the electrodes

2.10 Design of reactor for electrocoagulation process

The design of the reactor is a crucial factor in the electrocoagulation process. How well the reactor design suits are mainly dependent on wastewater types and the application's purpose. Many other factors are influencing the electrocoagulation performance including mode of operation (batch or continuous), electrode configurations (monopolar or bipolar), electrode material, electrode distance, effects of pH, current density, reaction time, conductivity and stirring speed. The reactor design can be divided into two categories: physical (mode of operation, reactor geometry, reactor scale-up, current density, and conductivity) and chemical (electrode material, electrode distance, pH, reaction time and passivation) aspects. The design considerations of the electrocoagulation reactor are shown in Table 2.4.

Table 2.4: The design considerations of the electrocoagulation reactor

Category	Factors
Physical	Mode of operation Reactor geometry Reactor scale-up Electrode configurations Current density and reaction time Conductivity
Chemical	Electrode material Electrode distance pH

2.10.1 Physical aspect

2.10.1.1 Mode of operation (continuous and batch operation)

A continuous system is stable in terms of performance and dynamic in terms of operation. The water and wastewater solution could be observed at the effluent samples' different flow rates. With study the effects of reaction time, the rates of electrode passivation and corrosion can also be checked (Sahu et al., 2014b). Continuous systems are more suitable for industrial processes with large effluent volumes. Meanwhile, the batch system requires simple reactor set-up and easy to operate than the continuous system. A batch system is subjected to a single pass through the system. This system is preferable for a feasibility study time-dependent behaviour, effects of pH, effects of initial concentrations and evaluate performance under controlled experimental conditions. Also, this system is more suitable for small-scale industries with low heavy metals concentration and maximum efficiency of metals can be successfully removed. The optimum parameters in the batch processes served as a guideline in operating the electrocoagulation reactors in a continuous mode. Castañeda-Díaz et al. (2017) studied the performance of the electrocoagulation and adsorption processes for dye removal from aqueous solutions. They used batch and continuous systems to study the effects of operating parameters. The results reveal that the maximum dye removal was attained at 60min using batch mode system compared to continuous mode system requires 90min to achieve high removal of dye. They stated that, the removal efficiency achieved in the batch system was higher than that achieved in the continuous electrocoagulation process (Castañeda-Díaz et al., 2017).

2.10.1.2 Reactor geometry

The geometry of the reactor also influences the electrocoagulation performance. Electrocoagulation reactors were designed using a number of configurations, such as tall (vertical/ horizontal) plate, short (horizontal parallel) plate, perforated plate, mesh electrode, cylindrical electrode, tube reactor, solid tube reactor, 2D reactor, 3D reactor (packed bed), fluidized bed, spouted bed and etc (Eiband et al., 2014; Hamdan & El-Naas, 2014; Moussa et al., 2017; Tezcan Un et al., 2013). Each system has its pros and cons, which are different regarding electrode life span, current efficiency and mass transfer. A variation of the electrocoagulation reactor was reported by Tezcan Un et al. (2013) investigated the removal of fluoride using a cylindrical anode and a rotating impeller cathode. Eiband et al. (2014) developed a new reactor geometry using rotating screw reactor to study the performance of electrocoagulation process for the removal of Pb(II). Hamdan & El-Naas (2014) studied the performance of electrocoagulation process for the removal of Chromium (VI) using cylindrical reactor. The results reveal that 100% of chromium was removed after treatment with 7.94 mA/cm^2 of current density and at pH 8. Several recent studies using various types of reactor geometry in the electrocoagulation process are listed in Table 2.5.

Table 2.5: Recent studies of various types of reactor geometry in the electrocoagulation process

Wastewater/ Pollutant	Process	Initial concentration (mg/L)	Electrode shape	Removal (%)	References
Aqueous solution	Batch	Pb: 1500	Titanium mesh coated with RuO_2 and IrO_2	91	(Abou-Shady et al., 2012)
Wastewater	Batch	Pb: 4	Titanium mesh coated with RuO2 and IrO2	99.7	(Basha et al., 2011)
Aqueous solution	Fluidized bed	Pb: 150	Perforated stainless steel 316	99	(Segundo et al., 2012)
Aqueous solution	Batch	Pb: 4	Stainless steel nets coated with single wall carbon nanotubes	99.6	(Liu et al., 2013)
Aqueous solution	Batch	Cr(VI): 500	Vertical and horizontal cylindrical	90	(Khalaf et al., 2016)
Battery industry	Batch	Pb: 9	Plate	97.2	(Mansoorian et al., 2014)
Aqueous solution	Spouted bed reactor	Cd: 50-270	Titanium mesh coated with IrO2 and RuO2	97.8	(Baghban et al., 2014)
Wastewater	Cylindrical packed-bed	As(III): 0.03-0.2	Iron ball	95.8	(Şık et al., 2017)
Aqueous solution	Batch	Pb: 5-20	Perforated	99.9	(Hussin et al., 2017)
Aqueous solution	Batch	Cr(III)/Cr(VI): 100	Vertical cylindrical	94.97-99.97	(Zewail & Yousef, 2014)

2.10.1.3 Reactor scale-up

The surface area to volume ratio (S/V) was regarded as an important scale-up parameter. The increase in S/V ratio, results in the reduction of the current density consumption (Belhout et al., 2010). Thus, this parameter should be considered in developing a scale-up electrocoagulation reactor due to its influencing the performance of the electrocoagulation process. Orescanin et al. (2011) have proven that the optimum conditions of the electrocoagulation treatment process from the laboratory scale could be applied in the pilot plant scale. They observed that 100% removal of Pb(II) was achieved with the pilot plant scale (Orescanin et al., 2011). In a research article by Khaled et al. (2015) observed that with increasing S/V ratio, the removal efficiency obtained also increases (Khaled et al., 2015). This result was further supported by a research from Bougerra et al. (2015) in which removal efficiency increases from 76.17% to 98.85%, the S/V ratio increases from 8.4 to 14.4 m^{-1} (Bouguerra et al., 2015). In order to ensure proper sizing and reactor proportioning, the dimensionless scale-up parameters, which are the Reynolds number (fluid flow regime) and Froude number (buoyancy) were calculated.

2.10.1.4 Electrode configurations

Electrocoagulation reactors commonly built up of plate electrodes using two electrodes that connected to electricity. Monopolar and bipolar are two types of electrode arrangement typically used in the electrocoagulation process. Each arrangement system has its pros and cons. Selection of suitable electrode configuration and usage of the electrode's large surface area are main characteristics to increase the electrocoagulation process' performance. In the monopolar systems (Figure 2.3a), all anodes and cathodes are connected to each other. In the bipolar systems (Figure 2.3b), the outermost electrodes

are linked to electricity, and the current passes over the other cathode electrodes, thus polarising them. In the connection of the bipolar system, only the first anode electrode and the last cathode electrode are connecting to power source. Various researches have reported on the comparison between monopolar and bipolar configurations on the removal of lead ions (Eiband et al., 2014; Garcia-Segura et al., 2017; Hansen et al., 2007; Heidmann & Calmano, 2008; Mansoorian et al., 2014; Pociecha & Lestan, 2010; Sahu et al., 2014a). The results of these studies showed that the lower operating cost is obtained via the monopolar configuration. However, higher heavy metals removal can be obtained with the bipolar configuration, which could be due to extra side reactions.

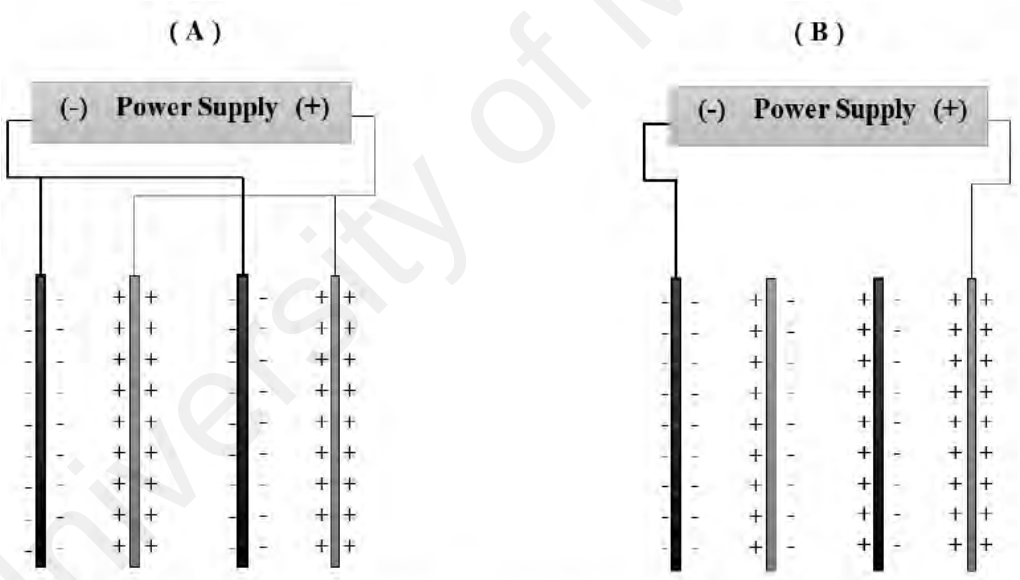

Figure 2.3: Electrodes arrangement a) Monopolar b) Bipolar in electrocoagulation reactor
(adopted from (Khandegar & Saroha, 2013; Naje et al., 2017)).

2.10.1.5 Current density and treatment time

Operating current density and treatment time are extremely important in electrocoagulation since it is the one and only operational parameter that could be controlled directly (Kabdaşlı et al., 2012). Both coagulant dosage and bubble generation rates are determined by current density. In addition, solution mixing and mass transfer at electrodes are also strongly influenced by current density. The amount of electricity made to pass through the electrolytic solution determines the quantity of metal dissolved or deposited (Refer to Equation 2.6). To run a reactor, the maximum current density may not necessarily be the mode with best efficiency. It is notable that the optimum current density will constantly involve an exchange-off between operational expenses and effective utilisation of the introduced coagulant. The other parameters like pH, flow rate and temperature must also be monitored along with operating times to ensure a high current efficiency. The amount of ions produced or charge loading, the product of current and treatment time will determine the quantity of the treated water (Sahu et al., 2014a). In a review article by Hakizimana et al. (2017) stated that very high current density values may negatively affect the electrocoagulation efficiency (Hakizimana et al., 2017). Using high current density is not recommended due to its could increase voltage, ohmic resistance and the operational cost (Garcia-Segura et al., 2017). Naje et al. (2017) reported that the increase in treatment time, resulted in an increase in the generation of flocs resulting and the pollutant removal efficiency (Naje et al., 2017).

The amount of electricity passing via the electrolyte solution will determine the amount of metal ion dissolved. The amount of metal ions dissolved during the reactions at the anode will be calculated using Faraday's law (Equation 2.6) (Chaturvedi, 2013; Ghosh et al., 2008).

$$Electrode\ consumption\ (kg/m^3) = \frac{I\ x\ t\ x\ M}{z\ x\ F\ x\ V} \quad (2.6)$$

where I is the current (A), M is the molecular mass of Zn (65.39 g/mol), t is the treatment time (s), F is Faraday's constant (96,487 C/mol), V is volume (m^3) and z is number of transferred electrons (z = 2).

2.10.1.6 Solution conductivity

The greater ionic strength causes an increase in the current density of wastewater. The current density efficiency increases with increasing electrolytic conductivity due to the decrease of ohmic resistance of wastewater. Therefore, it is important to investigate the effect of effluent conductivity on the electrocoagulation process (Hakizimana et al., 2017; Sahu et al., 2014a). There are three types of electrolyte (supporting electrolyte) typically used in the electrocoagulation process to increase the conductivity such as NaCl, KCl and Na_2SO_4. Before adjusting the pH value of the aqueous solution, supporting electrolyte is added and mixed in the solution. Current density rises with high in conductivity at a constant cell voltage, thus decreasing the energy consumption (Dalvand et al., 2011; MollahPathak et al., 2004). The supporting electrolyte could also reduce the energy consumption of electrocoagulation process. A similar observation made by Hakizimana et al. (2017) stated that the increase in conductivity resulted in decrease the energy consumption and produce a high removal of heavy metal ions.

2.10.2 Chemical aspect

2.10.2.1 Electrodes materials

Selection of suitable electrode material is vital to ensure the effectiveness of elimination in the electrocoagulation treatment process. The electrode material plays a key role in reactor design that emphasis on high activation energies in order to prevent an undesirable occurrence on side reaction during an electrocoagulation process. Aluminum, iron, graphite, mild steel, carbon and stainless steel are commonly electrode material used for electrocoagulation treatment (Garcia-Segura et al., 2017). Nevertheless, aluminum and iron are materials used widely as sacrificial electrode as they readily available, low in cost and proven to be effective (Bayramoglu et al., 2004; Hakizimana et al., 2017; Kobya et al., 2003). Aluminum and iron electrodes were combinedly used in some researches (Katal & Pahlavanzadeh, 2011). The electrolyte's chemical properties and pollutants to be removed determine the best material selection. If the efficiency of the treatment is the only factor in consideration, aluminium ought to be the best when compared to iron in most cases, generally. This could be due to high adsorption capacity of hydrous aluminum oxides. Nevertheless, it is notable that price of aluminum material is more expensive than iron material in certain countries (Emamjomeh & Sivakumar, 2009). Also, using Al as the electrode during the treatment process would release Al^{3+} ions and produced hazardous effect towards the environment and human being. One of the most common side effects of Al^{3+} emission is Alzheimer disease (Dermentzis et al., 2011).

Using Fe as electrode would lead to the presence of Fe^{3+} and Fe^{2+} ions. Fe^{2+} ions are commonly generated during Fe electrolysis, and these ions can easily be oxidised into Fe^{3+} in the presence of dissolved oxygen in the water. Fe^{3+} ions are fine, yellow $Fe(OH)_3$ particles with poor settleability and are ineffective in the removal of other metal ions

(Kobya et al., 2006). In addition, a large quantity of sludge after the treatment can occur due to high amount of iron ions in the treated water. In a few constructions, metal oxide coated titanium, which are inert electrodes, are used as cathodes. Inert cathode is suggested when wastewater has notable amounts of magnesium or calcium ions (Chen, 2008). Liu et al. (2013) obtained a high removal of Pb(II) with 97.2–99.6% after 90 min of treatment using a stainless steel net electrode coated with single-walled carbon nanotubes (Liu et al., 2013) . Shakir & Husein (2009) investigated the effects of several operating parameters on the removal of Pb(II) using stainless steel and aluminium as the cathode and anode, respectively. They achieved a removal efficiency of 100% after 120 min of treatment at a pH of 10 (Shakir & Husein, 2009). Mohamed & Al-Mureeb (2010) compared the performance of aluminium-aluminium (Al-Alwani et al.) and aluminium-stainless steel (Al-St) electrode pairs. The Al-Al electrode pair showed outstanding performance, with a Pb(II) removal efficiency of 99.08% (Mohammed & Al-Mureeb, 2010). In contrast, Mansoorian et al. (2014) demonstrated that the iron-iron (Fe-Fe) electrode pair has superior performance compared with the St-St and Al-Al electrode pairs (Mansoorian et al., 2014). Kara et al. (2013) reported a Pb(II) removal efficiency of 98% after 120 min of treatment using Fe-Fe electrode pair (Kara et al., 2013). Even though different electrodes materials give a different degree of removal efficiencies, it is important to choose a suitable electrode material to be used as anode and cathode in the electrocoagulation process. These important factors that should be considered are high removal efficiency, low cost of material and low sludge production.

2.10.2.2 Effect of electrodes distance

The distance between electrode plays an important role in the electrocoagulation process

where it not only significantly effects the removal efficiency, but also influences the solubility of the metal hydroxide precipitates due to the electrostatic field depends on the distance between the anode and cathode. The highest elimination of pollutant is obtained by keeping a short distance between the electrodes (Khandegar & Saroha, 2013). The removal efficiency of pollutant decreases with an increase in the inter-electrode distance. This is due to the fact that, further increase in the distance between the electrodes decreases the electrostatic effects resulting in a slower movement of the generated ions (Khaled et al., 2015). Increasing in the distance between electrode, will reduces the percentages of pollutant elimination efficiency. This is due to the movement time of the ions between electrodes become slow and decreases the ability of metal hydroxide ion production during the process. Consequently, energy consumption diminutions with reducing the distance between electrodes. As the inter-electrode distance become lower, additional electrochemically produced gas bubbles bring about turbulent hydrodynamics, thus leading to increase mass transfer rate as well as to increase reaction rate among the coagulant species and contaminants (Hakizimana et al., 2017).

2.10.2.3 Effect of pH

The pH of the solution plays an important role on the performance of electrocoagulation process. It influences the conductivity of the solution, dissolution of the electrodes, speciation of hydroxides and zeta potential of pollutants. Destabilisation of colloids produce by metal hydroxides ion. In slightly alkaline and neutral pH are suitable for formation of effective coagulant species. In highly alkaline pH, metal hydroxide ions are formed, and these ions have inefficient coagulation performance due to precipitation. Initial and final pH value will change in the electrocoagulation process, making it one of the important parameter need to be monitored. Thus, mechanistic investigations of

electrocoagulation process are difficult to estimate. At certain condition, acidic pH is suitable to be used for eliminating of pollutant, but it depends on type of pollutant need to be removed. For example, at acidic pH, the dissolution of metal ions was effective even without electricity connection. According to Naje et al. (2017), the dissolution rate reduces at high pH, which is comprehensible as the corrosion rate of metal ion declines in high alkaline pH in the presence of oxygen due to passive layer forms on the surface of electrode (Naje et al., 2017). Garcia-Segura et al. (2017) reported that pH mediums significantly differ the physiochemical possessions of coagulants, for instance: (i) the solubility of metal hydroxides, (ii) the electrical conductivity of metal hydroxides and (iii) the size of colloidal particles of coagulant complexes. Thus, neutral and alkaline pH are chosen as the suitable pH medium for coagulation and electrocoagulation and pH should monitor before and after treatment (Garcia-Segura et al., 2017).

2.11 Challenges of applying electrocoagulation process

Although electrocoagulation has numerous advantages, there are several challenges in applying electrocoagulation process, especially in large-scale applications. Firstly, the sacrificial electrode used needs to be replaced regularly due to oxidation. Then, the cost of electrode material in some countries may be expensive which may cause the application of electrocoagulation process to become unsuitable in those countries (Bayramoglu et al., 2004). In addition, the use of electricity is expensive in many places and some places might not have access to electricity. Moreover, the initial capital costs of electrocoagulation are higher compared to other technologies (Kobya et al., 2003). Therefore, a lot of effort should be made in order to progress from the electrocoagulation properties of electrodes to reactor scale-ups for applications. Some criteria that need to be considered are environmental viability, economical aspect and potential technology to

be applied. In the next section, new technology for the removal of lead ions are discussed whereby this technology uses renewable energy and is more economical and high effective.

2.12 Solar Photovoltaic electrocoagulation system

The increasing of energy cost in recent years together with operation cost of water treatment have led to a strong awareness to discover an alternative treatment strategy to replace a conventional technology. Electrocoagulation treatment process powered by solar photovoltaic energy represent an ecofriendly alternative for numerous types of water treatment around the world.

2.12.1 Brief history of solar photovoltaic

The photovoltaic process discovered in 1839 refers to conversion of a quantum of light, "photo", into electricity within a designed solar cell, "voltaic" (Grossiord et al., 2012). The first observation of PV effect on solid selenium was made by Adams and Day in 1877 (Adams & Day, 1877). Further development of solid-state PV devices paved the way for the fabrication of silicon solar cell with 6% energy conversion efficiency in 1954. This solar cell was used to convert solar energy into electricity in Vanguard 1 satellite in 1958 (Fraas, 2014). Since then, solar cells have been used in space technology to power satellites (El Chaar et al., 2011). The tremendous hike in oil price in the 1970s forced governments to relook at the initiatives to develop and promote renewable energy technologies. Much research has been done by the scientists around the world to enhance the efficiency of photovoltaic cells, and now the efficiency of these cells has increased up

to 40%. A brief history of solar photovoltaic cells is summarised in Table 2.6. It can be seen that PV technology has progressed tremendously over the years, becoming more sophisticated, more efficient and cost-effective due to advancements in materials science and research. Solar PV technology has great potential due to the fact that solar energy is free, available in abundance, and moreover, solar energy is powerful, noiseless and free of emissions. In brief, solar energy offers everything that fossil fuel energy cannot. Moreover, modern PV systems are very safe and highly reliable requiring a low maintenance cost and easy installation (Fraile et al., 2009; Ortiz et al., 2008).

Table 2.6: Brief history of solar photovoltaic

Scientists and innovation	Year
Alexandre-Edmond Becquerel discovers the photovoltaic effect	1839
Adams and Day observe the photovoltaic effect in solid selenium	1877
Charles Fritts develops a solar cell made from thin sheets of selenium and coated with gold which produce less than 1% efficiency	1883
Wilhelm Hallwachs develops a semiconductor-junction solar cell (copper and copper oxide)	1904
Wilson develops theory of high purity semiconductor	1931
Audobert and Stora discovers the photovoltaic effect in cadmium sulfide (CdSe)	1932
Chapin, Fuller and Pearson the scientists at Bell laboratory develops a silicon solar cell with 6% efficiency	1954
First use of solar cells on an orbiting satellite Vanguard 1	1958
Hoffman electronic develops a solar cell with 14% efficiency	1960

2.12.2 Photovoltaic system design

The basic PV system is comprised of a PV module, a charge controller or regulator, a battery, an inverter and alternating current (AC) load. Each component has a function and control method. In principle, a PV system is contingent upon the solar radiation incident on the PV module's surface which results in its transformation into direct current which is electrical energy. The electricity that is generated is passed to a regulator or charge controller before it is accumulated in a battery (Mook et al., 2014). The regulator or charge controller's function is to protect the battery from overcharge or excessive discharge. The battery provides power during low solar radiation periods, cloudy days or during night time. The direct current is converted into AC by and inverter for devices working in AC mode (Valero et al., 2008).

2.12.3 Types of solar photovoltaic system

Generally, solar PV systems can be divided into two fundamental types: stand-alone (off-grid) and grid-connected (grid-tied). Stand-alone PV systems are suitable for places that do not have power grid. At present, aforementioned solar PV systems are installed in rural areas or offshore islands where the main power system is too far away. A stand-alone PV system is normally operated at small power capacities and it does not produce very high current and voltage. The direct-coupled system is the simplest type of stand-alone PV system, whereby the DC load is being directly connected to DC output of a PV module or array. The load only operates during daytime, in the presence of sunlight considering the fact that there is no electrical energy storage (batteries) in direct-coupled systems. Hence, these systems are suitable for normal use like ventilation fans, small circulation pumps and water pumps in solar thermal water heating systems (Solanki, 2013). Batteries

are applied in order to have energy storage in numerous stand-alone PV systems. Such systems will be used when there is very few or no output that comes from the solar PV system, for example during the night time. The components of stand-alone PV system consist of the following items: 1) Solar PV module, 2) inverter, 3) charge controller, 4) battery, 5) AC load, 6) DC load and 7) cables. There are several parameters which need to be considered in designing stand-alone PV systems, namely, the orientation and tilt angles of the PV module, load requirements, sizing of the PV module, as well as temperature and solar radiation intensity at the place the PV system would be located (Ali & Salih, 2013; Pal et al., 2015).

Whereas, grid-connected system is connected to local grid and solar electricity generated is allocated via a local power supplier (Kaundinya et al., 2009; Mook et al., 2014). Grid-connected are normally found in urban areas where located near to the utility grid (Kaundinya et al., 2009). PV grid-connected systems are usually mounted on the solar PV power plants and rooftop of a residential or commercial building (Pillai et al., 2014). The solar PV power plants are free standing, which are normally placed on the ground as they have large generating capacity, reaching up to hundreds of megawatts. Some solar plants fix their PV panels into a static position, other PV plants are connected with agriculture whereas some other employ tracking systems that move the PV panels to track the sun's path on a daily basis in order to produce more electricity (Misolar, 2016; Tiwari & Dubey, 2010). The biggest PV power plants have been built in the California, USA. These PV stations generate electricity to power approximately 255,000 homes in the region (Jegede, 2016). The lists of world's largest solar PV power plants are given in Table 2.7.

Table 2.7: Lists of world's largest solar PV power plants

Country/State	Location	Power capacity	PV module types	Project duration/ commissioned
California	Kern and Los Angeles	579	Monocrystalline Silicon	(2013-2015) Solar Star Projects
California	Desert sunlight solar farm (Riverside County and Carrizo Plain)	550	Cadmium Telluride Solar	(2011-2015) First Solar
California	Topaz Solar Farm (San Luis Obispo)	550	Monocrystalline silicon	(2011-2014) First Solar
China	Longyangxia Dam Solar Park	320 (Phase I)530 (Phase II)	-	Phase I (March- December 2013). Phase II (2014-2015)
China	Golmund Solar Park (Qinghai Province)	60	-	(2009-2011)
India	Charanka Solar Park (Gujurat)	345	-	(2010-2012) Gujarat Power Corporation Limited (GPCL)
France	Cestas Solar Farm (Bordeaux)	300	-	(2014-2015) Eiffage, Schneider Electric and Krinner and went online
Nevada	Copper Mountain Solar Facility (Boulder)	552	-	(2010-2016) Sempra US Gas and Power

Grid-connected PV systems are easily found on the roofs of buildings or integrated into buildings because these systems require very little maintenance. In this case, the PV systems are also known as building-integrated photovoltaic (BIPV) systems. BIPV systems allow achieving the zero-emissions building target that addresses issues of energy resource depletion and environmental deterioration (Jelle & Breivik, 2012). BIPV are generally installed on facades, building windows and as flexible rolls on roofs. As a rule, BIPV systems have flexible orientation depending on particular conditions of the installation requirements (Makrides et al., 2010). It is predicted that the global market of BIPV and Building Applied Photovoltaic (BAPV) products will increase five-folds from 400 MW in 2012 to 2,250 MW in 2017 (Chan, 2013). Grid-connected PV systems function only when the supply source is available. The gird-connected PV systems' principal part is the inverter that gets the DC power generated by the PV module converted into AC power (Solanki, 2013). In a grid-connected PV system, the local grid functions like a battery with unrestricted storage capacity (Yanine & Sauma, 2013). The local grid accounts for seasonal load variations and therefore, the grid-connected PV system's overall efficiency is superior to that for stand-alone PV systems. Since the storage capacity of grid-connected PV systems is virtually limitless, the electricity generated can always be stored and any extraneous generated electricity need not be 'thrown away' (Kaundinya et al., 2009).

Cost of a solar PV system greatly depends on the type of system and panel installation location (ground or roof-mounted). Besides that, typical interval energy data and electricity tariff also influence the installation of solar PV system. Therefore, the total operating costs of a PV system are determined from the costs of PV panels, type of PV system installation and energy consumption. The PV installation power can be classified into four main PV systems: (1) Residential PV systems normally not exceeding 20 kW

(roof-mounted system), (2) Large-scale building PV systems on average not exceeding 1 MW (commercial buildings, hospitals, universities and schools), (3) Utility-scale PV systems usually exceed 1 MW capacity (ground-mounted/solar PV power plant) and (4) Off-grid or stand-alone applications varying in size (small to mid-size systems) (IRENA, 2012).

2.12.4 Operating principle of solar PV cells

The intensive research into the physicochemical and photonic properties of the most abundant on earth element on earth, silicon, allowed development of semiconductor material and PV cells manufacturing (Energy, 2012). Solar PV is made of a semiconductor material. Semiconductors could be categorised as: (1) extrinsic (impure semiconductor) and (2) intrinsic (pure semiconductor). In the intrinsic semiconductor, an electron-hole pair is created at room temperature, but it has low electrical conductivity. The flow of current is a mixture of electron and hole pairs. Hence, a little quantity of impurity is added in order to improve the intrinsic semiconductor's conductivity, which then becomes an extrinsic semiconductor. Doping is the process of adding impurities to intrinsic semiconductor. There are two categories of impurities that can be added; which are (1) trivalent and (2) pentavalent. Doping a trivalent element results in formation of the extrinsic semiconductor with excess of holes that, accept electrons in the semiconductor becomes a p-type extrinsic semiconductor. Hence, trivalent impurities are also known as acceptor impurities (Figure 2.4). Doping a pentavalent element leads to the formation of the extrinsic semiconductors with excess of electrons forming an n-type extrinsic semiconductor. The pentavalent impurities are also recognised as donor impurities (Figure 2.5) (Kumar et al., 2015).

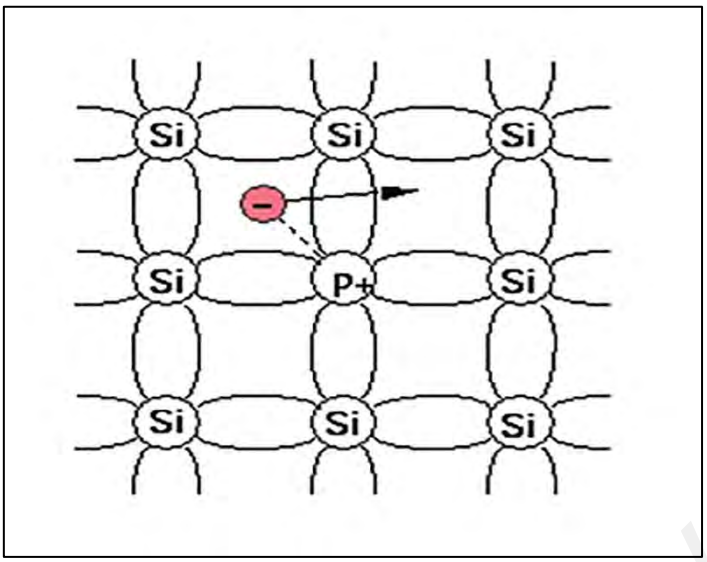

Figure 2.4: Formation of p-type semiconductor
(Reproduced from Kumar et al., (2015), Copyright 2017, with permission from Springer)

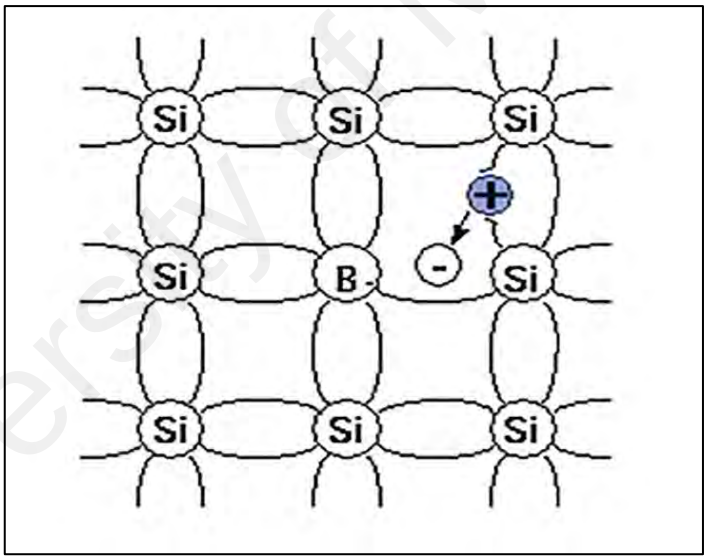

Figure 2.5: Formation of n-type semiconductor
(Reproduced from Kumar et al., (2015), Copyright 2017, with permission from Springer)

The main working principles of a PV solar cell can be summarised as follow: p-type and n-type refer to the holes and electrons, respectively, in a semiconductor material. In order to form a p-n junction in a single solar PV cell, p-type and n-type semiconductors are sandwiched together (Figure 2.6). When the PV cell is exposed to sunlight, photons are

absorbed promoting electrons to the conduction band. The electrons and holes move toward negative and positive terminal, respectively, in order to generate an electrical current. The electrons flow only from p to n layer, representing a short circuit; whereas in the reverse direction, the current does not flow and it represents an open circuit (Kreith & Goswami, 2007; Kumar et al., 2015).

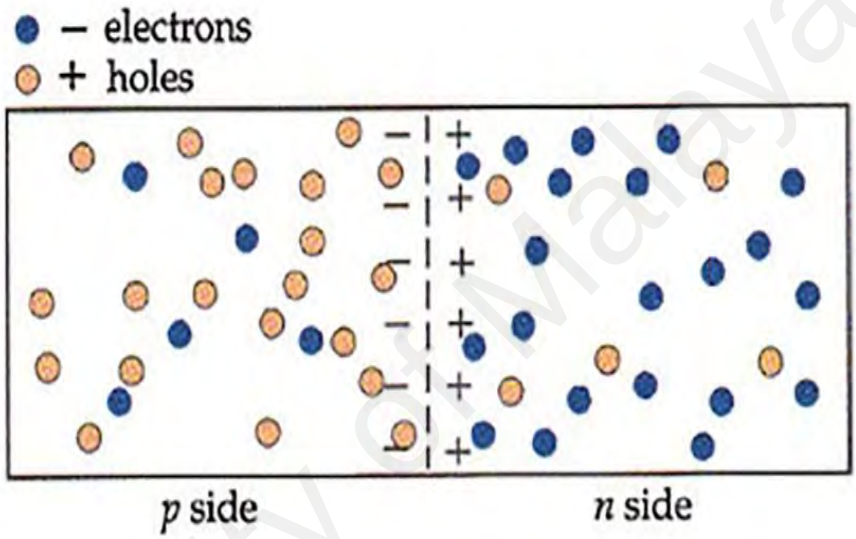

Figure 2.6: Structure of p-n junction
(Reproduced from Kumar et al., (2015), Copyright 2017, with permission from Springer)

2.12.5 PV cell materials

Silicon is the most preferred semiconductor material used for fabrication of PV cells; its purity and physical state are significant factors affecting solar cell functionality and efficiency. One particular grade of silicone is high-grade crystalline silicon which is presently the dominant material to produce high efficiency solar cells (Mah, 1998). Numerous types of PV cells have been developed worldwide, with more than 350 companies involved in the production of PV cells. Table 2.8 shows a list of top ten

manufacturers of PV cells (Mints, 2016). The majority of companies are located in China. However, the list also includes companies producing PV systems using crystalline silicon materials and cadmium telluride (CdTe) materials; whereby the latter corresponds to thin film PV technology (Mints, 2016). Only a few companies produce third generation PV systems based on dye-sensitised, organic polymer and quantum dot materials. The aforementioned PV technologies are discussed in the following section.

Table 2.8: Lists of companies producing materials for solar cells fabrication

PV Cell Manufacturer	PV Cell Materials	Country
Trina Solar	Crystalline silicon	China/Netherlands
JA Solar	Crystalline silicon	China/Malaysia
Hanwha Q-cells	Crystalline silicon	China/Germany/Malaysia/South Korea
Canadian Solar	Crystalline silicon	China
First Solar	Crystalline silicon/Cadmium Telluride	United States/Malaysia
Jinko Solar	Crystalline silicon	China/Malaysia
Yingli Solar	Crystalline silicon	China
Motech Solar	Crystalline silicon	Taiwan/China
NeoSolar	Crystalline silicon	Taiwan/China
Sungfeng-Suntech	Crystalline silicon	China/United States

Commercial solar cells may be categorised into two main types: crystalline silicon (c-Si) and thin-film, based on the technology used to produce them. Their properties differ in terms of light absorption efficiency, manufacturing technology, energy conversion efficiency and production cost. The c-Si category, called first-generation PV cell, consists of single crystalline (sc-Si) or monocrystalline and multicrystalline (mc-Si) or poly-crystalline silicon cells, which roughly represents 85-90% of the entire world market at present (Simbolotti & Taylor, 2013). The thin-film type of PV cells, called second-generation PV cells, may be classified into three categories: amorphous silicon, copper

indium selenide (CIS)/copper indium gallium diselenide (CIGS) and cadmium telluride (CdTe)/cadmium sulfide (CdS). Multi-junction PV cells is another second- generation PV cell technology which utilises multiple layers of semiconductor materials (elements from chemical element periodic table group III and V) to absorb a wider solar spectrum that is not possible for single-junction cells. By combining sophisticated sun-tracking systems and light-concentrating optics, these cells have demonstrated superior conversion efficiencies, above 40% as compared to any other PV technologies so far. Ongoing research and development in this field has led to the emergence of third-generation PV technology which comprise dye-sensitised, organic PV and quantum dot PV cells. These cells only have average conversion efficiency, but they have strong potential for commercialisation in future because of the significant reduction in material and manufacturing costs (Ardani & Margolis, 2010).

Figure 2.7 shows a progressive increase in PV cells conversion efficiencies between 1975 and 2015. The highest PV cell efficiency of 46.0% was obtained in 2015 for a multi-junction concentrator. Energy conversion efficiencies for crystalline silicon cells range from 21.2% to 27.6%; for thin film PV cells they are in 13.6% - 23.3% range; and it is around 10.6-12.6% for emerging PV technologies (Kurtz & Wilson, 2016). The following sections of the review provide descriptions on past research and recent developments pertaining to materials and solar cells configurations of different generations of PV cells.

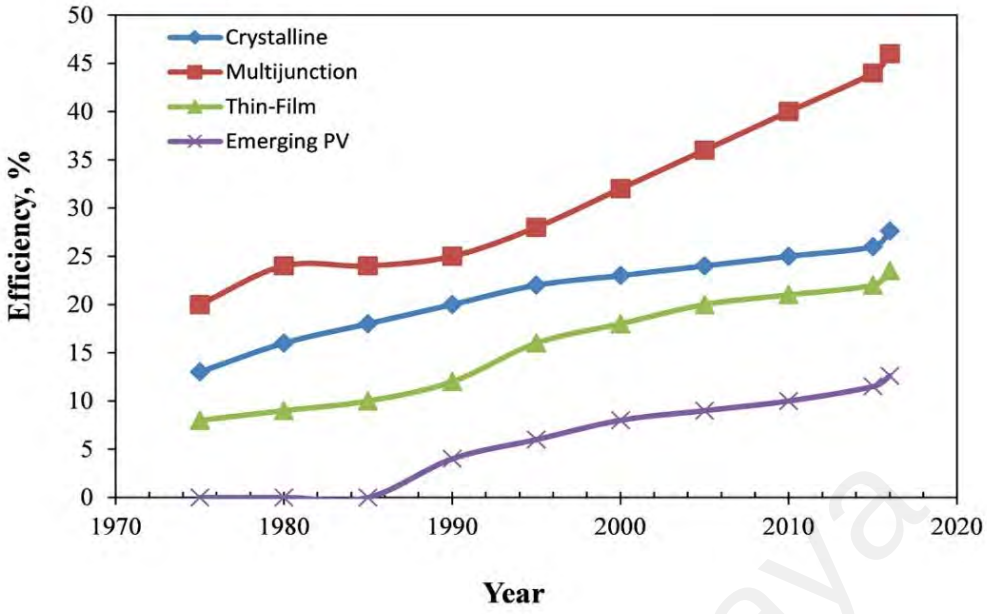

Figure 2.7: PV cell efficiencies from 1975 to 2015
(redrawn from the data of (Kurtz & Wilson, 2016)

2.12.6 Applications of PV technology

The rapid growth of the solar PV industry over the past years is also associated with the expanded range of PV systems applications in the municipal and industrial sectors. The use of solar PV systems for various applications shows positive effect on socio-economic and environmental sustainability. Table 2.9 summarises the societal and economic benefits of solar PV systems.

Table 2.9: Summary benefit of solar PV system to society and economic

Benefits	Remarks
Employment opportunity	-Reduce unemployment in rural area (e.g: solar PV technician) - Increase income for household -Enhance work productivity because can extend working hour with better lighting - Enhance production capacity for small industry
Improvement of quality of life of rural people	- Increase the family quality time among rural household because receive better lighting facility for entertainment. - Enhance the facility for education in the school such as lighting, computer and internet. - Increase the hospital accessibility for health treatment.
Creation of facilities for social activities:	-Increase the social activity among family -Rural people able to do night activity with friend like education program
Reduction in distribution and transmission cost of electricity	- PV system is more effective and viable option for rural electrification compared to grid expansion to those areas as there is no distribution and transmission lines losses
Improvement of environmental sustainability	- Reduces greenhouse gas emissions and make a significant contribution to climate protection

2.12.7 PV technology for water and wastewater treatment

Clean water and pollution-free energy remain as the very important issues in the agenda of the international environmental and economic development. Renewable energy used to treat water and wastewater is the most desirable direction for the green technologies applications capable of mitigating environmental impact. Conventional wastewater treatment processes to remove particles include coagulation, sedimentation, flotation and filtration. Biological treatment includes advanced oxidation, adsorption and membrane

processes to eliminate organic compounds (Chen, 2008). However, the main disadvantage of conventional wastewater treatment processes is the production of large volumes of sludge (which often contains toxic compounds), leading to waste handling and disposal issues. In contrast, advanced electrochemical methods such as electro-coagulation, electroflotation, electrooxidation, electrodisinfection and electroreduction processes offer higher treatment efficiency, complete destruction of pollutants and zero emissions (Chen, 2008; Mook et al., 2014). However, installation of a conventional water and wastewater treatment system in rural areas is economically unfeasible due to the high capital and operational costs required. In contrast, PV systems have flexibility to be designed for various applications, sizes and capacity and are much suitable for installations in rural areas. One good example is water desalination via reverse osmosis process, powered by PV system, to provide drinking water in small communities. Photovoltaic reverse osmosis (PVRO) system has minimal environmental impact; it is simple in design, assembly, maintenance and repair. The main feature of the system is the PV energy source that energises a feed pump and a high-pressure pump to pressurise the incoming water through the reverse osmosis membrane array leaving brine on one side and purified water on the other side of membrane (Bilton et al., 2011).

Kershman et al., (2003) evaluated the performance of a seawater reverse osmosis (SWRO) plant in Libya. The plant was operated using renewable energy sources (RES) including wind energy conversion (WEC) and PV power generation units. The RES was integrated into a grid-connected power supply for the plant (Kershman et al., 2003). Hasnain & Alajlan (1998) evaluated performance of a simple single-effect solar stills plant (Sadous reverse osmosis plant) of 5.8 m^3 water per day capacity to treat sea water. The single effect solar stills provided all the required for desalination process energy. The results showed that the single-effect solar stills are feasible for a desalination plant in

isolated areas where the land value can be neglected due to the ease of installation and maintenance of solar stills, especially if they are fabricated locally using available materials (Hasnain & Alajlan, 1998). The sustainability of electrochemical oxidation of wastewater can be enhanced through the utilisation of PV cell energy. This is indeed an area of active research activities in with the aim of reducing reduce the economic cost of solar power (Dermentzis et al., 2015; Marmanis et al., 2015; Palahouane et al., 2015; Valero et al., 2010; Zhang et al., 2014; Zhi et al., 2010). Connecting the PV modules directly to the electrochemical unit for wastewater treatment radically reduces the dependency of the unit on non-renewable energy sources. The photovoltaic solar electrooxidation (PSEO) process is particularly an attractive solution for wastewater treatment in isolated communities where standard treatment solutions are hard to apply.

Dominguez-Ramos et al. (2010) investigated the capability of a PSEO process to remove organic matter from lignosulphonate wastewater. Four monocrystalline silicon PV modules were connected to provide a total peak power of 640 W. The PV modules were installed on the roof tilted at 38° and oriented 20° west of south. The results showed that there is a reduction of 90% in the total organic carbon of the treated wastewater (Dominguez-Ramos et al., 2010). Similarly, Alvarez-Guerra et al. (2011) designed a PSEO system for water and wastewater treatment in remote areas where it is impossible to install conventional treatment systems. They used electrochemical oxidation in which boron-doped carbon was used as the anode and evaluated the characteristics of the effluent, wastewater flow rate, required yield and solar irradiance. They discovered that the feasibility of the PSEO process is dependent upon the geographical location. The effectiveness of wastewater treatment by PV technology is higher in sunny locations but the demand for PV technology is higher in locations with lower solar irradiance (Alvarez-Guerra et al., 2011). Valero et al. (2010) studied PV electro-oxidation system for dye-

containing wastewater treatment, where 40 PV polycrystalline silicon modules with a 38.48W peak power were used to achieve more than 95% of the wastewater decolourization (Valero et al., 2010). Sharma et al. (2011) investigated the feasibility of an electro-coagulation (EC) system powered by a PV module for water and wastewater treatment. The highest turbidity (91%) and reduction of organic content (95%) were achieved by the EC system powered by solar PV system, respectively. This indicates the great potential of solar PV electrocoagulation systems as alternatives for small-scale decentralised water and wastewater purification systems (Sharma et al., 2011). ZhangZhang et al. (2013) investigated removal of phosphate from landscape water using an electrocoagulation process with aluminium electrodes powered directly by PV module. Higher removal of total phosphate was achieved in sunny days; however, in overcast days, higher removal efficiency was achieved by extending treatment duration. The energy consumption for removing total phosphate was estimated to be 0.71kWh/m^3 (ZhangZhang et al., 2013). Palahouane et al. (2015) studied removal of fluoride ions in PV powered electrocoagulation process and achieved high removal efficiency at low energy consumption of 0.32kWh/m^3 (Palahouane et al., 2015). García-García et al. (2015) evaluated reduction in the chemical oxygen demand (COD), total organic carbon (TOC), colour, and turbidity through electrocoagulation (EC) and electrooxidation (EO) processes powered by PV modules. The reduction of TOC of up to 70.26% and 100% of COD was achieved in the combined EC + EO processes (García-García et al., 2015). Valero et al. (2014) investigated the removal of a real industrial wastewater using electrochemical oxidations powered by solar photovoltaic. They studied the removal of COD for three different anode materials (Ti/Pt, Ti/RuO_2 and Ti/IrO_2). They found that the optimum conditions for removal of COD are as follows: (1) anode material: Ti/RuO_2, (2) pH: 9, and (3) current density: 50 mA/cm^2. The removal of COD was 75% at these optimum conditions. They also attained high removal of COD (80%) when the solar PV

electro-oxidation system was applied at the pre-industrial scale (Valero et al., 2014). Table 2.10 presents summary of PV technology for water and wastewater treatment.

Table 2.10: A summary of PV technology for water and wastewater treatment

Country/State	Location	Power capacity	PV module types	Project duration/ commissioned
California	Kern and Los Angeles	579	Monocrystalline Silicon	(2013-2015) Solar Star Projects
California	Desert sunlight solar farm (Riverside County and Carrizo Plain)	550	Cadmium Telluride Solar	(2011-2015) First Solar
California	Topaz Solar Farm (San Luis Obispo)	550	Monocrystalline silicon	(2011-2014) First Solar
China	Longyangxia Dam Solar Park	320 (Phase I) 530 (Phase II)	-	Phase I (March- December 2013). Phase II (2014-2015)
China	Golmund Solar Park (Qinghai Province)	60	-	(2009-2011)
India	Charanka Solar Park (Gujurat)	345	-	(2010-2012) Gujarat Power Corporation Limited (GPCL)
France	Cestas Solar Farm (Bordeaux)	300	-	(2014-2015) Eiffage, Schneider Electric and Krinner and went online
Nevada	Copper Mountain Solar Facility (Boulder)	552	-	(2010-2016) Sempra US Gas and Power

2.13 Adsorption

Adsorption process is known to be effective economical for heavy metal wastewater treatment and is a promising method for a long-term treatment. The adsorption process is more flexible in terms of design and operation whereby it mostly produces high-quality treated effluent (Ariffin et al., 2017). In addition, due to occasional reversible properties, adsorbents used can be regenerated using proper desorption process. The adsorption process is suggested to remove metal ions in wastewater due to low concentrations of metal ions found in wastewater. The physical and chemical characteristics of the adsorbents and adsorbate, the concentration of adsorbate in liquid, temperature, contact time and pH are the parameters that should be considered in this treatment (Abbaszadeh et al., 2016) .

The adsorption is attractive technique because of its simplicity, low cost, effectiveness, and flexibility in design and operation. Moreover, this technique does not produce undesirable by-products (Lee & Hamid, 2015). Selection of appropriate adsorbent materials is the most important factor in an adsorption process. The adsorbent most commonly used to remove heavy metals is activated carbon because of its high surface area, well-developed porosity and special surface chemical properties that have been proven to be effective (Hameed et al., 2009). The world demand for activated carbon has increased rapidly over the years. The global market for activated carbon has reached US$ 2.1 billion in 2014 and the market demand is expected to increase to US$10.15 billion by 2024 (Ceskaa, 2015; Cestari et al., 2005). Even though activated carbon is attractive due to its broad range of industrial applications, sometimes its application is limited due to its high cost. Therefore, a lot of research is needed to explore and produce green adsorbent which low cost, availability, high effectiveness and can be reused and regenerated. There

is a great interest in exploring adsorbents from agricultural waste materials such as coconut shells and palm tree (Gueu et al., 2006), apricot seeds (Kobya et al., 2005), pomegranate peels (El-Ashtoukhy et al., 2008), hazelnut and almond shell (Bulut & Tez, 2007), tamarind wood (Acharya et al., 2009), palm shell (Mook et al., 2013), cashew nutshells (Subramaniam & Kumar Ponnusamy, 2015), and papaya peel (Brudey et al., 2016) and these types of activated carbon have been successfully used for heavy metals removal. Numerous studies have been recently published on the removal of Pb(II) ions using adsorbent materials. The type of adsorbents used are different during the years. Several studies have been emphasis on the agricultural byproducts of lignocelluloses materials as adsorbent due to its low cost and availability. The study investigated the performance of adsorbent on the kinetics and adsorption equilibrium data (Langmuir and Freundlich isotherms). Comparison of recent studies on Pb(II) removal with different type of adsorbent materials are presented in Table 2.11.

Table 2.11: Comparison of recent studies on Pb(II) removal with different type of adsorbent materials

Adsorbent	Surface area (m^2/g)	Adsorption equilibrium	References
Palm shell waste	772.1	Freudliuch	(Choong et al., 2018)
Palm oil mill waste	59.1989	Langmuir	(Adebisi et al., 2017)
Almond shell	1133.25	Langmuir	(Thitame & Shukla, 2017)
Punica granatum L. peels	-	Langmuir	(Ay et al., 2017)
Peanut shell	570	Freudliuch	(Xu et al., 2017)
Commercial AC	4273	Langmuir	(Asuquo et al., 2017)
Typha angustifolia and Salix matsudana	234.42	Langmuir	(Tang et al., 2017)
Palm oil leaves	122	Langmuir	(El-Sayed & Nada, 2017)
Cucumber peel	-	Langmuir	(Basu et al., 2017)
Sugarcane bagasse		Langmuir	(Salihi et al., 2017)

The presence of an "adsorbent" solid binding molecules using ion exchange, physical attractive forces and chemical binding imply the adsorption process. The adsorbents should be best obtainable in large amount, at a lower cost and should be regenerable easily. There are various adsorbents used for adsorption of lead ions. Selection of appropriate adsorbent materials is the most crucial aspect in an adsorption process. For adsorption process, three key operating parameters that should be considered for selecting adsorbent are large surface area, pore volume and surface functional groups (Abbaszadeh et al., 2016). Many different porous natures of materials are being developed such as activated carbon, zeolites, mesoporous oxides, pillared clays, carbon nanotubes, polymers, metal organic, graphene oxide and graphene nanosheets. Among them, the adsorbent that is most commonly used to remove heavy metals is carbonaceous-based adsorbents such as activated carbon as it has high surface area, well-developed porosity and special surface chemical properties that have been proven to be effective (Gautam & Chattopadhyaya, 2016). Commercial activated carbon is the adsorbent that being extensively used in many adsorption processes especially for heavy metal removal. Hence, converting agricultural wastes into activated carbon is a reasonable proposition since this helps tackle environmental and waste disposal problems, improves economic value and provides a potential alternative for commercial activated carbon.

2.13.1 Operating parameters

Various factors, such as oxygenous functional groups and thickness of adsorbent, species of heavy metal ions in solution and experimental conditions, affect the adsorption of heavy metal ions on the surface of adsorbent. It had been confirmed that the oxygenous functional groups on the adsorbent surface played a significant characteristic in the maximum adsorption capacity of heavy metal ion due to the decrease in oxygenous

functional groups. In addition, activated carbon adsorbent was more effective to adsorb lead ion than conventional adsorbent as more oxygenous functional groups exist on the surface. Furthermore, the experimental conditions, for instance initial solution pH, adsorbent dose, contact time and temperature also notably influence the adsorption (Abbaszadeh et al., 2016).

Although many researches were made on the adsorption of heavy metal ions, there is still diminutive information on a complete research on the optimum and effective parameters for obtaining the highest adsorption capacity. Two methods are commonly used for designing experiments to obtain the optimum operating conditions such as one-factor-at-a-time (OFAT) and design of experiments (DOE). The OFAT method requires more runs for the same precision in effect estimation and is suitable for screening test. Meanwhile, the design of experiment especially response surface methodology (RSM) is a method that is effective and to be used for modelling and process optimisation. Designing and planning an experiment are involved in the technique. The data obtained is later analysed and interpreted. The purpose of employing this approach in this technique is to reduce the number of experiments, enhance statistical interpretation and determine the optimum parameters. However, a screening test must be conducted before study on the DOE technique in order to obtain a successful optimum condition. There are many factors affecting the adsorption capacity which include type of adsorbent used, pH, adsorbent dosage, initial concentration, effect of time and temperature. In this section the most effective parameters on the adsorption of lead ions are determined.

2.13.1.1 Effect of pH

The surface charge, the adsorbate species and the degree of ionization are influenced by the solution's pH. As the pH of solution increases, the amount of metal adsorbed also increases until a specific point. After that, any increase in pH will reduce the amount of metal adsorbed. Moyo et al. (2013) reported that as the solution's pH increases, the adsorption efficiency increase progressively, and optimum pH was obtained at pH 5.4 (Moyo et al., 2013). Cataldo et al. (2016) have developed a new adsorbent material for the removal of Pb(II) ion from aqueous solution. The results indicated that high adsorption capacity of 15.7mg/g and 10.5mg/g was achieved at pH 5 (Cataldo et al., 2016).

2.13.1.2 Effect of adsorbent dosage

The capacity to uptake heavy metals by adsorbents is influenced by dose of adsorbent used. Normally, increasing the adsorbents' dosage will result in increasing amount of metals adsorbed until it reaches a specific point. After this point, further increasing the dosage will render the adsorption capacity constant. Gaya et al. (2015) examined the effect of operating parameters on the removal of cadmium and lead by adsorption on doum palm shell. The results reveal that when the adsorbent dose increased, the removal efficiency also increased. This could be due to the increasing of adsorption sites (Gaya et al., 2015).

2.13.1.3 Effect of initial concentration

The initial concentration of heavy metals makes the adsorption dosage gain a strong effect. The initial concentration affects the overcoming of all resistance of mass transfer between aqueous and solid phases, whereby initial concentration plays a role as an important driving force. The efficiency of heavy metal removal is depending on concentration and a decreasing trend occurs if the initial concentration is further increased. As reported by Farghali et al. (2013) stated that the removal efficiency decreases with the increasing of initial Pb(II) concentration. This could be due to the increase in the driving force from the concentration gradient (Farghali et al., 2013).

2.13.1.4 Effect of contact time

The adsorption capacity of adsorbate into adsorbent is the result of interaction of functional group between the surface of adsorbent and solution. In order for the process to undergo completion, the interaction should be maintained at equilibrium for a particular period of time. Abbaszadeh et al. (2016) observed that the adsorption capacity and removal efficiency increase from 19.54mg/g to 37.2mg/g and 48.8% to 93.2%, respectively, with increasing treatment time from 10 to 120 min. They stated that the removal efficiency enhanced quickly at the initial reaction time due to additional unsaturated surface and active sites are present on the adsorbent surface area (Abbaszadeh et al., 2016) . This result is further supported by a research from Moyo et al. (2013) stated that a high adsorption capacity was achieved at short treatment time (60 min) (Moyo et al., 2013). In contrast, Farghali et al. (2013) reported that the maximum adsorption was obtained after 4 h treatment time (Farghali et al., 2013).

2.13.1.5 Effect of temperature

The adsorption equilibrium that is influenced by the temperature used determines the nature of the processes, which can either be either exothermic or endothermic. As the temperature increases, the adsorbates' uptake capacity increases. This occurs due to the pores enlargement and the sorbent surface's activation (Ariffin et al., 2017).

The sorption isotherms are employed in explanation in order to illustrate the mechanism of how adsorbate ions interact on adsorbent's surface although there is no particular mechanism in the adsorption process (Ariffin et al., 2017). Table 2.12 illustrate the adsorption model that are commonly employed to ascertain the reaction between adsorbent and adsorbate.

Table 2.12: Adsorption models of the batch system
(Szlachta & Chubar, 2013)

Types of mechanism	Equations	Nomenclature
Adsorption isotherms -Freundlich -Langmuir	$q_e = KC_e^n$ $q_e = \frac{q_m \cdot bC_e}{1+bC_e}$	Where *qe* and *qm* are the equilibrium and maximum monolayer adsorption capacities (mg/g), respectively, *Ce* is the equilibrium concentration of adsorbate in the solution (mg/L), *b* is the Langmuir adsorption equilibrium constant related to the binding energy (L/mg), *K* is the Freundlich constant related to the adsorption capacity ((mg/g) or (L/mg)) and *n* is the adsorption intensity parameter.
Adsorption kinetics -pseudo-first order -pseudo-second order -Elovich model -Intra-particle diffusion model	$q = q_e\left(1-e^{-k_1^t}\right)$ $q = \frac{k_2 q_e^2 t}{1+k_2 q_e t}$ $q = \frac{1}{b}\ln(ab) + \frac{1}{b}\ln(t)$ $q = k_{ind}t^{0.5} + I$	Where q and *qe* are the amounts of Pb(II) adsorbed at time t and during equilibrium (mg/g), respectively, *t* is the contact time (min), k_1 is the rate constant of pseudo-first-order adsorption (1/min), k_2 is the rate constant of pseudo-second-order adsorption (g/mg min), *b* is the desorption constant (g/mg), *a* is the initial adsorption rate (mg/g min), kind is the intra-particle diffusion rate constant (mg/(g min0.5)), and *I* is the constant for the boundary layer thickness (mg/g).
Activation energy	$\ln k_2 = \ln A - \left(\frac{E_a}{RT}\right)$	Where *A* is the temperature independent factor (g/mg min), E_a is the activation energy (kJ/mol), *R* is the gas constant (8.314 J/mol.K) and *T* is the temperature (K).

2.14 Combinations of electrocoagulation with other treatment technologies

Although a lot have been achieved in the field of electrocoagulation and adsorption, more research should be carried out to ensure efficient treatment of wastewater. Combining two or more methods of treatment could produce high removal of lead, which is also more economical viable. Numerous studies have been investigated on the combination of electrocoagulation (EC) with other methods like membrane filtration, electro-flotation (EF), electrooxidation (EO), chemical coagulation (CC) and sedimentation (Khandegar & Saroha, 2013; Sahu et al., 2014b). A greater removal efficiency is obtained when numerous methods to treat effluents are combined as compared to using single treatment method. An effective and safe way to remove pollutants is electrocoagulation that is used in combination with other method of treatment. A few studies that combine the electrocoagulation with other treatment techniques were reported in literature and these findings are summed in Table 2.11. Nevertheless, no prior studies to combine electrocoagulation with adsorption process were made, especially for the treatment of Pb(II) from aqueous solution or wastewater to reduce the sludge toxicity. Therefore, many studies should be carried out to investigate the possibility of combining electrocoagulation with other methods in order to formulate a cost effective and environmentally friendly solution with high removal efficiency.

Table 2.13: Electrocoagulation process combined with other methods

Combination process	Effluent	Results	References
EC +Gas sparging	Aqueous solution	Cr (more than 90%)	(Daous & El-Shazly, 2012)
EC + Adsorption	Aqueous solution	Indigo carmine dye (90.5%)	(Secula et al., 2012)
EC + EF	Aqueous solution	NH_3 (98%), PO_4^3 (98%), COD (72%)	(Mahvi et al., 2011)
EC + EO	Aqueous solution	As (95%), F^- (90%)	(Zhao et al., 2011)
EC + Adsorption	Aqueous solution	Cr (VI) (92%)	(Narayanan & M., 2009)
EC + EF	Laundry	COD (62%)	(Wang et al., 2009)
EC + EF	Industrial	F^- (86%)	(Shen et al., 2003)
EC + Air injection	Wastewater	Cr (95%), As (90%)	(Parga et al., 2005)
EC + Adsorption	Textile wastewater	Dye (90%)	(Castañeda-Díaz et al., 2017)
EC + CC +Adsorption	Textile wastewater	Dye (44.5%)	(Bazrafshan et al., 2016)
EC + EO	Wastewater	COD (60%)	(Chakchouk et al., 2017)
EC + EF	Aqueous solution	COD (67%)	(Jiang et al., 2002)

2.15 Summary

In this chapter, electrocoagulation and adsorption processes for the removal of lead ions have been presented. Nevertheless, although there are many publications in literature on both processes, there is still a lack of information on a complete study with regards to the relationship between economic point of view and environmental aspect. Besides, there are other important criteria that needed to be considered such as types of heavy metal compounds in the wastewater, types of combination process and suitable operating parameters. Electrocoagulation and adsorption processes for the heavy metal removal have attracted a lot of attention in the recent years. Findings from literature have proven that both processes can remove and recovering heavy metal ions from waste and wastewater. In addition, numerous case studies have demonstrated economic feasibility

and environmental sustainability of PV system installations in rural areas. Although presently the initial cost of PV system is high, continuous research in materials and energy efficiency would help to achieve its substantial reduction. Many developing countries have implemented PV energy projects in the past decade. However, a stronger solidarity between government agencies, NGOs, research community and industry is required to secure complete transition from fossil fuels to renewable solar energy within the next decades. Although this field has seen a lot of accomplishment, a lot of research should be made (i) to conduct in-depth study on more environmentally friendly new techniques for electrocoagulation (ii) to investigate an effective method to remove lead ions using combination of both processes which further enhances the removal performance of lead ion.

CHAPTER 3: MATERIALS AND METHODS

3.1 Workflow of research methodology

This chapter describes the experimental method, design of experiment and characterisation of the electrocoagulation process, adsorption process and integrated system. The first investigation of this research is to compare the performance of electrode materials. Performance of four different electrode materials, namely Al, Cu, Fe, and Zn electrodes were compared using the electrocoagulation process. In addition, other parameters such as sludge volume index (SVI), anode geometry, current distribution, energy consumption and particle size were also investigated. The produced sludge was characterised, and the particle size of sludge were measured. The electrodes surface was also characterised. The second work was aimed to study the effects of parameters on solar PV electrocoagulation process. After several scientific results were obtained, the study then continued to determine the best parameter that can influence electrocoagulation process. In this regard, the effects of electrode distance, stirring rate, pH, current density and initial Pb(II) concentration on Pb(II) removal using solar PV electrocoagulation system were investigated. Furthermore, the next study examines another method that has capability to remove Pb(II) from aqueous solution which is adsorption using palm shell activated carbon as adsorbent. The effects of initial Pb(II) concentration, treatment time, pH, adsorbent dosage and temperature were investigated, along with kinetic, isotherm and sludge product characterisation. Finally, integrated system was developed using combination of two techniques to enhance the removal efficiency. The optimum parameter obtained from solar PV electrocoagulation and adsorption process was used as benchmark in the integration system to obtain more detailed information about the integration process parameters. Figure 3.1 shows graphical presentation of overall work (methodology).

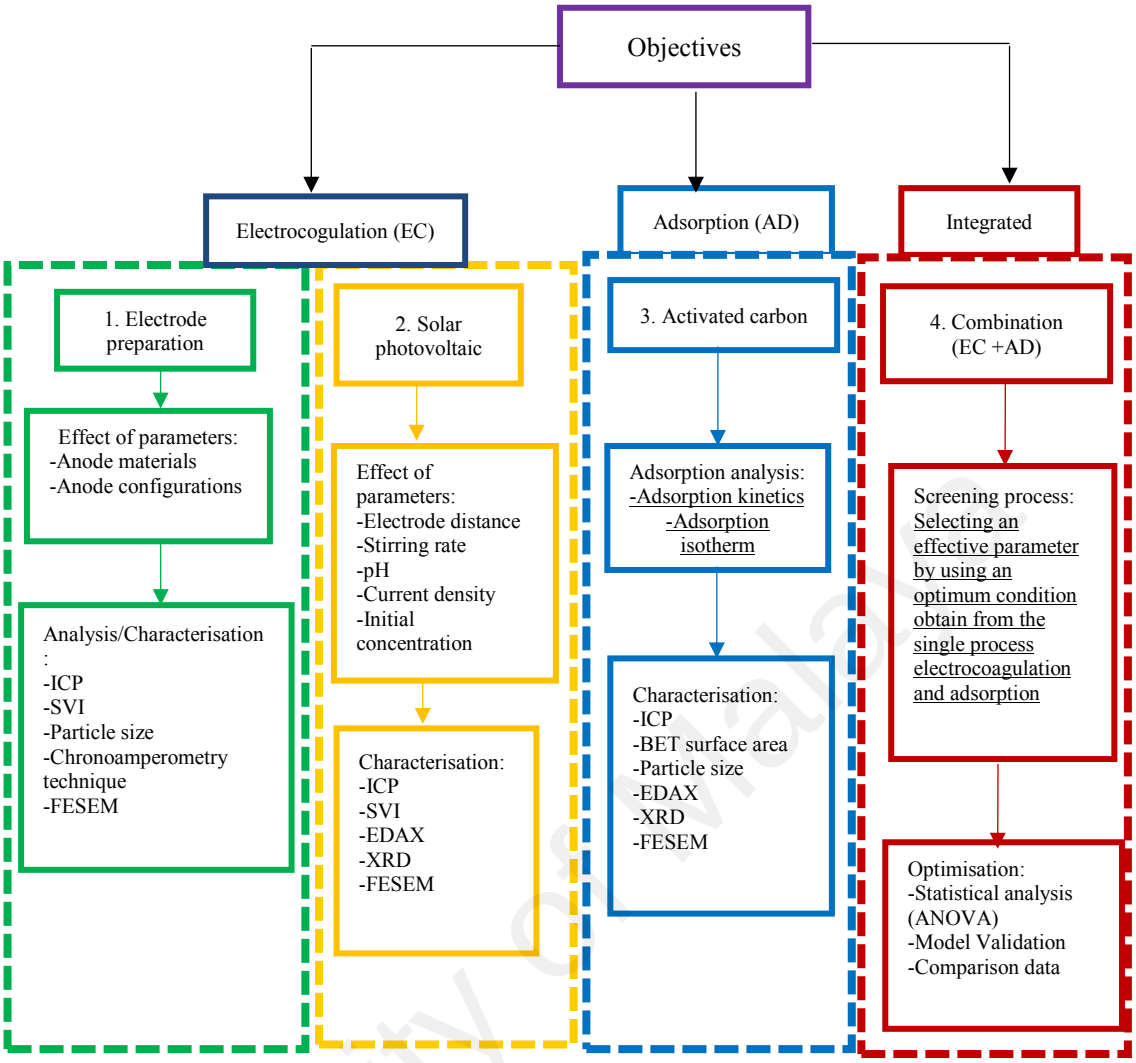

Figure 3.1: Detailed workflow of the thesis

3.2 Chemicals

Lead nitrate $Pb(NO_3)_2$ (Sigma-Aldrich), sodium hydroxide (NaOH, Merck), sulphuric acid (H_2SO_4, Merck), hydrochloric acid (HCl, Merck), and sodium chloride (NaCl, Merck) of analytical grade were used to prepare aqueous solutions for the experiments. The pH of the solutions was adjusted by adding 0.01 M H_2SO_4 or 0.01 M NaOH. H_2SO_4 was preferably used for pH adjustment because it is fast acting, highly effective, and low cost.

3.3 Electrocoagulation process set-up

The experiments were conducted using a 1000 mL borosilicate glass beaker placed on a magnetic stirrer. The electrochemical system was set up with a bipolar configuration. The bipolar configuration connected only the first perforated electrode to the anode and the last perforated electrode to the cathode. The plane sacrificial electrodes were then placed between the two parallel electrodes without any electrical connection. Figure 3.2 shows the schematic of the electrochemical system set-up. The perforated Zn, Cu, Fe and Al electrodes (dimensions: 7 cm × 10 cm) with hole diameters ranging from 0.2 cm to 0.5 cm, were used as the anode and cathode pairs for electrocoagulation treatment (Figure 3.3). An inter-electrode distance was studied in the range from 1.0 cm to 4.0 cm in all electrocoagulation experiments. The electrode surface was polished with fine sandpaper, rinsed with diluted hydrochloric acid (HCl) and washed with distilled water. The electrodes were then connected to a digital DC stabilised power supply (GPR16H50D) with bipolar configuration at 0–10 A level (current) and 0–40 V level (voltage). The stirring rate of the solution was investigated by varying the stirring rate from 0 rpm to 350 rpm for the electrocoagulation treatment. The supporting electrolyte was 0.01 M NaCl. All samples were filtered (0.45 μm pore size) to separate generated sludge for further analysis.

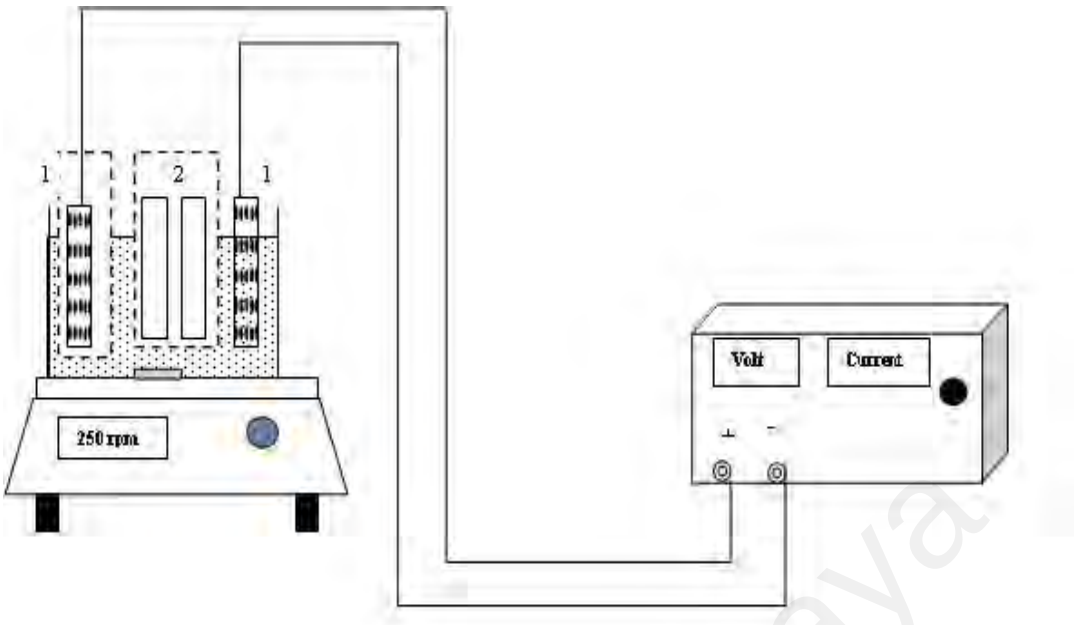

Bipolar reactor set-up:

1: Perforated anode and cathode electrodes, 2: plane electrode (without any electrical connection)

Figure 3.2: Schematic of the electrochemical set-up with conventional power

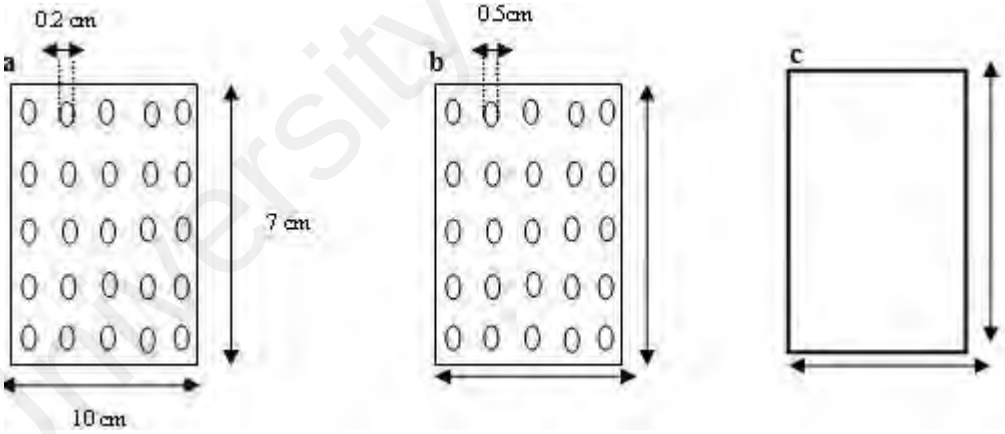

Figure 3.3: Electrode geometry for the electrocoagulation process. a) hole diameter (0.2 cm), b) hole diameter (0.5 cm) and c) without hole (plane)

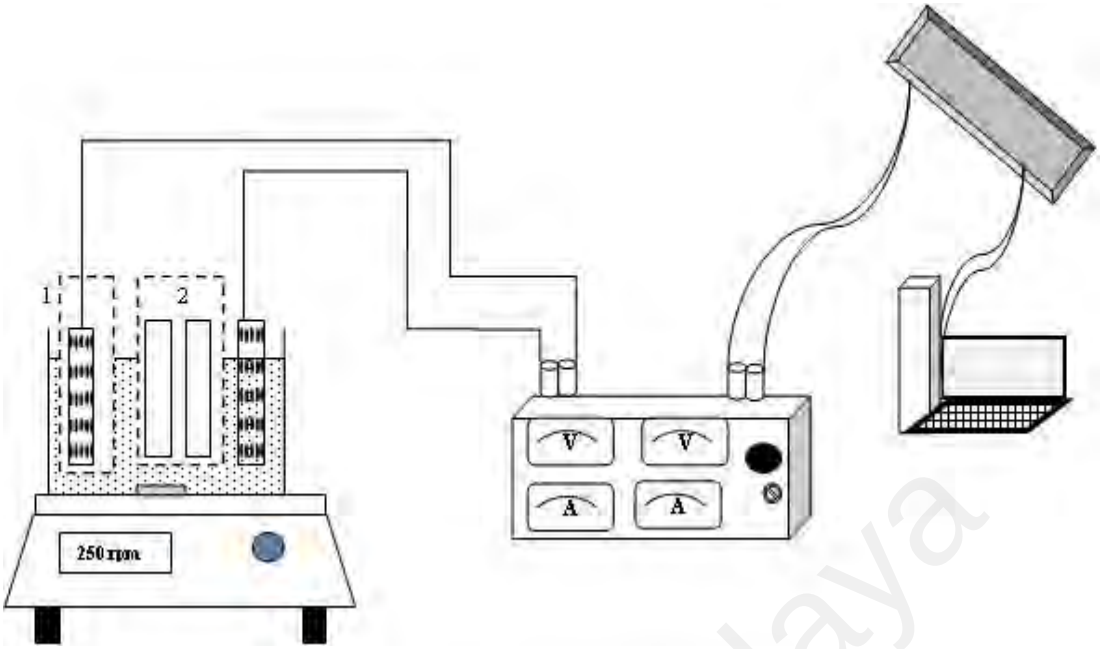

Bipolar reactor set-up:

1: Perforated anode and cathode electrodes, 2: plane electrode (without any electrical connection)

Figure 3.4: Schematic of the electrochemical set-up with solar PV power source

3.4 Solar photovoltaic set-up

The solar photovoltaic module (KINVE, KV250-60P) was purchased from BOS Asia Company (Malaysia). It consists of 12 monocrystalline silicon cells, each with a length and width of 1640 and 990 mm, respectively. The optimum operating current (McAlister et al.), optimum operating voltage (V_{mp}), short circuit current (I_{sc}) and open circuit voltage (V_{oc}) of the solar PV module are 8.3 A, 30.2 V, 9.02 A and 37.1 V, respectively. The PV panels were fixed to the roof of the Chemical Engineering Department, University of Malaya, Malaysia, located at (3° 7' 1") north latitude and (101° 39' 12") west longitude. The current and voltage of the DC-DC charge controller were within 0–10A and 0–12V ranges, respectively. The electrodes were powered by connecting the anode and cathode to the positive and negative outlets of the DC-DC charge controller and a battery,

respectively (Figure 3.4). Solar panel data such as cell voltage, photovoltaic voltage, current intensity and solar irradiation were collected using a data acquisition system connected to a computer.

3.5 Experimental procedure (Electrocoagulation process)

The experiments were divided into two stages. In the first stage, the performance of perforated Zn as the new anode material was tested and then compared with the performance of conventional electrode. For preliminary experiments, the Pb(II) concentration and initial pH was maintained at 5 mg/L and 5.68. The anode and cathode were connected to a DC power supply at a fixed current density of 0.81mA/cm^2. The process conditions were optimised in the second stage. The effects of pH (3–10), current density (0.161–1.61 mA/cm^2) and initial Pb(II) concentration (5–20 mg/L) were investigated throughout a series of experiments using a solar PV setup. The parameter ranges were selected based on the experimental data of the first stage. All experiments were performed at an ambient temperature. In electrocoagulation studies, distance between electrode, stirring rate, pH, current density and initial Pb(II) concentration were used as an important parameter to investigate their performance on the removal of Pb(II) from aqueous solution, and the details parameters are given in Table 3.1.

Table 3.1: Electrocoagulation experimental parameters

Parameters	Chosen parameter ranges
Distance between electrodes (cm)	1.0, 2.0, 3.0, 4.0
Stirring rate (rpm)	0, 200, 250, 300, 350
pH	3, 5, 7, 10
Current (A)	0.01, 0.03, 0.05, 0.07, 1.0
Current density (mA/cm^2)	0.161, 0.484, 0.81, 1.13, 1.61
Initial Pb(II) concentration (mg/L)	5, 10, 15, 20

3.6 Analytical methods (Electrooagulation process)

Pb(II) concentrations were analysed using Inductively Couple Plasma-Optical Emission Spectrometry (ICP-OES) (Perkin Elmer, Optima 7000 DV). Standard stock Pb(II) ion solutions (1000 mg/L) were prepared by dissolving $Pb(NO_3)_2$ in deionised water. Each analysis was conducted in triplicate. Removal efficiency, electrode consumption, electrical energy consumption and operating cost were determined using the following equations (Ghosh et al., 2008):

$$\text{Removal Efficiency } (\%) = \frac{Co - Ct}{Co} x\,100 \tag{3.1}$$

where *Co* is the initial Pb(II) concentration (mg/L) and *Ct* is the Pb(II) concentration after treatment (mg/L).

$$\text{Electrode consumption } (kg/m^3) = \frac{I\ x\ t\ x\ M}{z\ x\ F\ x\ V} \tag{3.2}$$

where *I* is the current (A), *M* is the molecular mass of Zn (65.39 g/mol), *t* is the treatment time (*s*), *F* is Faraday's constant (96,487 C/mol), *V* is volume (m^3) and *z* is number of transferred electrons (z = 2).

$$E\ (kWh/m^3) = \frac{U\ x\ I\ x\ t}{V} \tag{3.3}$$

where *E* is the energy consumption (kWh/m^3), *U* is the voltage (V), *I* is the current (A), *t* is the treatment time (h) and *V* is the volume of aqueous solution (m^3).

$$Operating\,\text{cost}\ (US\$/m^3) = aC_{energy} + bC_{electrode} \quad (3.4)$$

where *a* represents the 2015 electricity price in Malaysia (US$ 0.06/kW h), *b* represents the 2015 retail Zn price in Malaysia (2.73 US$/kg Zn); C_{energy} represents the electrical energy consumption (kWh/m^3) and $C_{electrode}$ represents the consumption of zinc electrode (kg/m^3).

The settleability of the precipitates is indicated by the sludge volume index (SVI), which refers to the volume in millilitres occupied by 1 gram of suspension after 30 min. The SVI is given by the following (Beyazit, 2014):

$$SVI(mL/g) = \frac{H_{30}}{H_0 SS} 1000 \quad (3.5)$$

where *SVI* is the sludge volume index (mL/g), *SS* is the initial sludge concentration after treatment (g/L), H_0 is the initial height of the sludge in the settling column (cm) and H_{30} is the height of the sludge once it has settled after 30 min (cm).

The current-time behaviour of Pb(II) towards both perforated and plane electrodes were estimated using chronoamperometry technique. The experiments were performed by potentiostat (Bio-Logic, SP-300) with EC-lab10.44 software. The solution was 5 mM Pb^{2+} in 0.01M NaCl as the supporting electrolyte. The kinetic rate constant was calculated using the pseudo-first-order (equation 3.6) and pseudo second order (equation 3.7) models (Al-Shannag et al., 2015).

$$C_t = C_o e^{-k_1 t} \tag{3.6}$$

$$C_t = C_e + (C_o - C_e) e^{-k_2 t} \tag{3.7}$$

where *Co* is the amount of Pb ions at the initial concentration (mg/L), *Ct* is the amount of Pb ions after treatment (mg/L), *t* is the treatment time (min) and *k* is the first order rate constant (min^{-1}).

3.7 Characterisation of electrode and sludge (Electrocoagulation process)

Particle size distribution was measured using zeta potential analyser (Malvern 2000, UK). Examination of the surface morphology and elemental analysis of the electrodes were carried out using JEOL field emission scanning electron microscope (FESEM) cross-beam workstation equipped with an energy-dispersive X-ray spectroscopy (EDX) facility (AMETEK, Advanced Microanalysis Solutions, UK) operated at an accelerating voltage of 10 kV. The presences of crystalline forms and compound phases in the sludge and electrodes surface were determined via an X-ray diffractometer (D8 Advance X-ray diffractometer (XRD)-Bruker AXS) with Cu-Kα monochromatic radiation. The XRD was operated at 40 kV and 40 mA, with a scanning rate of 1° 2Θ/min and scanning interval range from 10° to 90°. All visual images of the electrodes surface were captured using Dinocapture 2.0 version 1.5.13 digital camera at an image dimension of 1.0 mm.

3.8 Experimental procedure (Adsorption process)

3.8.1 Batch experiments

Granular OPSAC was purchased from Bravo Green Sdn. Bhd. which is a local supplier located in Sarawak, Malaysia and the activated carbon (adsorbent) was sifted to particle size (700-850 μm). The adsorbent was subsequently washed by using distilled water in order to eliminate impurities and then was left to dry in an oven for 24 hours with a temperature of 110 °C to remove moisture. Batch adsorption experiments were conducted in centrifuge tubes whereby each tube contained 30 mL of Pb(II) solution with different initial concentrations (10-130 mg/L) and 0.06 g of OPSAC. The samples were stirred at 180 rpm via an orbital shaker with the temperature being controlled at 27 ± 1°C for 96 hours until reaching the equilibrium state at a constant pH (6, 8 or 10). The experimental flowchart of adsorption process is depicted in Figure 3.5.

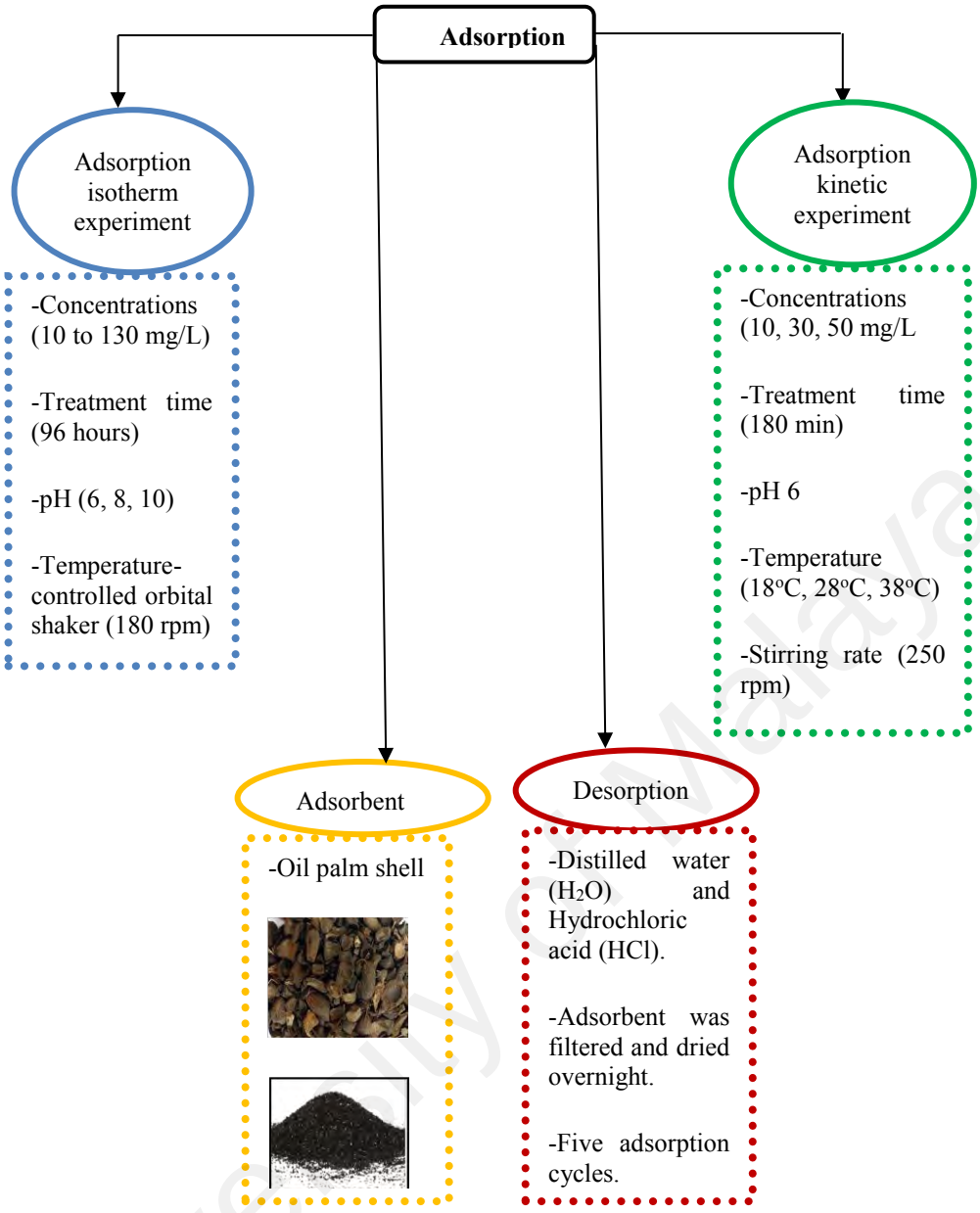

Figure 3.5: Experimental flowchart of adsorption process

The Langmuir and Freundlich equations as well as the non-linear regression approach were applied to estimate isotherm parameters. Statsoft Statistica software version 12 was used for data analysis. The nonlinear regression approach was the most viable method to select the optimum isotherm. This method gave minimum error distributions between predicted isotherms and the experimental data (Szlachta & Chubar, 2013). The Langmuir and Freundlich equations are provided by equations 3.8 and 3.9 correspondingly:

$$q_e = \frac{q_m \cdot bC_e}{1 + bC_e} \tag{3.8}$$

$$q_e = KC_e^n \tag{3.9}$$

where q_e and q_m represent the equilibrium and maximum monolayer adsorption capacities (mg/g), correspondingly, C_e stands for the equilibrium concentration of adsorbate in solution (mg/L), b represents the Langmuir adsorption equilibrium constant associated with the binding energy (L/mg), K represents the Freundlich constant associated with the adsorption capacity ((mg/g) or (L/mg)) and n stands for the adsorption intensity parameter.

The Pb(II) adsorption capacity (q_{exp}, mg/g) was computed via the following equations:

$$q_{\exp} = \frac{(C_O - C_e)V}{m} \tag{3.10}$$

where Co represents the initial Pb(II) concentration (mg/L), C_e represents the equilibrium concentration of the adsorbate (mg/L), V represents the volume of the solution (L) and m represents the mass of the dry adsorbent (g).

The adsorption kinetics experiments were conducted at three different Pb(II) concentrations (10, 30 and 50 mg/L) as well as three different temperatures (18, 28 and 38 °C) for 3 hours. The experiments were performed with an initial pH of 6 via 4 g/L of adsorbent dose. In the kinetics study, the agitation speed used to stir Pb(II) solution was 250 rpm. In order to obtain a fixed temperature throughout the process, a temperature-controlled water bath was utilised.

To fit the data related to adsorption kinetics, there were four models which were applied, namely pseudo-first-order kinetic model (equation 3.11), pseudo-second-order kinetic model (equation 3.12), Elovich model (equation 3.13) and intra-particle diffusion model (equation 3.14) proposed by (Ho & McKay, 1998; Weber & Morris, 1963):

$$q = q_e\left(1 - e^{-k_1 t}\right) \tag{3.11}$$

$$q = \frac{k_2 q_e^2 t}{1 + k_2 q_e t} \tag{3.12}$$

$$q = \frac{1}{b}\ln(ab) + \frac{1}{b}\ln(t) \tag{3.13}$$

$$q = k_{ind} t^{0.5} + I \tag{3.14}$$

where q and q_e represent the amounts of Pb(II) adsorbed at time t and during equilibrium (mg/g) correspondingly, t represents the contact time (min), k_1 represents the rate constant of pseudo-first-order adsorption (1/min), k_2 represents the rate constant of pseudo-second-order adsorption (g/mg min), b represents the desorption constant (g/mg), a represents the initial adsorption rate (mg/g min), k_{ind} represents the intra-particle diffusion rate constant (mg/(g $\text{min}^{0.5}$)), and I represents the constant for the boundary layer thickness (mg/g).

Activation energy (E_a) of Pb(II) adsorption onto palm shell based activated carbon was calculated as follow (Szlachta & Chubar, 2013):

$$\ln k_2 = \ln A - \left(\frac{E_a}{RT}\right) \quad (3.15)$$

where A represents the temperature independent factor (g/mg min), E_a represents the activation energy (kJ/mol), R represents the gas constant (8.314 J/mol.K) and T represents the temperature (K).

3.9 Characterisation of adsorbent

JEOL field emission scanning electron microscope (FESEM) cross-beam workstation (Hitachi, Japan) which was equipped with an energy-dispersive X-ray analysis (EDAX) facility (AMETEK, Advanced Microanalysis Solutions, UK) was utilised to examine the surface morphology of the adsorbent and the device was run at an increasing voltage of 10 kV. The adsorption and desorption measurements were performed in liquid nitrogen at 77 K via TriStar II 3020 surface area as well as porosity analyser (Micromeritics ASAP 2020, United States). The surface area of Brunauer-Emmett-Teller (BET) was ascertained by using the nitrogen adsorption isotherm data. The average pore diameter was calculated by analysing desorption isotherms via the Barrett-Joyner-Halenda (BJH) method. To ascertain the point of zero charge (pH_{PZC}), which is the point in which pH_{final} versus $pH_{initial}$ intersects with the line where $pH_{initial} = pH_{final}$, the pH drift technique was applied. The pH of the background solution (0.01 M of NaCl) was regulated to the needed pH by using 0.1 M of HCl or NaOH before adding 0.15 g of activated carbon. The solution was stirred for 24 hours in order to achieve pH equilibrium. The particle size distribution was ascertained via Malvern Mastersizer 2000 particle size analyser (Malvern, UK).

3.10 Error analysis

3.10.1 Adsorption kinetics

According to Asgari et al. (2012), besides correlation coefficient (R^2), the applicability of kinetic models were further assessed by comparing with normalised standard deviation (NSD) and average relative error (ARE) (Asgari et al., 2012):

$$NSD = 100\sqrt{\frac{1}{N-1}\sum_{i=1}^{N}\left[\frac{\left(q_e^{\exp}-q_e^{cal}\right)}{q_e^{\exp}}\right]^2} \tag{3.16}$$

$$ARE = \frac{100}{N}\sum_{i=1}^{N}\left|\frac{q_e^{\exp}-q_e^{cal}}{q_e^{\exp}}\right|_i \tag{3.17}$$

where $q_e{}^{calc}$ represents the equilibrium, capacity determined from the model (mg/g), $q_e{}^{exp}$ represents the equilibrium capacity obtained from experiments (mg/g) and N represents the number of experimental points. The smaller NSD and ARE values show more precise approximations of q_e values.

3.10.2 Adsorption Isotherm

The capability of adsorption isotherm in explaining the process of adsorption was proved by root mean square error (RMSE) and chi-square test statistic (Ho, 2004; Ramavandi et al., 2014), which were indicated as follow:

$$RMSE = \sqrt{\frac{1}{N-2}\sum_{i=1}^{N}\left(q_e^{\exp} - q_e^{cal}\right)^2} \tag{3.18}$$

$$\chi^2 = \frac{\left(q_e{}^{\exp} - q_e{}^{calc}\right)^2}{q_e{}^{calc}} \tag{3.19}$$

where $q_e{}^{calc}$ is the equilibrium capacity determined from the model (mg/g), $q_e{}^{exp}$ is the equilibrium capacity obtained from experiments (mg/g) and N is the number of experimental points. The smaller RMSE and χ^2 values indicate a better curve fitting.

3.11 Desorption experiment

The desorption process is important to attain practical and economical adsorption. A promising adsorbent is needed not only to produce high adsorption capacity but also the ability to regenerate as well as potential to recycle. To determine the most effective desorption solution, 0.06 g of OPSAC was placed in three different Erlenmeyer flask that contained 50 mL of 0.1 M hydrochloric acid (HCl), nitric acid (HNO_3) and distilled water (H_2O) without any pH adjustment for 3 hours via an incubator shaker at a temperature of 27°C and a speed of 180 rpm. Then, the mixture was filtered after desorption and was analysed by ICP.

3.12 Experimental procedure (Integrated system)

In the integrated electrocoagulation and adsorption process, the experiment was carried out in one system. The integrated system was established through a bipolar configuration. The schematic diagram of establishing the integrated system is depicted in Figure 3.6. The perforated Zn, which has the dimension of 7 cm × 10 cm and hole diameter of 0.5

cm, was utilised as the anode and cathode pairs in integrated process. The distance and current density of an inter-electrode were fixed at 1.0 cm and 1.13 mA/cm^2 respectively in all experiments. The solutions were agitated at 250 rpm with a constant temperature of 27 ± 1°C. After the experiments, the residual Pb(II) concentration was sifted using 0.45 μm pore size and the samples were then analysed immediately using ICP to determine the removal efficiency of Pb(II) ion. All the experiments were conducted at room temperature. The main aim of integrated system is to maximise the removal efficiency, minimise the power consumption and reduce the amount of adsorbent used in removing Pb(II) from aqueous solution. The results were optimised by response surface methodology (RSM) in order to obtain an appropriate parameter for optimisation as well as to attain optimum condition of the integrated process (Figure 3.7).

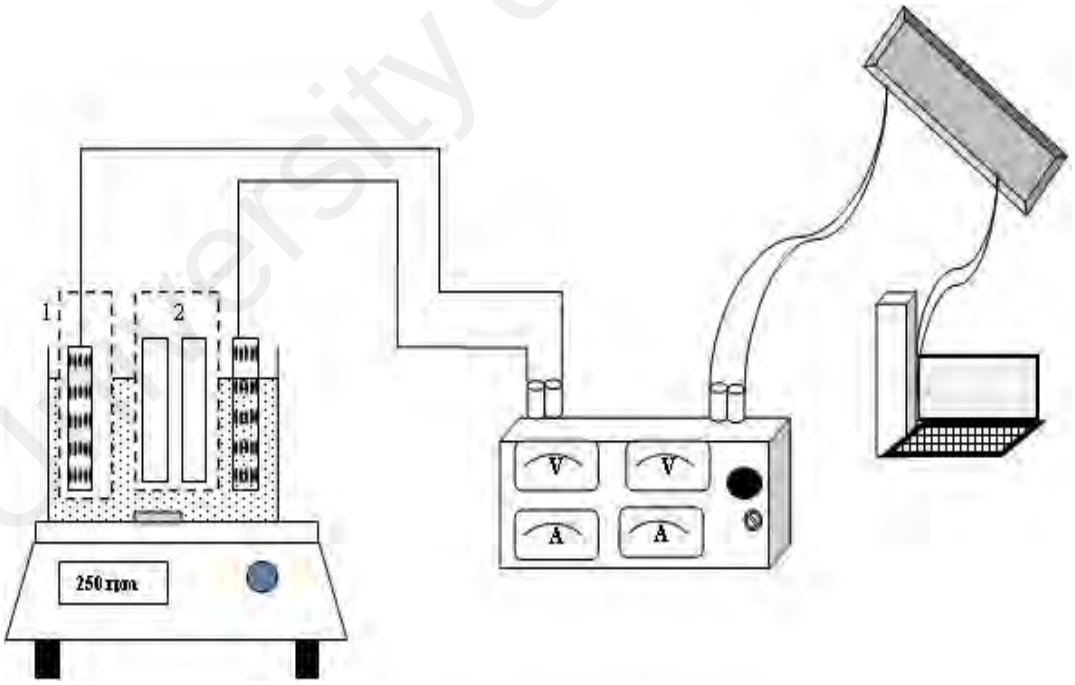

Figure 3.6: Schematic diagram of establishing the integrated process using solar PV power source

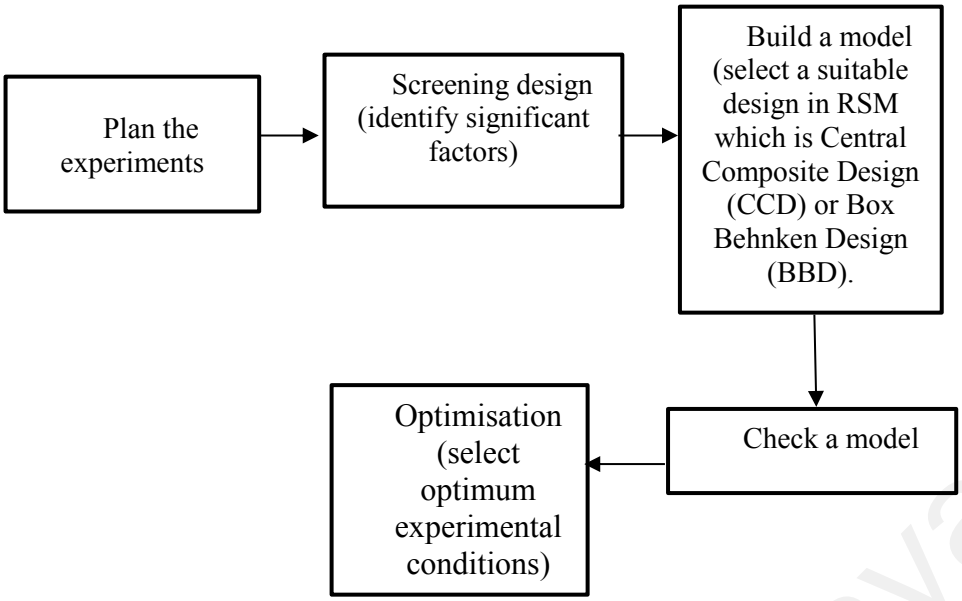

Figure 3.7: Optimisation process flowchart by response surface methodology

3.12.1 Screening design

For an optimisation process, there are two steps required which include the screening technique to select the best and important parameters as well as response surface methodology. In the present study, the main parameters were studied according to the results obtained from the single electrocoagulation process and adsorption process whereby the pH, initial Pb(II) concentration and adsorbent dosage were selected to be the major variables in the integrated process. The experiment design was produced by the Design Expert software version 11.0 (Stat Soft Inc., Tulsa, USA). Table 3.2 shows the optimum experimental conditions of the single electrocoagulation and adsorption process. Based on the experimental results, the main parameters such as pH, initial Pb(II) concentration and adsorbent dosage were changed within the range of 5-7, 15-25 mg/L and 2-4 g/L respectively.

Table 3.2: Optimum experimental conditions of the electrocoagulation and adsorption process

Parameters	Electrocoagulation	Adsorption
Initial Pb(II) concentration (mg/L)	5	10
pH	7	6
Adsorbent dosage (g/L)	-	4
Current density (mA/cm^2)	1.13	-
Removal efficiency (%)	99.9	99.1

3.12.2 Response surface methodology

As a powerful statistical and mathematical technique, response surface methodology (RSM) is effective to be used in analysing and modeling as well as examining crucial processes by decreasing the number of trials in experiments (Myers & Montgomery, 2002). This technique can be applied to solve various lab-scale or industries problems within a reasonable amount of time. Optimisation process via RSM is certainly a quicker, easier and cost-effective approach in terms of collecting results of experimental research as compared to the conventional approach (one-factor-at-a-time), in which interaction effect between parameters is not measurable and takes longer time to examine all factors (Alim et al., 2008). The primary aim of this method is to improve the response surface which is affected by several process parameters. There are several steps in applying RSM. Firstly, a sequence of experiments is carried out in order to obtain sufficient and dependable dimension of the response of interest. Secondly, a mathematical model of the second-order response surface which has the suitable model fit is produced. Thirdly, the ideal set of experimental parameters which forms a maximal or minimal value of response is ascertained. Finally, the direct and connection effects of process parameters are depicted via two and three-dimensional (3-D) plots (Gunaraj & Murugan, 1999).

Among several methods of response surface methodology, central composite design (CCD) and Box–Behnken design (BBD) were discovered to be the most extensively applied design in RSM (Zolgharnein et al., 2013). BBD design is a round, rotatable, or closely rotatable second-order design. It is formed according to three-level incomplete factorial design, containing the center point and middle points of the edges from a cube. As for CCD design, it has been applied extensively as the experimental design in recent years. This technique is suitable in fitting a quadratic surface. Besides that, it can improve the significant parameters through a least number of experiments and examine the connection between parameters.

.

The CCD contains two levels of factorial design that have 2^n factorial points, with 2n axial points that have every factor in turn to be adjusted to its low and high levels while the other factors at their central and n_c central points that have all factors are adjusted to their central level (Asaithambi et al., 2016; Asfaram et al., 2015). To ascertain the experimental error as well as the reproduction of data and model which are less fit, the center points are usually applied. They are effective in solving research problems, especially when attempting to find an ideal condition. In the present study, since the number of independent variables was three, the total number of experiments was 17. There were 14 experiments which were amplified with three repetitions at center point to assess the error. Generally, there are two vital models which are applied in RSM, namely first order and second order polynomial (Equation 3.20 and 3.21) (Asaithambi et al., 2016; Khuri & Mukhopadhyay, 2010).

$$y = \beta_o + \sum_{i=1}^{k} \beta_i x_i + \varepsilon \tag{3.20}$$

$$y = \beta_o + \sum_{i=1}^{k} \beta_i x_i + \sum_{i<j} \sum \beta_{ij} x_i x_i + \sum_{i=1}^{k} \beta_{ii} x_i^2 + \varepsilon \quad (3.21)$$

Where *y* represents the predicted response or removal efficiency, *Xi* and *Xj* represent independent variables, and ε represents the residual term. Meanwhile, β_i, βj and βij stand for the linear coefficient, quadratic coefficient and cross-product coefficients (Asfaram et al., 2015).

In CCD design, experimental data were fitted to a second order polynomial equation, and regression coefficients were attained. To validate the importance and adequacy of the developed regression model, the analysis of variance (ANOVA) was carried out. The sufficiency of the response surface models was assessed by computing determination coefficient (R^2) and examining it for the lack of fit. According to p- and F-values, the significant variables were determined and the 3-D plot of responses against the significant variables was formed to predict the best functioning requirements. Desirability function is an ordinary and well-known technique to ascertain the ideal requirements (Rebane & Barham). The major benefit of desirability function is its capability to get qualitative and quantitative responses through easy and instant transformation of various responses for one measurement (Asfaram et al., 2015). Generally, desirability function is within the range between 0 and 1. The optimum experimental conditions with the highest desirability which equal to 1 provides more useful response. However, if the values equal to zero, this indicates minimum applicability or undesirable condition.

CHAPTER 4: RESULTS AND DISCUSSION

4.1 Electrocoagulation

4.1.1 Performance of different electrode materials

Selecting an electrode material is crucial for electrocoagulation treatment. Therefore, electrode material is the first parameter examined in this study. We tested the Pb(II) removal performance of Al, Cu, Fe, and Zn electrodes in the electrocoagulation treatment system powered by a conventional electric power source. Figure 4.1 shows that the highest Pb(II) removal efficiency of 97.5% was achieved when using the Zn electrode, whereas the lowest Pb(II) removal efficiency of 74.1% was achieved when using the Cu electrode. The shortest treatment time of 30 min was also achieved with the use of Zn electrode. The Pb(II) removal efficiencies of 84.2% and 81.1% were achieved with the Al and Fe electrodes only after 50 min of treatment using the current density of 0.81mA/cm^2.

In particular, Pb(II) removal by the Fe electrode initially increased from 31% to 81%, but it began to decrease after 50 min of treatment. After 50 min of treatment with Fe anode, the colour of the treated water became greenish because the formation of iron particles made the solution turbid and yellowish. Chen et al. (2000) observed a similar trend which is attributed to the presence of Fe^{3+} and Fe^{2+} ions. Fe^{2+} ions are commonly generated during Fe electrolysis, and these ions can easily be oxidised into Fe^{3+} in the presence of dissolved oxygen in water (Chen et al., 2000). Fe^{3+} ions are fine, yellow $Fe(OH)_3$ particles with poor settleability and are ineffective in the removal of other metal ions (Kobya et al., 2006). An image of Fe anode in Figure 4.2(a) indicates the presence of little corrosion pitting. Kobya et al. (2006) reported a similar observation and stated that Fe electrodes are less effective and cause corrosion (Kobya et al., 2006). In contrast, water treated using

Zn electrode was clear and odourless. These results demonstrate the potential application of Zn in electrocoagulation due to its ability to remove high Pb(II) concentrations within the short treatment time and least corrosion. Besides that, in order to ensure that Zn electrode is suitable to be used for further studies without impacting the environment, the concentration of Zn after electrocoagulation treatment was investigated. It is found that, all analysis tested gave effective results in 100% Zn was eliminated after the electrocoagulation treatment. According to Malaysia's environmental law, the standard limit of Zn in effluent is 1.0 mg/L (IWK, 2016). Based on the ICP analysis results, the average Zn content in the solution is very low, which is approximately 0.0011mg/L. Therefore, it can be concluded that, the use of Zn electrode did not impact the environment negatively and that this electrode is appropriate to be used for removing Pb(II) ion.

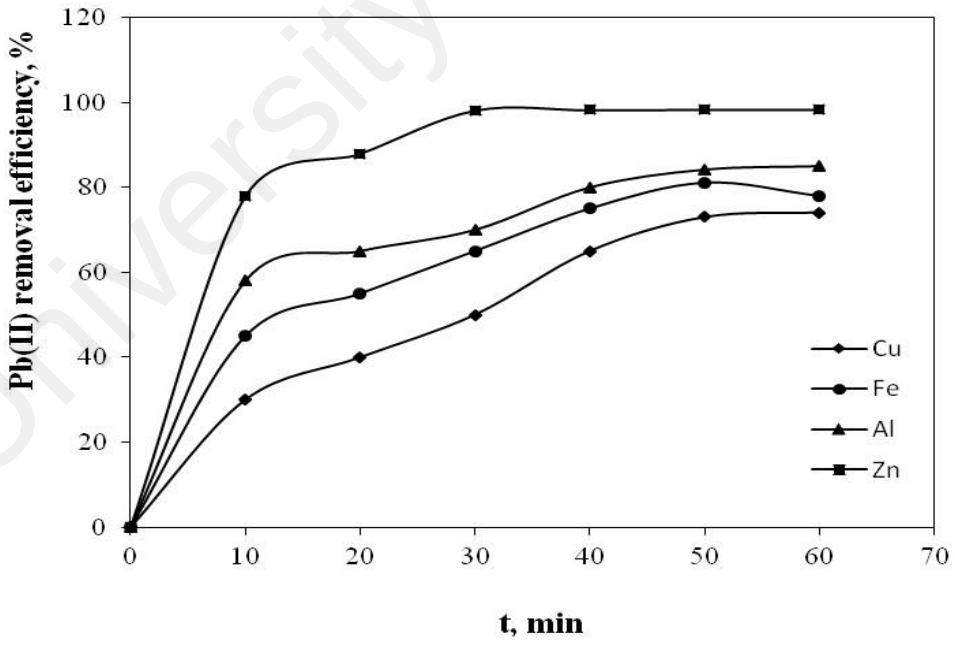

Figure 4.1: Effects of different anode materials on Pb (II) removal efficiency (initial pH 5.68, Co = 5 mg/L, current density = 0.81 mA/cm2, agitation rate = 250 rpm, hole size = 0.2 cm)

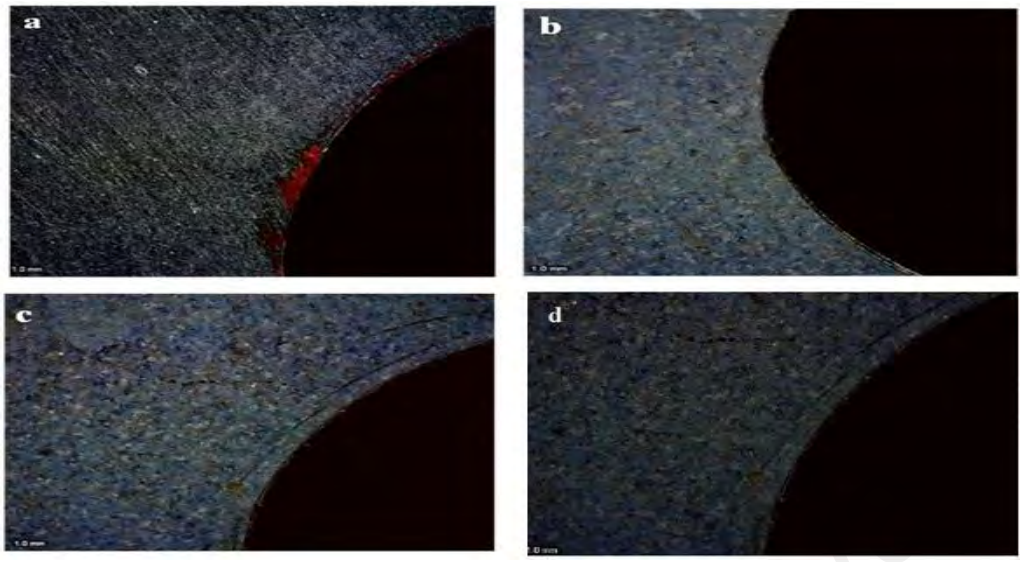

Figure 4.2: Images of the anodes surface after treatment: (a) Fe, (b) Zn, (c) Al and (d) Cu

The results obtained in this study show that the use of Zn is more superior when compared to results obtained from the literature. Mansoorian et al. (2014) reported that the highest Pb(II) removal efficiency, which is 97.2%, was obtained with the use of Fe electrode and the current density of 6mA/cm^2 for the duration of 40 min (Mansoorian et al., 2014). In contrast, Assadi et al. (2015) observed that the highest Pb(II) removal efficiency, which is 94%, was achieved using Al electrode under the optimum current density of 33mA/cm^2 for a 30 min duration treatment (Assadi et al., 2015).

Table 4.1 presents the performance data of the four electrode metals (Fe, Cu, Zn and Al) in terms of sludge production and Pb (II) removal efficiency. Sludge produced from electrocoagulation treatment is related to the characteristics of wastewater, coagulant concentration, current density and treatment time. An SVI < 100 mg/L is considered as a good settling characteristic (Beyazit, 2014). All four electrodes showed an SVI < 100 mL/g after treatment. However, the SVI was relatively higher for the Fe electrode, which is associated with the formation of extraneous iron hydroxide flocs suspended in the

solution. In contrast, the Zn electrode had the lowest SVI (68.5 mL/g) among the four electrodes. In the electrocoagulation process, the electric current causes the dissolution of metal electrode and thus, generating a series of coagulant species which are metal hydroxides, that can destabilise and combined the suspended particles or precipitates to become flocs and absorb dissolve contaminants (Katal & Pahlavanzadeh, 2011). The metal hydroxide flocs form great surface areas that are useful for an accelerated adsorption, enhancing the chances of the attachment of pollutants to flocs. At last, these flocs are eliminated from aqueous solution easily by the sedimentation process or H_2 flotation (Daneshvar et al., 2006). The size and growth of flocs can influence the electrocoagulation removal rate. Thus, an increment in the floc production in aqueous solution can be observed, which leads to the enhancement in the lead removal efficiency (Uğurlu et al., 2008).

Based on the results, it was found that the average particle size in the treated water were 2898, 2885, 2925 and 2956 nm for Cu, Fe, Al and Zn electrodes, respectively. Notably, large flocs were present in the Zn electrode solution and these large surface areas could generate active surface for accelerated adsorption of compounds, trap colloidal particles and eliminate contaminants from aqueous solution easily. Thus, the larger floc significantly enhanced Pb (II) removal efficiency during electrocoagulation. These findings are supported by the results reported by Daneshvar et al. (2004), where it is stated that increasing the treatment time from 2 to 4 min increased the removal efficiency significantly and the increment also occurs in the production of hydroxide flocs production (Daneshvar et al., 2006). The Zn electrode also recorded the lowest energy consumption (0.325 kWh/m^3) and operating cost (0.664 US$/$m^3$). Based on these results, the Zn electrode demonstrated a superior performance in terms of Pb(II) removal efficiency, energy consumption and sludge production.

Table 4.1: Performance of different anode materials during electrocoagulation process

Electrode materials	Removal efficiency (%)	Energy consumption (kWh/m^3)	SVI (mL/g)	Particle size (nm)
Cu	74.1	0.327	75.3	2898
Fe	81.1	0.390	80.2	2885
Al	84.2	0.355	75.1	2925
Zn	97.5	0.325	68.5	2956

4.1.2 Comparison of anode configurations

Three types of anode geometry were compared in this study: hole with a diameter of 0.2 cm, (2) hole with a diameter of 0.5 cm and (3) plane (no hole). Between three types of anode geometry, the type (2) with 0.5 cm hole diameter poses highest surface area. The anode geometry with the largest surface area will increase current distribution, and hence increase the Pb(II) removal. Figure 4.3 confirms that the perforated electrode with a 0.5 cm hole diameter exhibits a higher Pb(II) removal efficiency, lower treatment time and lower voltage. Larger hole diameters are associated with higher removal efficiency probably because of increased current distribution throughout the electrode surface, including the additional exposed surface of the perforated holes (Kuroda et al., 2003). The Pb (II) removal efficiency increased with increasing hole size, with the plane electrode having the lowest removal efficiency recorded. Figure 4.4 shows the amount of current generated by anodes using different electrode geometry. The anode with 0.5 cm hole diameter produced the highest amount of current whereas the anode with plane geometry generated the lowest amount of current. The anode with 0.5 cm hole diameter was also more active as compared to other anode geometries in removing Pb(II) ions during electrocoagulation. All subsequent experiments were carried out using perforated Zn electrode with a hole diameter of 0.5 cm.

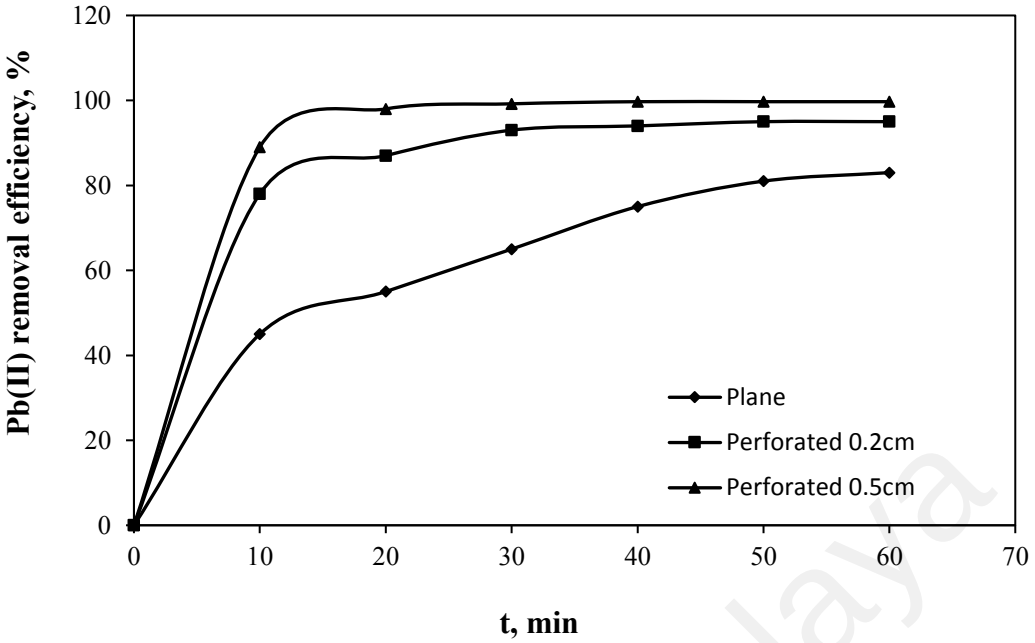

Figure 4.3:Effects of different anode geometries on Pb (II) removal efficiency (pH 5.68, C_{Pb} = 5 mg/L, current density = 0.81 mA/cm^2, agitation = 250 rpm).

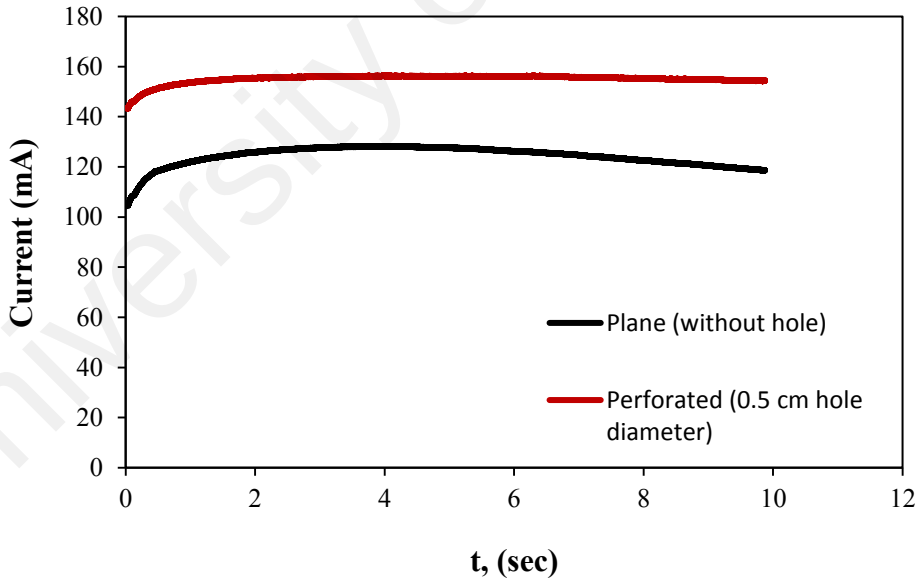

Figure 4.4: Chronoamperometry of perforated and plane electrodes in Pb(II) solution (5mM Pb(II) + 0.01M NaCl)

4.2 Meteorological conditions (solar PV)

Meteorological conditions are important to solar PV module performance as they influence the Pb(II) removal efficiency of the electrocoagulation system. Experiments were conducted under three various weather conditions (sunny, partly cloudy and cloudy). All experiments were recorded in triplicate measurements for each of the three different weather conditions for the same treatment time (12:00–1:00 pm) in order to identify the most optimum weather condition. Table 4.2 presents the performance data of the three different weather conditions in terms of removal efficiency. The highest and lowest Pb(II) removal efficiencies were obtained on the sunny and cloudy day, respectively. Table 4.2 demonstrates that the Pb(II) removal efficiency was 99% on the sunny day and that the solar radiation (950 W/m^2) produced was higher than those of the other weather conditions. Table 4.2 also shows that the removal efficiency gradually decreased as solar irradiation power decreased, which can be attributed to the variation in weather. In addition, under partly cloudy and cloudy weather conditions, the solar radiation power dropped, and the Pb (II) removal efficiency decreased. Therefore, further experimental studies on solar PV system were conducted under sunny weather conditions.

Table 4.2: Performance of solar photovoltaic electrocoagulation under different meteorological conditions (initial pH 5.68, Co = 5 mg/L, current density = 0.81 mA/cm^2)

Weather conditions	Sunny	Partly cloudy	Cloudy
Solar radiation (W/m^2)	950	410	165
Temperature (^oC)	33	28	26
Removal efficiency at 1hour treatment time (%)	99.1	78.8	74.5

4.3 Process optimisation of the solar PV electrocoagulation treatment system

Electrocoagulation treatment is influenced by several operating parameters, such as treatment time, initial pH, initial Pb(II) concentration and current density, which were investigated in this study and discussed in this section.

4.3.1 Effect of distance between electrodes

The distance between electrodes and its effects (anode-cathode distance) were studied in the range of 1.0 cm to 4.0 cm, while keeping other parameters constant. The variation in removal percentage of Pb(II) with different distance between electrodes is illustrated in Table 4.3. Based on the results, it is clear that the removal percentage of Pb(II) increased with decreasing distance between electrodes, whereby the highest removal efficiency recorded was 97.5% at an electrode distance of 1.0 cm, as shown in Table 4.3. A similar observation has been made by Bouguerra et al. (2015), where they reported that when the inter electrode distance increases from 0.5 cm to 2.0 cm, the percentage of heavy metals removal decreases. They also stated that a short inter electrode distance of 0.5 cm is considered sufficient to attain the highest removal of heavy metal ion and produce less energy consumption (Bouguerra et al., 2015). The electrostatic attraction reduced as the distance between the electrodes increased. During the electrocoagulation process, the anodic oxidation occurs when the potential is applied to the electrodes. When the anodic oxidation rate reduces, the number of cations at anode also reduced. These cations play an important role for the formation of coagulant. As the electrolysis time increased, an ultra-thin layer of metal hydroxide was created on the anode generating. The formation of this fine film increased with the increase in the distance between electrodes, causing an increase in the ohmic loss (IR resistance). The incremental drop in IR is not encouraged

for electrocoagulation due to the fact that the loss of ohmic for both cathode and anode over voltage values and mass transfer resistance turned larger, hence leading to a slowdown in the kinetics of transfer charge and consequently a lower removal efficiency of heavy metal ions (Ghosh et al., 2008) . This is in line with the observation made by Vasudevan et al. (2011b) for the removal process of Pb(II) from water via electrocoagulation, Mansoorian et al. (2014) for electrocoagulation evaluation in treating wastewater from electroplating, as well as Kobya et al. (2006) for the heavy metals removal from aqueous based solutions via electrocoagulation (Kobya et al., 2006; Mansoorian et al., 2014; Vasudevan & Lakshmi, 2011b).

Moreover, increasing the distance between electrodes lowered the rates of both particle aggregation and Pb(II) adsorption, which resulted in decrement in the elimination of Pb(II) ion. In fact, the highest Pb(II) removal was attained at a short distance (1.0 cm) between the electrodes. Thus, the selection of an optimum electrode distance at 1.0 cm is recommended in order to reduce electrode consumption, energy consumption as well as to enhance the removal efficiency of Pb(II) ion.

Table 4.3: Effect of distance between electrodes in the solar PV electrocoagulation (pH 5.68, C_{Pb} = 5 mg/L, current density = 0.81 mA/cm^2, agitation = 250 rpm)

Electrode distance (cm)	Removal Efficiency (%)	Voltage (V)	Electrode consumption (kg/m^3)
1	97.5	2.8	0.225
2	90.2	3.3	0.283
3	81.2	3.8	0.296
4	70.1	4.5	0.323

4.3.2 Effect of stirring rate

The effects of stirring rate on the Pb(II) ion removal was investigated at different stirring rates (0, 200, 250, 300 and 350 rpm) (Table 4.4). It is obvious that the stirring rate of 250 rpm was found to be the most effective in removing Pb(II) ion from aqueous solution. Based on the observation, as the stirring rate increases, the coagulant matter is formed, which get attached between one another and effectively disperse in the reactor, resulting in a homogenous content of the reactor and making precipitation easier. These findings are supported by the results reported by Can et al. (2003), where the effect of stirring rate between 100 and 500 rpm was studied. They found that the greatest efficiency of removal was obtained at 200 rpm, whereby it then decreases significantly (Can et al., 2003). This result is further supported by a research from Khaled et al. (2015) who found that at a moderate agitation speed, the elimination of heavy metal ions was much faster than at a higher agitation speed due to high formation of metal hydroxide flocs and high energy consumption, which lead to higher cost (Khaled et al., 2015).

On the other hand, at 0 rpm (without stirring), the Pb(II) removal was low and the percentage of removal rarely exceeds 73% for a treatment time of 30 min. Increasing the stirring speed lowers the efficiency of Pb(II) removal because enhancing stirring speed reduces the competence of flock formation of metal hydroxide (Khaled et al., 2015). However, it can be observed that the removal efficiency decreased rapidly when a high stirring speed of 350 rpm was applied. The results show that it is clear that the Pb elimination was low at a high stirring speed whereby the percentage of removal did not exceed 90% for a treatment time of 30 min. This may be due to the breaking of coagulant due to the effect of strong stirring rate (Bouguerra et al., 2015). The operation at high stirring speed enhances restructuring and particle fragmentation, which leads to the

production of smaller and more compact aggregates of metal hydroxide flocs. In addition, it is important to note that the amount of sludge produced increased by increasing the stirring rate. With a high agitation speed, a greater amount of metal hydroxide flocs was formed during the electrocoagulation, producing more sludge (Bouguerra et al., 2015). Therefore, the sludge reduces thePb(II) removal efficiency. A similar observation had been made by Can et al. (2014), whereby they reported that high stirring speed created negative pressure on the flow of electrons which slows the flow of electrons or creates an additional resistance causes higher energy required (Can et al., 2014). Therefore, based on the observation, it can be stated that the optimum stirring rate of 250 rpm was selected and used for further studies.

Table 4.4 illustrates the pH changes after electrocoagulation process. It is evident that the final pH for all experiments increased slightly as compared to the initial pH. However, at high stirring speed (350 rpm), the final pH increased significantly than the initial pH (Table 4.4). This is due to the aqueous solution precipitating and producing high amount of sludge and hence, increasing the pH values. It is important to monitor a pH value before and after electrocoagulation treatment as well as maintain a pH value between pH 6 to pH 7 in order to avoid high amount of metal hydroxide flocs precipitation and high sludge production.

Table 4.4: Effect of stirring rate in the solar PV electrocoagulation (pH 5.68, C_{Pb} = 5 mg/L, current density = 0.81 mA/cm^2, electrode distance = 1.0 cm)

Stirring rate (rpm)	Removal Efficiency (%)	Final pH
200	96.1	6.2
250	97.5	6.5
300	95.8	6.8
350	90.3	7.1

4.3.3 Effect of pH

Initial pH is one of the most important operating parameters that influences electrocoagulation performance. A series of batch experiments was performed under varying pH levels (3.0 to 10.0) to determine the optimum pH. The current density and agitation rate were kept constant at 0.81 mA/cm^2 and 250 rpm, respectively. Figure 4.5 illustrates that the removal efficiency increased as the pH increased from 3.0 to 7.0. These results clearly demonstrate that the highest Pb(II) removal was obtained at pH 7 (99.9% removal) after 10 min of treatment. On the other hand, at higher pH value (pH 10), the removal efficiency is found to be reduced significantly. According to the research article by Wippermann et al. (1991), the authors investigated the electrochemistry occurring on Zn surface and the effects of pH using Pourbaix diagram of Zn-H_2O in aqueous environment. They found that at pH 9 and 12.5, a formation of zincate ions will occur, and it causes a passive corrosion on the Zn surface, thus decreasing the removal efficiency. This is due to the amphoteric nature of active dissolution of zinc at higher pH (Wippermann et al., 1991).

However, as reported by Vasudevan & Lakshmi (2011b), the $Zn(OH)_2$ precipitation can only be significant at pH 8.6 based on the Zn–H_2O Pourbaix diagram. At pH > 8.6, Zn is insoluble in water, resulting in the formation of an oxide film on the zinc. which passivates zinc (Vasudevan & Lakshmi, 2011b). During the electrocoagulation process, the OH^- production from the reaction increased with increasing pH due to the production of hydroxides. Consequently, insoluble $Zn(OH)_2$ precipitates were formed at a higher pH value. The influent pH is a crucial parameter that influences the performance of the electrocoagulation process. When the pH of the aqueous solution was between 6.5 and 7.5, the maximum removal was achieved. However, the interfacial pH-increased during

electrocoagulation, which favoured $Zn(OH)_2$ formation and resulted in higher removal efficiency at pH 7.0. Similarly, Escobar et al. (2006) found that the Pb (II) removal efficiency progressively increases with pH up to 7.0. However, once the pH exceeded 7.0, the Pb(II) removal efficiency significantly decreased. At a higher pH (strong alkaline), the solid Zn hydroxide dissolved with the formation of zincate ($Zn(OH)_4)^{2-}$) ions. Thus, the electrode corroded and the Pb(II) removal decreased. Furthermore, the decrease is also linked to the amphoteric behaviour of cations and anions present at alkaline pH that do not contribute to Pb(II) removal. A strong acidic medium also diminishes metal ion oxidation at low pH, thus hindering the heavy metal removal (Costa et al., 2004; Escobar et al., 2006). All subsequent experiments were carried out using solutions that have pH 7.0.

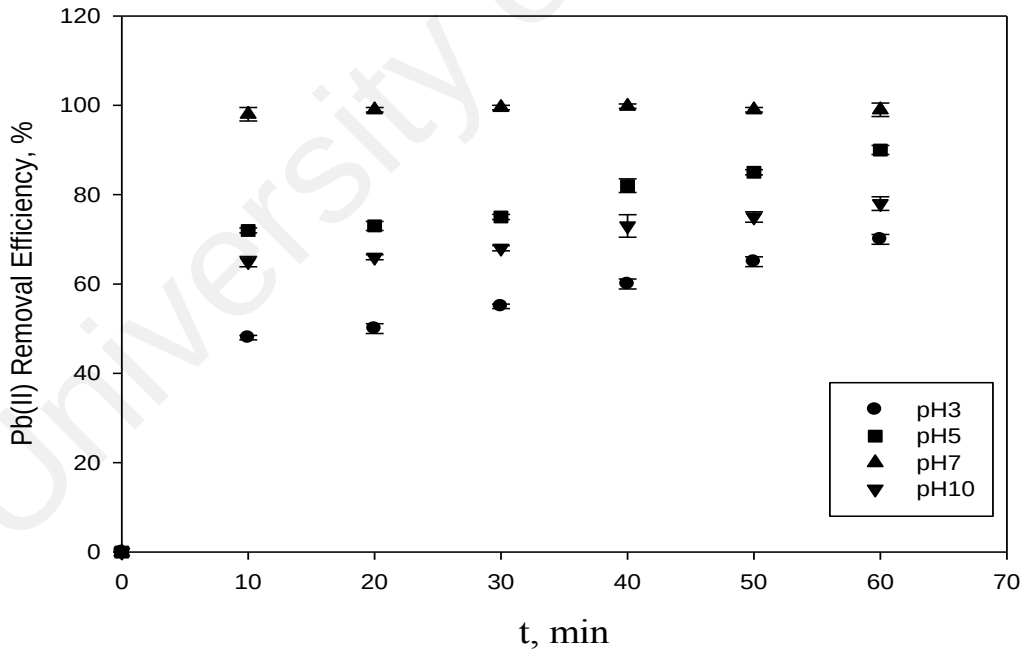

Figure 4.5: Effect of pH on Pb (II) removal by solar photovoltaic electrocoagulation (C_{Pb} = 5mg/L, current density = 0.81 mA/cm^2, agitation = 250 rpm)

4.3.4 Effect of current density

The optimum current density provides enhanced control of electrocoagulation and improves current efficiency and energy cost. In this study, we varied the current density of the perforated Zn electrode between 0.161 to 1.61mA/cm^2 (0.01 to 1.0 A) to determine the optimum range for Pb(II) removal. The pH of the solution was maintained at 7.0. Figure 4.6 shows that the Pb(II) removal efficiency increased as the current density increased. High current density is associated with higher coagulant and hydrogen bubble generation with smaller sizes at the cathode, thus leading to an efficient Pb(II) ion removal via flocculation (Kobya et al., 2005). The highest Pb(II) removal efficiency of 78% at the lowest current density of 0.161mA/cm^2 was obtained only after at least 1 h of treatment, whereas a removal efficiency of 99.9% was achieved at the highest current density of 1.61mA/cm^2 within the first 10 min of treatment.

However, the high current density resulted in higher sludge production. The higher current density was also responsible for the passivation of cathode because of intensive hydroxide anion production. During treatment, hydroxide anions formed a thick turbid sludge in the solution, thus increasing the applied voltage as well as the energy consumption. An optimum current density is recommended to prevent the excessive oxygen evolution and reduce other undesirable effects, such as heat generation (Daous & El-Shazly, 2012; El-Ashtoukhy et al., 2008). The current density of 1.13mA/cm^2 was selected for further experiments because it facilitates a high Pb(II) removal efficiency within a short period of time and at a reasonable operation cost.

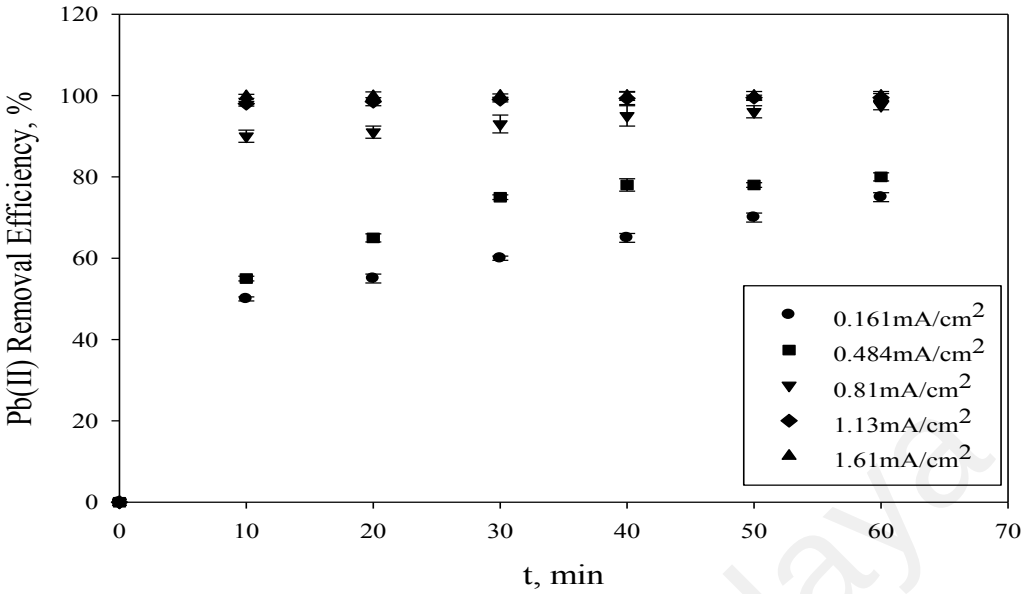

Figure 4.6: Effect of current density on Pb (II) removal by solar photovoltaic electrocoagulation (C_{Pb} = 5 mg/L, pH = 7.0, agitation = 250 rpm)

4.3.5 Effect of initial Pb(II) concentration

The effect of initial Pb(II) concentration on the performance of solar PV electrocoagulation was determined by varying the initial Pb(II) concentration from 5 to 20 mg/L (Figure 4.7). The current density and treatment time were kept constant at 1.13mA/cm^2 and 60 min, respectively. The results showed that the removal efficiency slightly decreased as the initial Pb(II) concentrations increased. The highest Pb(II) removal was achieved at 5 mg/L of initial Pb(II) concentrations. This is due to the fact that increasing Pb(II) concentration enhances concentration polarization via adsorption on the anode and cathode, thus resulting in the decrement of Zn dissolution rate at the anode and the hydrogen gas evolution at the cathode (Daous & El-Shazly, 2012). A similar observation for Pb(II) removal had been made by Assadi et al. (2015). Furthermore, this outcome was anticipated based on the theory of dilute solutions, which states that a longer time is required to remove higher Pb(II) concentrations from the

solution due to the formation of a diffusion layer within the vicinity of the electrode, thus resulting in a slower reaction rate. The diffusion layer did not affect the rate of diffusion as well as the migration of metal ions to the electrode surface in more concentrated solutions (Bazrafshan et al., 2012).

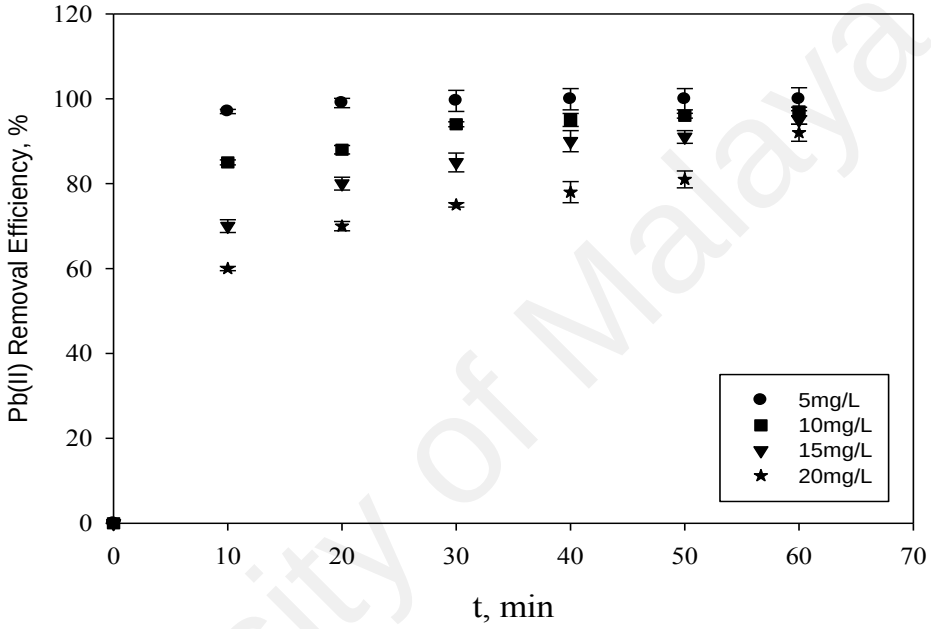

Figure 4.7:Effect of initial Pb (II) concentration on Pb (II) removal efficiency of solar photovoltaic electrocoagulation (pH = 7.0, current density = 1.13 mA/cm^2, agitation = 250 rpm)

To observe the relationship between initial Pb(II) concentration and time, the kinetic analysis for the removal of Pb(II) ions was studied by varying the Pb(II) concentrations from 5 mg/L to 20 mg/L. The experimental data fit very well into the pseudo second-order model. A dramatic reduction in the Pb(II) concentration was observed within the first 10 min at 5 mg/L of Pb(II) concentration (Figure 4.8). However, the concentration reduction was mitigated by increasing the treatment duration above 30 min, especially at high Pb(II) concentration. The results demonstrated that increasing the Pb(II)

concentration decreased the removal rate of Pb ions. It was observed that, longer treatment duration is required to achieve complete depletion of high initial Pb(II) concentration. The kinetic rate constant increased from 0.112 to 0.776 min^{-1} as the initial Pb(II) concentration decreased from 20 mg/L to 5 mg/L (Table 4.5).

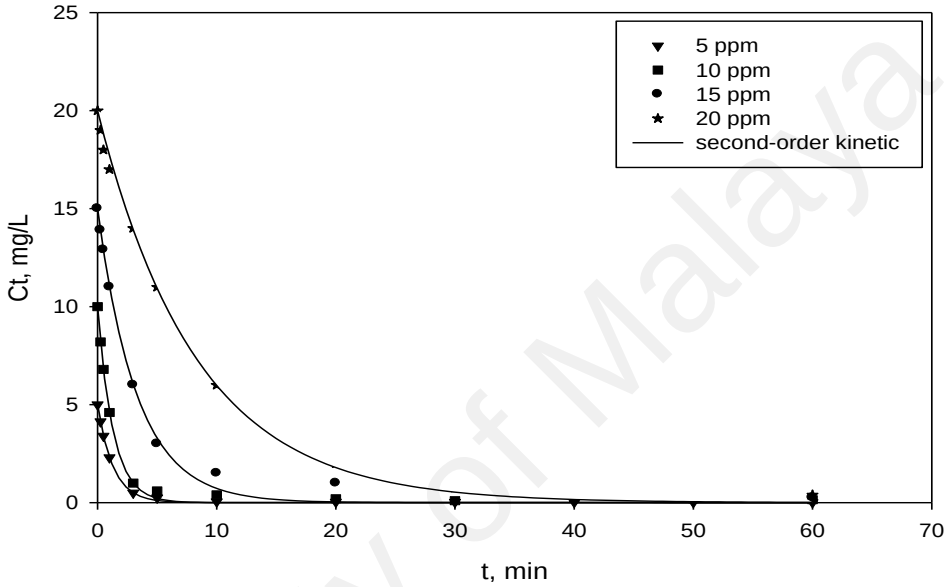

Figure 4.8: Effect of initial Pb (II) concentration on Pb (II) removal efficiency in solar photovoltaic electrocoagulation process (pH = 7.0, current density = 1.13 mA/cm^2, agitation = 250 rpm)

Table 4.5: Pseudo second-order removal rates of Pb(II) ions at different initial concentrations

Concentration of Pb(II) ions (mg/L)	Kinetic rate constant, K_2 (min^{-1})	R^2
5	0.776	0.9997
10	0.751	0.9985
15	0.303	0.9961
20	0.112	0.9822

4.3.6 Surface characterisation

Figure 4.9(a) and (b) present the microscopic images of the surface morphology of electrode materials. The images show that the Zn electrode features a smooth surface before treatment. The EDAX analysis (Figure 4.10) confirms that the Zn electrode exhibits a higher Zn content. The image of electrode after the treatment indicates the presence of ultrafine $Zn(OH)_2$ particles on the rather coarse electrode surface. Visible dents are also observed around the centre of the active sites of $Zn(OH)_2$ generation as a result of Zn electrode dissolution.

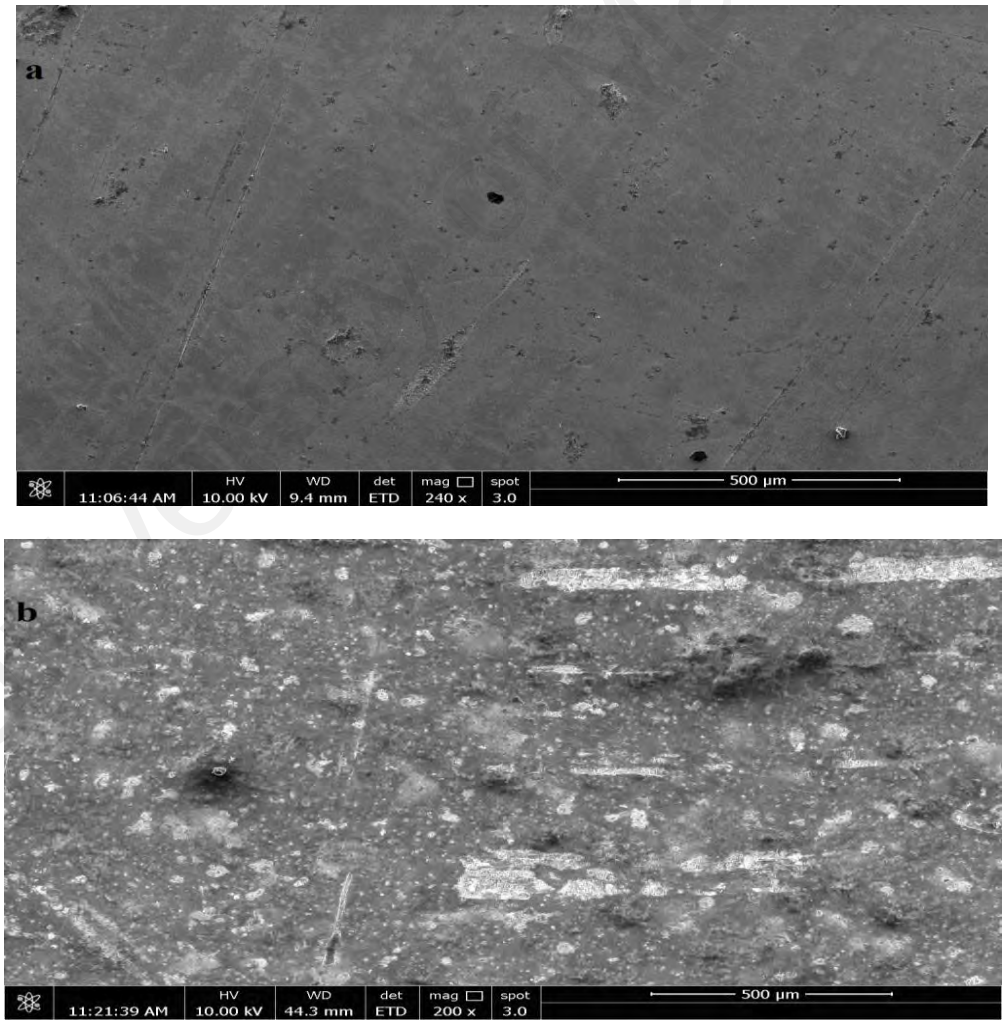

Figure 4.9: FESEM images of perforated zinc electrode (a) before and (b) after treatment

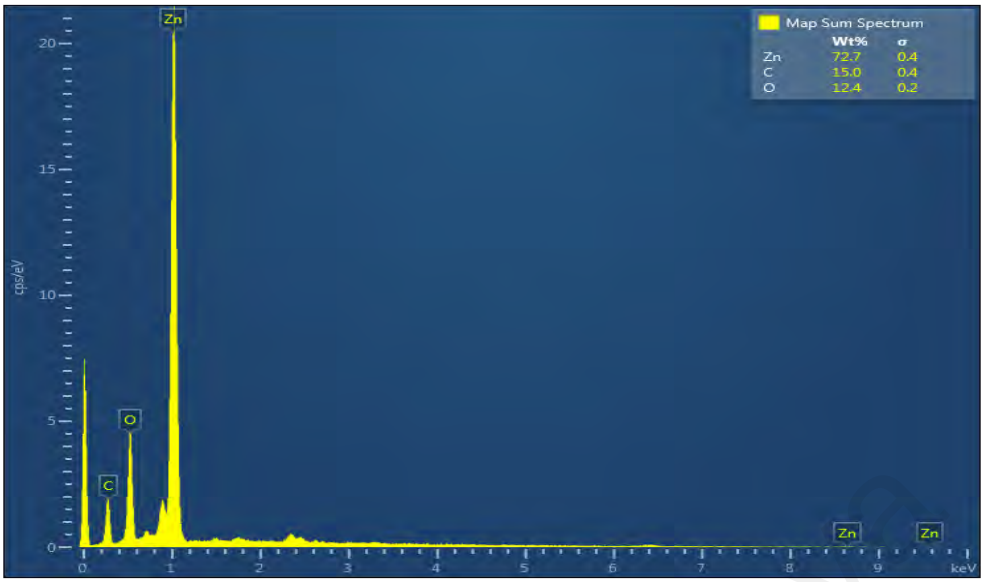

Figure 4.10: EDX elemental composition of zinc electrode before electrocoagulation

Figure 4.11 shows the EDX analysis data on the elemental constituents of sludge after electrocoagulation treatment. The analysis of sludge after treatment indicates the presence of Pb, Zn, C and O in the spectrum. This result confirms that Pb ions were adsorbed onto $Zn(OH)_2$. Figure 4.12 displays the XRD analysis results, which indicate a high peak at 36° to 43°, thus confirming the presence of zinc oxide. Other compound that appears in the image is zinc hydroxide carbonate which shows a peak at 39° to 70°.

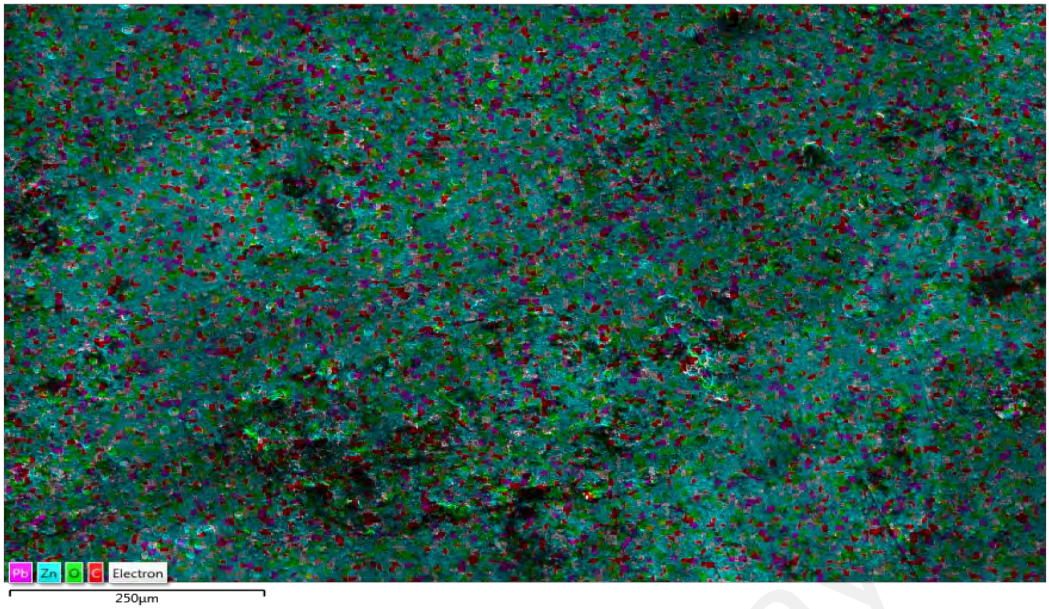

Figure 4.11: EDX elemental composition of sludge after electrocoagulation.

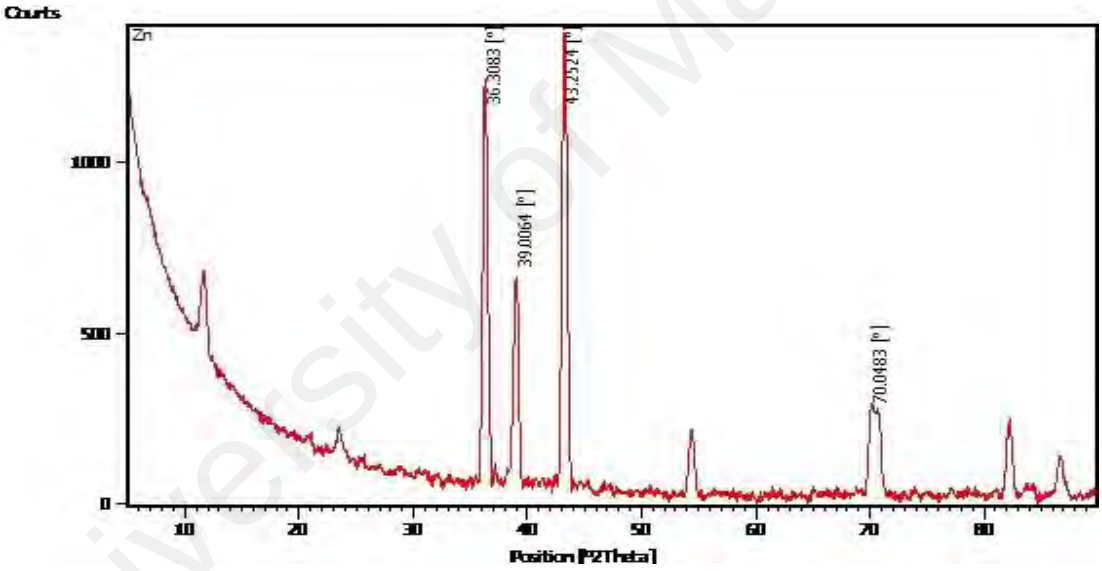

Figure 4.12: XRD image of sludge produced after treatment

4.4 Adsorption

4.4.1 Properties of oil palm shell activated carbon

Figure 4.13 shows the FESEM image of OPSAC. It can be observed from the surface morphological features that the OPSAC is a highly porous material, which is characterised by spongy and irregular-shaped particles. The pore size ranges between micro (<2 nm) to macropores (>50 nm).

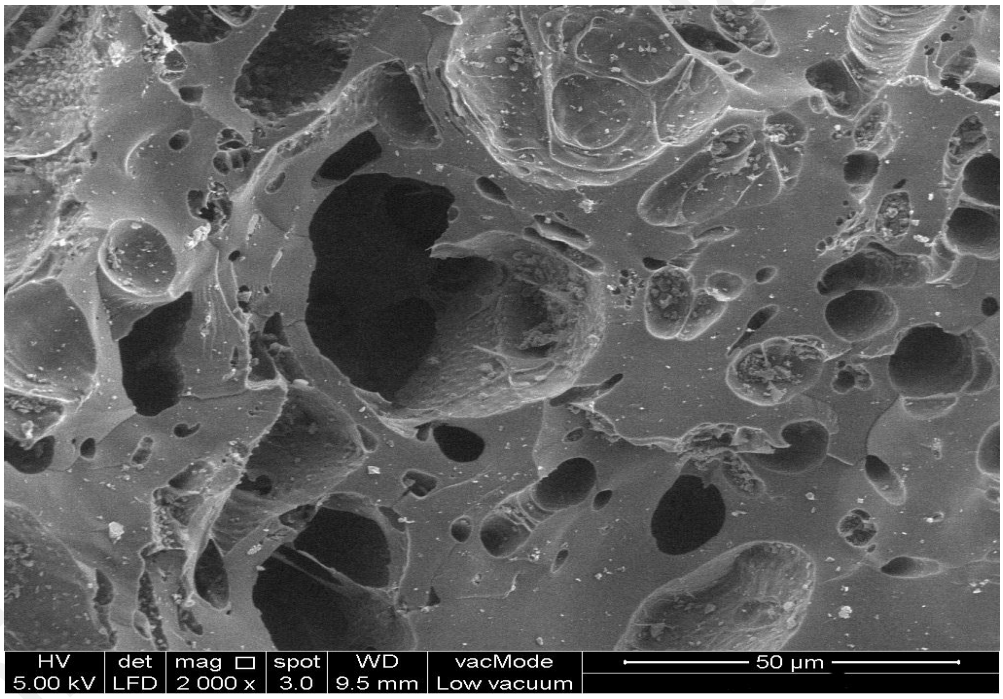

Figure 4.13: FESEM image of the oil palm shell-based activated carbon

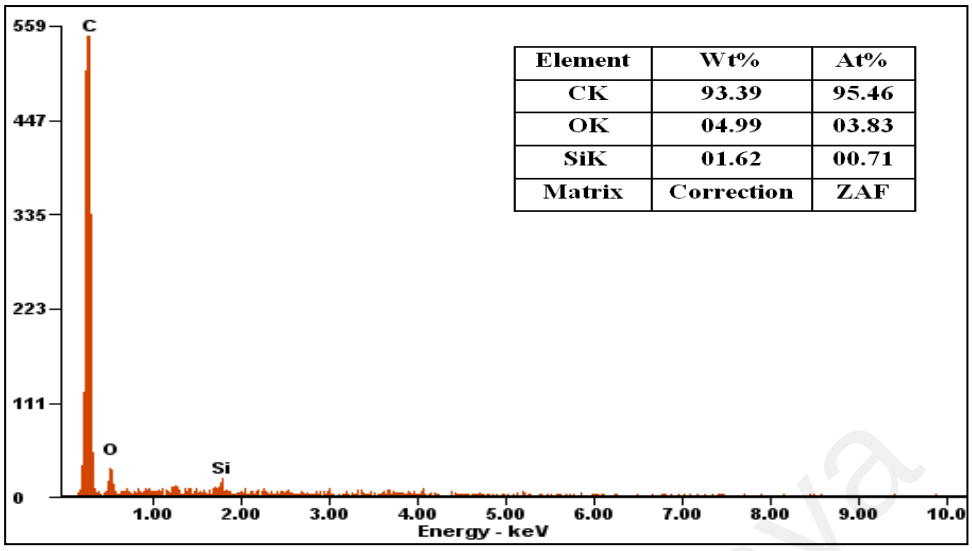

Figure 4.14: EDAX image of the oil palm shell-based activated carbon

Figure 4.14 shows EDAX analysis of the fresh OPSAC before treatment. The result indicates that carbon is the major element, whereas oxygen and silica are the minor constituents present in the adsorbent. Their features can be observed at 0.5-2.0keV as shown in Figure 4.14.

Figure 4.15 illustrates the nitrogen adsorption-desorption isotherms of the OPSAC. Based on the International Union of Pure and Applied Chemistry (IUPAC) classification, an OPSAC material corresponds to type I and IV isotherms. The results indicate that at the low relative pressure region (< 0.05), a steep adsorption of nitrogen corresponding to the isotherm of type I was observed, thus it is attributed to the presence of micropores. Furthermore, in the range between 0.3 and 0.6 of relative pressure, a slim and long hysteresis loop was observed, which corresponds to type IV isotherm. This is associated with the presence of micro and mesopores. The type of hysteresis loops of OPSAC is identified as type H4 according to the IUPAC classification. These characteristics correspond to the hysteresis loops with adsorption and desorption isotherms parallel to each other and almost horizontal branches, and is always related to narrow slit-like pores

which includes pores in the micropore region. The BET pore volume and surface area of OPSAC are given in Table 4.6. Surface area play a dominant role in the removal of heavy. In the adsorption process of Pb(II), the metal ion is attached to the active sites on the surface of adsorbent whereby it then diffuses into the pores. The pore volume effect on adsorption is because of the Pb(II) ion size which restricts the penetration into the structure of the pore. Therefore, the adsorption gets larger with the surface area and pore volume of the adsorbent. The analysis confirms that OPSAC adsorbent has a specific BET surface area of 1092.90m^2/g. The high specific surface area of the adsorbent can provide more adsorption sites, hence increasing the removal efficiency (Hu et al., 2017). The inset in Figure 4.15 shows that the distribution of pore width was at 12Å (1.2 nm), proving that OPSAC mainly consists of micropores. This wide range of pore width is considered sufficient to provide an effective active surface for the adsorption to take place, which is utilized to remove metal ions from aqueous solutions. As illustrated in Table 4.6, from the t-Plot analysis, OPSAC mostly contains micropores with 889.91m^2/g. The micropore area has contributed approximately 77% of the total pore area. OPSAC has an average pore diameter of 1.815 nm and total pore volume of 0.354cm^3/g. The pore size distribution enables it to adsorb metal molecules like Pb(II) ions. The Pb(II) ion has high electronegativity, large ionic radius (0.132 nm) and high atomic weight (207.2 g/mol). Thus, the attraction force between Pb(II) ions and binding sites of the adsorbent will be increased (Putra et al., 2014).

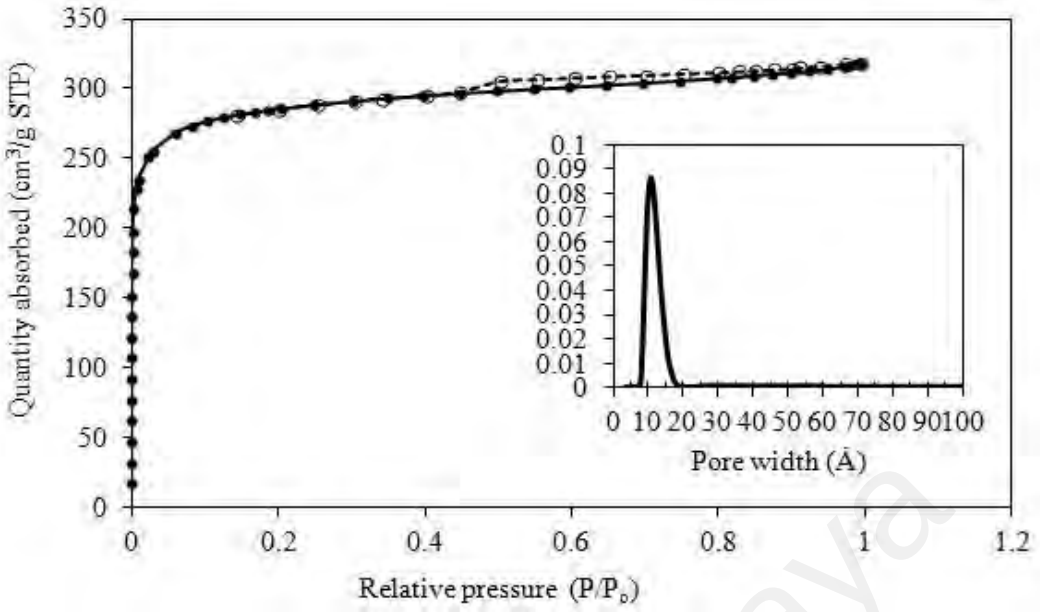

Figure 4.15: Nitrogen adsorption-desorption isotherms of the OPSAC

Table 4.6: Properties of the oil palm shell-based activated carbon

Parameters	Values
BET surface area (m^2/g)	1092.90
Micropore (m^2/g)	889.91
Pore volume (cm^3/g)	0.354
Average pore diameter (nm)	1.815
Particle size (μm)	765.65
pH_{PZC}	8.0

4.5 Adsorption kinetics

The effects of treatment time, initial Pb(II) concentration, solution pH, temperature and adsorbent dosage on the adsorption of Pb(II) onto OPSAC was investigated through a series of experiments with the aim to determine the optimum process conditions for adsorption kinetics.

4.5.1 Effect of treatment time and initial Pb(II) concentration

The effect of treatment time on Pb(II) removal by the OPSAC was studied at different initial Pb(II) concentrations and the results are presented in Figure 4.16. The results indicate that after 15 minutes of contact time, the Pb(II) ions quickly reach complete depletion at the lowest initial Pb(II) concentration of 10 mg/L. The adsorption capacity and Pb(II) removal efficiency is 4.89 mg/g and 99.1%, respectively. After this time, there was no significant increase in the adsorption of Pb(II). Based on the results, it is evident that the adsorption of Pb(II) increases progressively with respect to treatment time. When the Pb(II) initial concentrations are 30 and 50 mg/L, the adsorption reaches a plateau after 30 minutes of the treatment resulting in a Pb(II) removal efficiency of 97.6 and 96.3%, respectively. This indicates that when greater amount of Pb(II) is present in the solution, a longer time is needed to reach the equilibrium state. The observed behaviour can be described by the fact that the adsorption process is quicker when the number of active sites obtainable is much superior than the amount of metal ions that can be adsorbed. Additional significant characteristic is that the achievement of equilibrium is due to the the restricted mass transfer of liquid solution to the outer surface of the adsorbent, also by a deliberate mass transfer inside the activated carbon particles (Acharya et al., 2009; Cechinel et al., 2014). Bartczak et al. (2013) and Deiana et al. (2014) observed a similar trend, whereby the removal efficiency increases rapidly with increasing contact time at the earlier stage of treatment time (Bartczak et al., 2013; Deiana et al., 2014). Later, the removal efficiency remains almost constant once a certain treatment time is reached. This is because the adsorbent is saturated.

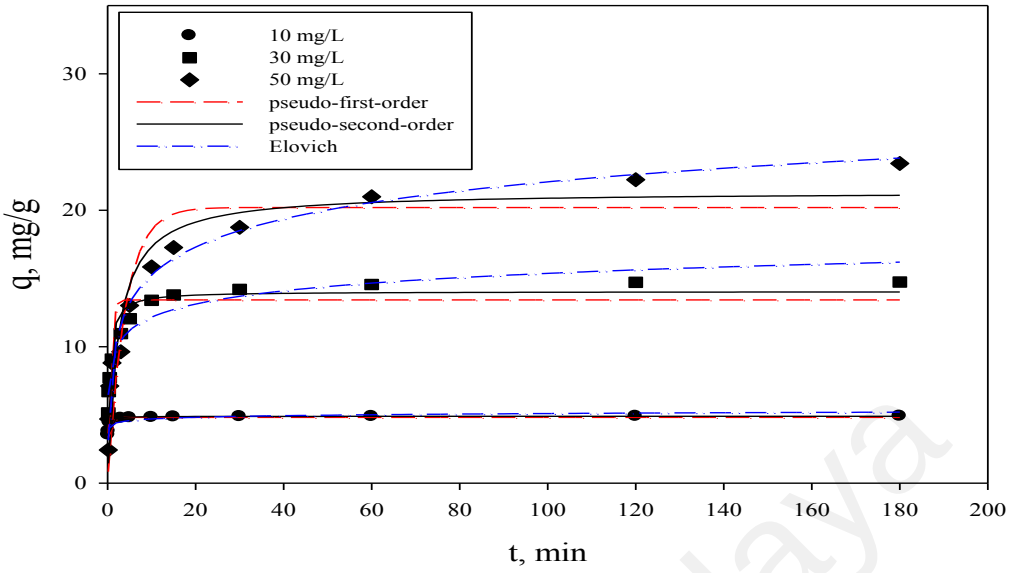

Figure 4.16: Kinetics of Pb(II) removal by palm shell based activated carbon at various Pb(II) concentrations and a constant temperature of 28°C

To analyse the kinetic mechanisms of Pb(II) adsorption, three models were used to fit with the experimental data: pseudo-first-order kinetic model, pseudo-second-order kinetic model and Elovich model. The kinetic parameters are listed in Table 4.7. It is identified that the pseudo-second-order model describes the Pb(II) adsorption kinetics very well, having the highest value of correlation coefficient. Error analysis using NSD and ARE was further applied on pseudo-first and pseudo-second order to validate the best fitting model to represent the kinetics of Pb(II) adsorption onto OPSAC. The value of this error analysis for the Pseudo-first order and Pseudo-second order is compared in Table 4.8. The equilibrium capacity values (q_e) obtained from the pseudo-second-order model align with those obtained from experiments (q_{exp}), unlike the results predicted using pseudo-first-order and Elovich models. The highest adsorption rate constant (k_1), which is 3.174 g/mg·min, is obtained at the lowest initial Pb(II) concentration (10 mg/L), since the availability of adsorption sites on the activated carbon surface is sufficiently high to eliminate more than 99.1% of Pb(II) from the aqueous solution.

Table 4.7: Kinetic model parameters for Pb(II) adsorption

		Pseudo-first order			Pseudo-second order			Elovich equation		
C_0, (mg/L)	q_{exp}, (mg/g)	k_1 (min)	q_e (mg/g)	R^2	k_2 (g/mg min)	q_e (mg /g)	R^2	A	b	R^2
10	4.91	6.96	4.81	0.996	3.174	4.896	0.999	0.70	1.00	0.799
30	14.73	1.859	13.42	0.952	0.184	14.04	0.984	0.97	0.75	0.763
50	23.42	0.250	20.19	0.937	0.020	21.37	0.968	1.40	0.50	0.777

Table 4.8: Error analysis of kinetic model

	Pseudo-first order		Pseudo-second order	
C_0, mg/L	NSD	ARE	NSD	ARE
10	0.570	0.152	0.082	0.022
30	2.571	0.685	1.361	0.363
50	3.974	1.059	2.536	0.676

The intra-particle diffusion model by Weber and Morris was used to decide on the adsorption kinetic process' rate limiting step. The time dependent intra-particle diffusion of the components is represented by this model. The adsorption kinetic is generally under the control of different diffusion mechanisms. The initial region relates to rapid external adsorbate diffusion in the boundary layer (Szlachta & Chubar, 2013). Whereas, the second region (gradual adsorption stage) is attributed to intra-particle diffusion. The equilibrium plateau region (final adsorption stage) indicates that intra-particle diffusion begins to slow down because of the low concentration in solution and lower availability of adsorption sites (Cestari et al., 2005). According to Toor & Jin (2012), intra-particle diffusion is involved in adsorption reaction if the plot of *q (mg/g)* versus the square root of time ($t^{1/2}$) results in a straight line that cuts across the origin (Toor & Jin, 2012). However, if the plot is multi-linear and does not cut across the origin, this would mean that there is a combination of two or more diffusion mechanisms which affect the adsorption process (Szlachta & Chubar, 2013).

In this study, the plots for intra-particle diffusion model are multi-linear and are split into three regions (Figure 4.17). The first region corresponds to boundary-layer diffusion in which the external volume is transferred to the adsorbent's surface and the Pb(II) ions are adsorbed rapidly in this region (Abbaszadeh et al., 2016). The intra-particle diffusion rate constant K_{ind-1} is high within this region, with a value of 7.939-13.310 mg/(g $min^{0.5}$) (Table 4.9). The second region corresponds to intra-particle diffusion from the Pb(II) ions to the internal sites of the adsorbent, whereby the K_{ind-2} values fall within a range of 0.187-3.341 mg/(g $min^{0.5}$), and are lower than those in the first region. In the third region, however, the adsorption becomes very slow and stable, nearing equilibrium with maximum adsorption. The K_{ind-3} values are close to zero and therefore, these values are excluded from the table. Unlike this study, Coelho et al. (2014) and Abbaszadeh et al.

(2016) obtained only two regions in their investigation of Pb(II) removal by cashew nut and papaya leaf-based adsorbent, respectively (Abbaszadeh et al., 2016; Coelho et al., 2014). Table 4.9 illustrates the data of boundary layer thickness, determined from the intercepts of plots I_1 and I_2. The extrapolated lines do not cut across the origin, indicating that there is an intra-particle diffusion during Pb(II) adsorption and it is not the only rate-limiting step (Figure 4.17). Moreover, the negative intercept values indicate that the effect of boundary layer is near to minimum.

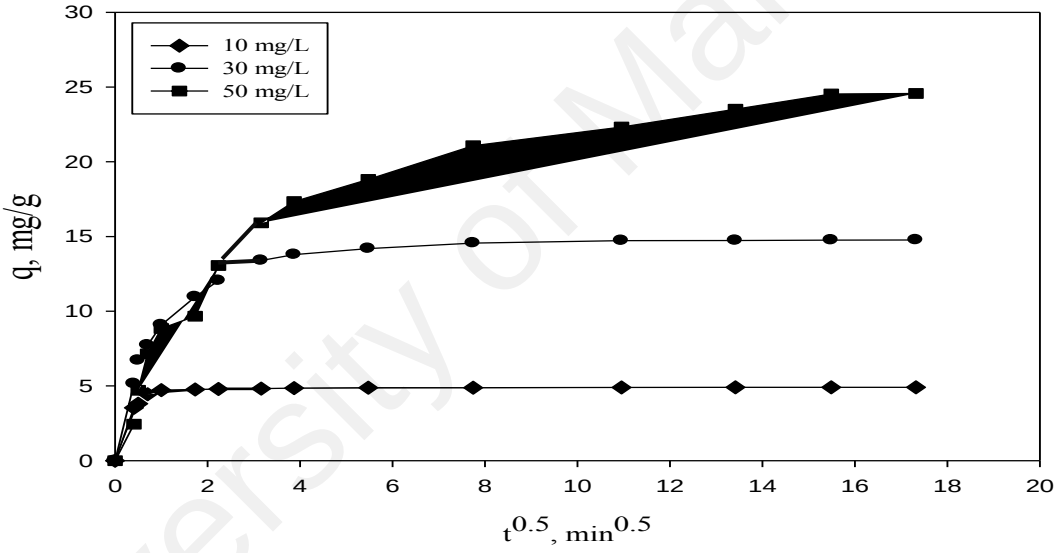

Figure 4.17: Weber and Morris intra-particle diffusion plots 28°C

Table 4.9: Parameters of intra-particle-diffusion model

C_0, mg/L	K_{ind-1}	I_1	R^2	K_{ind-2}	I_2	R^2
10	7.939	0.0464	0.988	0.187	4.412	0.976
30	12.15	-0.1438	0.959	2.748	5.615	0.975
50	13.31	-0.005	0.999	3.341	5.958	0.975

4.5.2 Effect of pH

Figure 4.18 shows the speciation profiles of Pb(II) ions as a function of pH, whereby the concentrations were computed using Visual Minteq software version 3.0. When the pH is below 6, about 80% of metal ions appear in the form of Pb^{2+}. This is due to excessive carbon surface protonation which decreases the adsorption of Pb(II). This finding aligns with the results found by Kobya et al. (2005). At high pH values, formation of $Pb(OH)^{+}$ and $Pb(OH)_2$ can be observed (Kobya et al., 2005). In addition, when the pH exceeds 7, precipitation occurs due to Pb(II) ion association with OH^- ions of the basic solution, forming lead hydroxides which decrease the rate of adsorption and thus increase the Pb(II) removal efficiency (Bouchelkia et al., 2016; Cechinel et al., 2014). Trace amount of other Pb species such as $Pb(NO_3)_2$ (aq), $Pb_4(OH)^{+}$ and $Pb_2(OH)^{3+}$ are also present in the solution. However, the concentrations do not vary greatly throughout the pH range tested in this study.

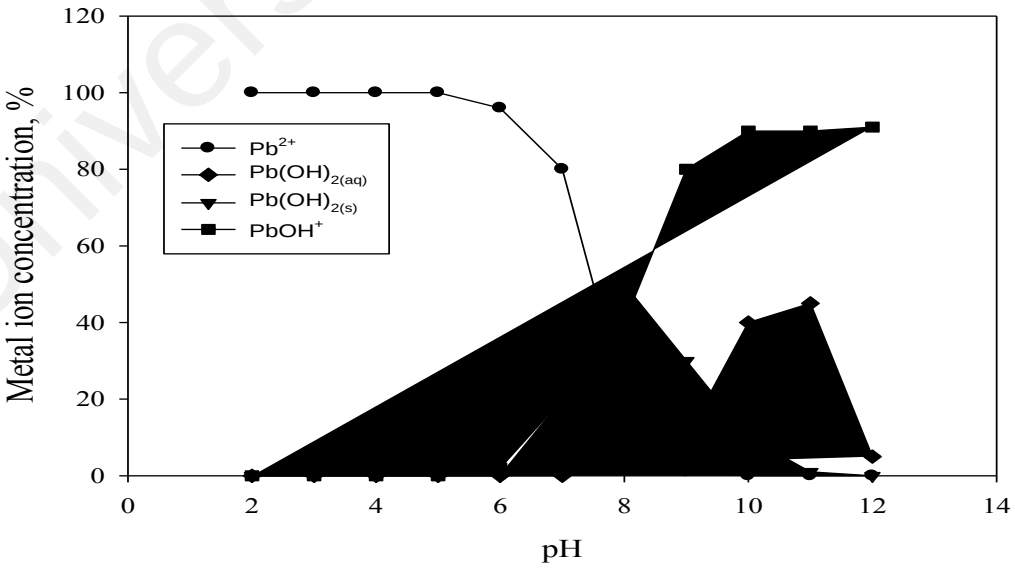

Figure 4.18: Speciation profiles of Pb(II) ions as a function of pH

The effect of pH on the Pb(II) removal efficiency by the OPSAC is illustrated in Figure 4.19. The Pb(II) adsorption is strongly dependent on pH because Pb(II) precipitates in solutions that have pH values higher than 7. The Pb(II) removal efficiency increased from 45 to 99.1% when the pH is increased from 2 to 6. It can be observed that the maximum Pb(II) removal occurs at pH 6 and the efficiency decreases gradually beyond this pH. Momčilović et al. (2011), Moreno-Barbosa et al. (2013) and Erdem et al. (2013) also observed a similar phenomenon using other types of activated carbons. At lower pH values, the Pb(II) removal slows down (Erdem et al., 2004; Momčilović et al., 2011; Moreno-Barbosa et al., 2013). This is due to competition between the Pb(II) and H^+ ions for active sites on the adsorbent surface (Rama Raju et al., 2013). However, this competition weakens at higher pH values, and the Pb(II) ions substitute the H^+ ions to bond with accessible surface functional groups such as –OH and –COOH on the adsorbent surface (Abbaszadeh et al., 2016). Since the Pb(II) ions have a tendency to precipitate at a pH greater than 7, pH 6 is considered to be the appropriate pH for further experiments.

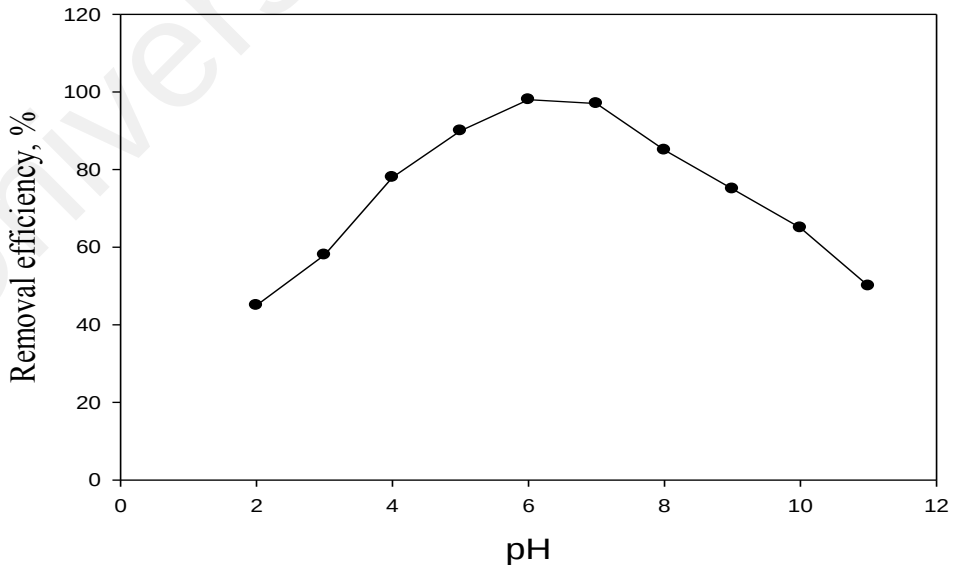

Figure 4.19: Effect of pH on the Pb(II) removal efficiency by oil palm shell-based activated carbon

4.5.3 Effect of adsorbent dosage

Figure 4.20 shows the effect of adsorbent dosage on the Pb(II) removal by OPSAC. It was observed that, increasing the adsorbent dosage from 2 to 8 g/L also increases percentage removal of Pb(II) from 65.5 to 99.8%. However, the equilibrium state had been attained for sorbent dosage higher than 4 g/L. The enhancement of Pb(II) adsorption is because of higher number of active adsorption binding sites available and the availability of a larger surface area for adsorption of Pb(II) (Rama Raju et al., 2013). However, Pb(II) removal efficiency slightly rose (3%) when the dose of adsorbent rose from 4 to 5 g/L. Besides that, the rate of Pb(II) adsorbed on OPSAC remains constant at adsorbent dosage greater than 5 g/L. This indicates that the adsorption of Pb(II) diminishes when the adsorbent dosage exceeds this value. This is due to active sites overlapping at greater adsorbent masses, and resulting in lowered effective surface area needed for adsorption (Asgari et al., 2012).

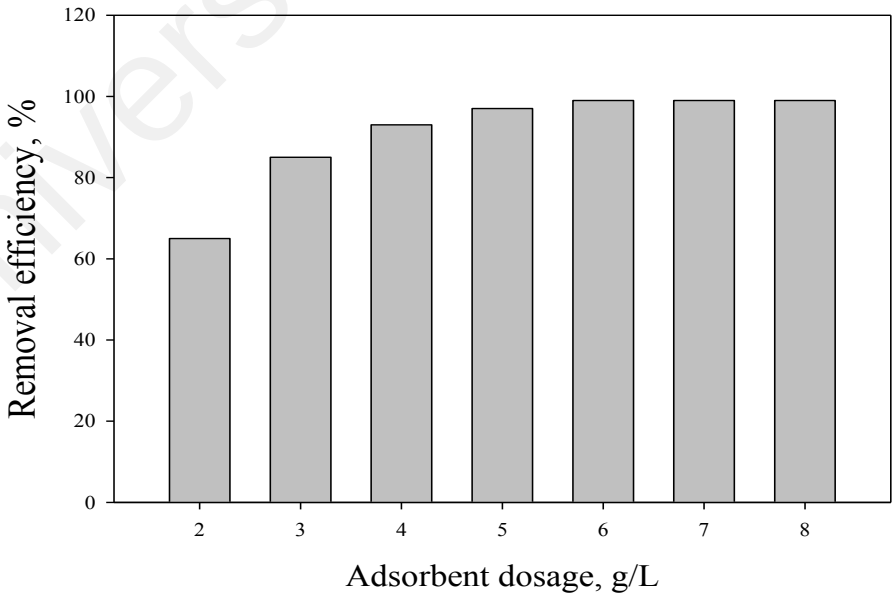

Figure 4.20: Effect of adsorbent dosage on the Pb(II) removal efficiency by oil palm shell-based activated carbon

4.5.4 Effect of temperature

Temperature is an important factor in adsorption process. The effect of temperature on the adsorption of Pb(II) onto OPSAC is shown in Figure 4.21. The enhancement in the adsorption capacity and Pb(II) removal efficiency from 14.21 to 15.25 mg/g and 65.0 to 99.1%, can be observed when the solution temperature increased from 18 to 38 °C. It is clear that higher process temperature enhanced the adsorption rate. The results also indicate that the adsorption process is endothermic in nature. This could be because of increased chemical interactions between the Pb(II) ions and functional groups on the activated carbon surface, which result in chemical adsorption. In addition, this observation could also be attributed to a greater number of adsorption sites created during the process as a result of the breakup of a few internal bonds near the edge of the active surface sites of the sorbent (Abbaszadeh et al., 2016). The higher the temperature of the process, the faster the adsorption equilibrium is obtained. The time required to reach adsorption equilibrium is less than 30 min for the three temperatures investigated in this study.

This observation is consistent with the findings of Acharya et al. (2009) and Mousavi et al. (2010) who reported a higher adsorption of Pb(II) when the temperature rose from 10 to 40°C (Acharya et al., 2009; Mousavi et al., 2010). As mentioned previously, the adsorption process is best illustrated by the pseudo-second-order kinetic model. For this reason, the same model was utilized to evaluate the activation energy. The values of the predicted adsorption capacity (q_e) are in good agreement with those obtained from experiments (q_{exp}) (Table 4.10). A high correlation coefficient is obtained for each temperature. The rate constant rose progressively from 0.005 to 0.012 min^{-1} for 18 to 38°C.

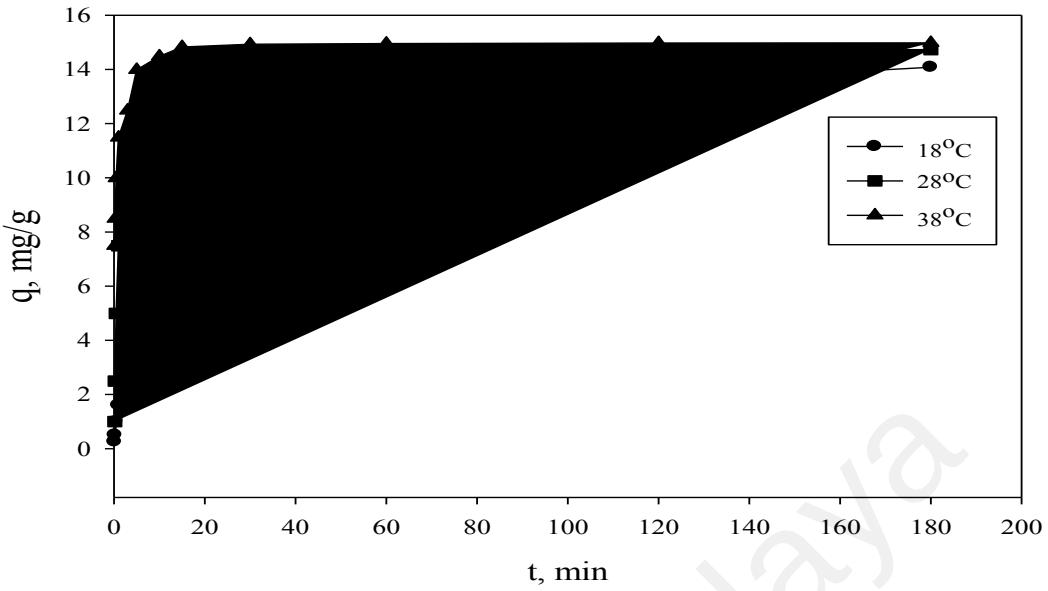

Figure 4.21: Adsorption kinetics of Pb(II) removal by oil palm shell-based activated at various temperatures with a constant Pb(II) concentration of 30mg/L

Table 4.10: Kinetic model parameters for Pb(II) adsorption at different temperature with a Pb(II) concentration of 30mg/L

		Pseudo-second order		
T ^{o}C	q_{exp} (mg/g)	k_2 (g/mg min)	q_e (mg/g)	R^2
18	14.21	0.005	14.18	0.991
28	14.89	0.007	14.73	0.984
38	15.25	0.012	14.97	0.968

These rate constant values were used to calculate the activation energy using the Arrhenius equation. The activation energy of adsorption is the free energy required for the metal ions to adsorb onto the activated carbon. Based on the activation energy data, the assessment of whether a physical or chemical adsorption process is involved in the reaction can be made. The reaction in physical adsorption can be easily reversed and the equilibrium can be attained rapidly. Therefore, a weak intermolecular force is involved that requires only small energy (less than 4 kJ/mol). Whereas, chemical adsorption

requires stronger bonding forces and has a greater E_a value that ranges from 8-800 kJ/mol (Ismaiel et al., 2013). In this study, the activation energy determined for Pb(II) from the slope of $\ln k_2$ versus 1/T (not shown in this paper) is 19.26 kJ/mol, which indicates that the Pb(II) adsorption is a chemical adsorption process.

4.6 Adsorption Isotherms

Equilibrium study is essential in studying adsorption process as it provides an insight into the adsorption isotherms, interactions among metal ions and active sites on the adsorbent surface as well as the adsorbent's capacity to prove its surface capability. In this study, the non-linear Langmuir and Freundlich models were utilized to evaluate the equilibrium data of Pb(II) adsorption onto OPSAC. The adsorption isotherm parameters and correlation coefficients are listed in Table 4.11. The Langmuir isotherm assumes that all available active sites are comparable and that there is no preference on one over the other, and optimum adsorption happens because of the saturated monolayer of metal ions on the adsorbent surface (Abbaszadeh et al., 2016). The adsorption energy is assumed to be constant and there is no adsorbate movement on the surface. The Langmuir equilibrium constant *b* indicates the adsorption energy and reflects the adsorptive material affinity for the solute. A higher *b* value results in a steeper isotherm slope, which suggests that there is a higher metal-ligand bond stability. The Freundlich isotherm, however, is applicable for highly heterogeneous surfaces and an adsorption isotherm that lacks a plateau region is indicative of multi-layer adsorption. An *n* value lower than 1, indicates a normal Freundlich isotherm, whereas an *n* value greater than indicates cooperative adsorption. In this study, the *n* values are within the range of 0.57-0.63, which indicate a normal Freundlich isotherm. In this study, the adsorption of Pb(II) shows an ascending trend, followed by a plateau region at higher equilibrium adsorbate concentrations (Figure 4.22).

The maximum adsorption of Pb(II) occurs at pH 6 and the adsorption capacity decreases beyond this pH. This is due to the electrostatic interactions between the adsorbent surface and Pb molecules present in the solution. The results obtained in this study show that the equilibrium values are well fitted by the Langmuir isotherm model with higher correlation coefficients (Abbaszadeh et al., 2016). In addition, the RMSE values and χ^2 tests are lower for the Langmuir model compared to the Freundlich model. The high adsorptive capacity of the adsorbent was 58.05 mg/g at pH 6 (Table 4.11). The Langmuir parameter (R_L) has been widely used to determine whether the adsorption process is favourable. According to Ismaiel et al. (2013), the process is favourable if R_L is within the following range: $0 < R_L < 1$. The type of isotherm is linear if R_L is equal to 1 and irreversible if R_L is equal to 0. In this work, the R_L values are within the range of 0.83-0.94, which again indicate that the adsorption isotherm of Pb(II) onto OPSAC is favourable (Ismaiel et al., 2013). A comparison of the maximum adsorption capacities of different types of adsorbents are shown in Table 4.12. These results showed that the competence of OPSAC to eliminate Pb(II) from aqueous solution is normally more effective than other adsorbents reported in the literature.

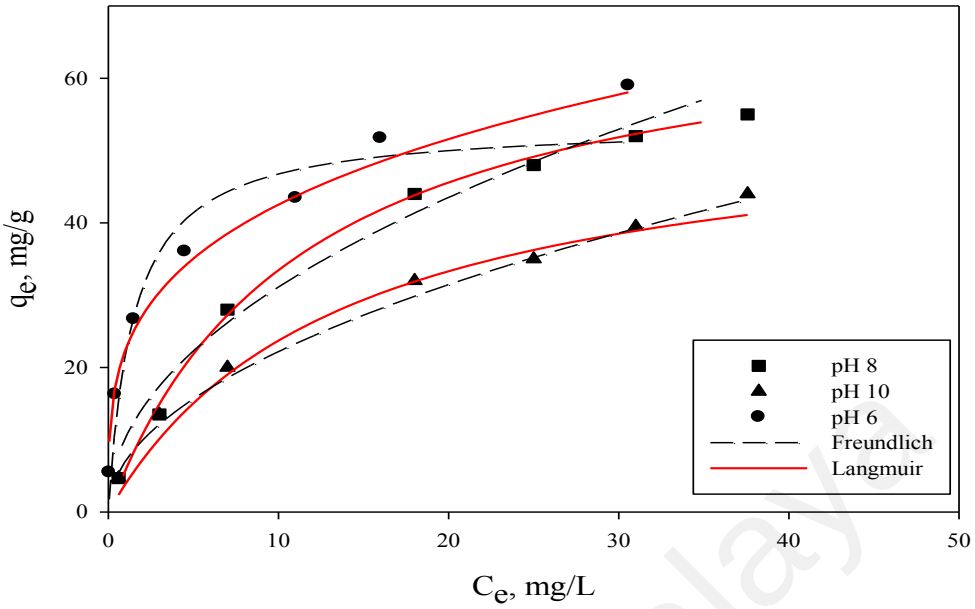

Figure 4.22: Langmuir and Freundlich adsorption isotherm of Pb(II) onto palm shell based activated carbon at pH 6, 8 and 10

Table 4.11: Langmuir and Freundlich isotherm model parameters, correlation coefficient and error analysis for Pb(II) adsorption

	Langmuir isotherm					Freundlich isotherm				
pH	q_m (mg/g)	b (L/mg)	R^2	RMSE	χ^2	K (mg/g) (L/mg)	N	R^2	RMSE	χ^2
6	58.05	0.45	0.999	0.586	0.030	20.447	0.57	0.986	0.686	1.282
8	53.90	0.14	0.987	0.268	0.007	11.66	0.60	0.978	0.414	1.721
10	42.08	0.07	0.978	0.740	0.065	6.91	0.63	0.965	0.868	1.431

Table 4.12: Comparison of adsorption capacity of Pb(II) adsorption by different types of activated carbon

Adsorbents	Adsorption capacity (mg/g)	References
Sugar cane bagasse	7.30	(Lara et al., 2010)
Carica papaya leaf powder	11.30	(Rama Raju et al., 2013)
Pine cone	27.53	(Momčilović et al., 2011)
Walnut wood	41.66	(Ghaedi et al., 2015)
Papaya peel	38.31	(Abbaszadeh et al., 2016)
Oil palm shell	58.05	This study

4.7 Desorption experiment

A promising adsorbent should not only produce high adsorption capacity but should also make the process economically effective by being able to be recycled and recovered. Numerous categories of desorbing agents for instance, HCl, HNO_3 and distilled water were tested for desorption of adsorbed Pb(II) from aqueous solution (Karaoğlu et al., 2013). Based on the experimental results, the recovery of Pb(II) ions can be ranked in the order of HCl > HNO_3 > distilled water, from the highest to lowest recovery rate. As it can be observed, the maximum desorption of Pb(II) ions was 98% with 0.1 M of HCl, while HNO_3 and distilled water exhibited about 78% and 50% of the adsorbed lead ions, respectively. A similar observation had been made by Shekinah et al. (2002) where they proved that the maximum desorption of Pb(II) was achieved using 0.025M to 0.175 M of HCl as the desorption agent (Shekinah et al., 2002). It can be concluded that, the OPSAC is possible to be regenerated and it can be recycled five times.

4.8 Integrated system

The focus of this combination process is to enhance the elimination of Pb(II) ion in the single solar PV electrocoagulation process and adsorption process by improving operating parameter in the integrated system. The influence of various operating parameters on the removal efficiency was also examined. Table 4.13 shows the optimum experimental data from the single electrocoagulation process and adsorption process. The obtained result showed that the highest removal of Pb(II) ion in the solar PV electrocoagulation process was attained at initial Pb(II) concentration of 5 mg/L and at pH 7. Meanwhile, in the adsorption process, the maximum elimination of Pb(II) ion was attained at initial Pb(II) concentration of 10 mg/L and at pH 6. It could be seen that high

removal of Pb(II) was attained at low initial Pb(II) concentration. However, industrial wastewater usually contains high concentrations of Pb(II) within a range of 1–25 mg/L, which is resulted from battery production and electroplating respectively (Wang et al., 2010; Zhou, 2015). Therefore, optimum operating conditions need to be obtained in order to apply integrated system in the industry process. The application of integrated system can be used in industrial applications because it gives several benefits such as low-cost adsorbent, easy to implement, short treatment time, low sludge production, low energy consumption (using solar energy), high removal efficiency and low operation cost (using combination of two methods).

Table 4.13: Comparison of optimum parameters of single electrocoagulation and activated carbon adsorption on the removal of Pb(II)

Parameters	Electrocoagulation	Adsorption
Initial concentration (mg/L)	10	10
Ph	7	6
Current density (mA/m^2)	1.13	-
Adsorbent dosage (g/L)	-	4
Removal efficiency (%)	99.9	99.1

4.9 Screening point of parameters

The purposes of the screening study were to attain the reference information that can be applied for the optimisation study and to determine the effect of individually parameter on the integration process. Three important parameters were used in this experimental design with each parameter being assessed at five dissimilar points. Each point was examined to choose the points that achieved the highest removal efficiency. The optimum data from the single solar PV electrocoagulation process and adsorption process was used

to determine the range of parameter in the integrated process. The operating parameters were optimised by using response surface methodology (RSM) model. Table 4.14 shows the selected range of parameters that were used in the integration process: initial concentration (15-35 mg/L), pH (5-7) and adsorbent dosage (2-4 g/L). Meanwhile, the current density, distance between electrode and stirring rate were remained constant during the integration process.

Table 4.14: Factors and their corresponding levels

Factors	Code/ Symbol	Units	Coded variable level				
			-1	-0.5	0	+0.5	+1
pH	X_1		5.0	5.5	6.0	6.5	7.0
Initial concentration	X_2	mg/L	15	20	25	27.5	35
Adsorbent dosage	X_3	g/L	2	2.5	3	3.5	4

4.10 Experimental Design (Response Surface Methodology)

Response surface methodology (RSM) is one of the approaches applied in the design of experiment, in which it is proven as a powerful and effective technique for process optimisation. The approach used in this technique is reducing the number of experiments while improving the statistical interpretation and locating the accurate optimum parameters. Box &Wilson (1951) was the first researcher that used and developed this RSM by as a regression method to explore the correlation between some explanatory factors and one or more responses (Box & Wilson, 1951). In this study, Design Expert Software trial version 11.0.3 (Stat-Ease, Inc., Minneapolis, USA) was used to improve the mathematical model and estimate the subsequent regression analysis. The software was also used in the analysis of variance (ANOVA) and response surfaces analysis. The parameters that were affected by the efficient removal of Pb were studied via a standard

RSM design which was based on the central composite design (CCD). Employing the CCD method as the experimental design is deemed suitable to fit a quadratic surface with minimum number of experiments in order to enhance the effectiveness of process parameters. In addition, this method also helps to analyse the interaction between these parameters (Arami-Niya et al., 2012). A several of statistical analysis like normal plot, residual analysis, interaction effects, perturbation plot and analysis of variance (ANOVA) were examined to check the precision of the fitted model (Aziz et al., 2016).

In the optimisation experiment, three important process parameters were chosen which included pH, initial Pb(II) concentration (mg/L) and adsorbent dosage (g/L). These parameters were denoted as X_1, X_2 and X_3, respectively. The range and levels of the factors were measured as stated by the experimental design, which is shown in Table 4.15. The coded values for these factors were set at five levels (-1, -0.5, 0, 0.5, 1). CCD designed 17 runs of experiment, including three replicates of experimental runs at the central point to eliminate errors and curvature.

In evaluating the experimental data, the response variable was fitted by a second-order model in the form of quadratic polynomial equation as given by Eq. (4.1)

$$Y = b'_0 + \sum_{i=1}^{n} b_i X_i + \sum_{i=1}^{n} b_{ii} X_i^2 + \sum_{i=1}^{n} \sum_{j>1}^{n} b_{ij} X_i X_j \qquad (4.1)$$

Where Y is the predicted response (efficient level of Pb removal, %) and the b's denote; b'_0 the constant coefficient, b_i the linear coefficients, b_{ij} the interaction coefficients and b_{ii} the quadratic coefficients. x_i, x_j are the coded values or independent factor.

Table 4.15: Experimental design matrix and results

Run order	Actual level of variables			Response (%)	
	X_1	X_2 (mg/L)	X_3 (g/L)	Actual Value	Predicted value
1	5	35	2	68.00	67.47
2	6	25	2.5	95.50	94.78
3	7	35	4	31.00	30.65
4	5.5	25	3	90.00	92.23
5	6	25	3	90.00	89.93
6	6	25	3	92.00	89.93
7	6	25	3.5	89.00	90.52
8	6	25	3	90.00	89.93
9	5	35	4	60.00	59.95
10	6.5	25	3	85.00	83.58
11	6	20	3	83.00	83.11
12	5	15	4	69.00	68.27
13	6	30	3	78.00	78.70
14	7	15	2	60.00	60.00
15	5	15	2	65.00	65.30
16	7	35	2	50.00	50.68
17	7	15	4	50.00	50.47

4.10.1 Development of regression model equation

The correlations between process variables on Pb removal was examined by using CCD. Runs 5, 6 and 8 at the center point were selected to investigate the experimental error. The models were chosen based on the maximum order polynomials where the extra terms were significant, and the models were not aliased in accordance with the sequential model sum of squares. The selection of the quadratic model was recommended by the CCD. The design of this experiment is illustrated in Table 4.15 along with the experimental and predicted results. The highest elimination of Pb was attained approximately at ~96%. A regression analysis was achieved to fit the response function on removal efficiency of Pb (%). The model is described by Eq. (4.1), where the variables are presented by the

following denotations: removal efficiency (Y) as a function of pH (X_1), initial concentration as X_2 and adsorbent dosage as X_3. Based on the experimental results shown in Table 4.15, the second-order polynomial model equation for optimisation was recognised and presented in terms of coded factors.

The final empirical model in terms of coded factors for the efficient level of Pb removal (Y) is given in Eq. (4.2):

$$Y = +89.93 - 8.65X_1 - 4.41X_2 - 4.26X_3 - 2.88X_1X_2 - 3.13X_1X_3 - 2.68X_2X_3 - 36.11X_2^2 \quad (4.2)$$

The negative signs in Eq. (4.2) indicate antagonistic effects, whereas positive signs indicate synergistic effects. A multiple regression analysis technique which was included in the RSM was used to estimate the coefficient in order to better understand the response of the respective variables (Arami-Niya et al., 2012). The fitness of the model was measured from its coefficients of correlation and determination**.** Based on Table 4.16, t and p tests were performed to obtain the significance of the predicted coefficient in the regression model (Equation 4.2). The t test value was attained by dividing each factor with its standard error (SE). According to Rengadurai et al. (2012), larger t value and lowest p value indicate more significant coefficient for the variable. The results of the current study exhibited that the linear factors (X_1, X_2, X_3) and the square factors (X_2^2) were highly significant in the model, followed by the quadratic or interaction factors (X_1X_2, X_1X_3, X_2X_3) that were also extremely significant in the model.

Table 4.16: ANOVA results for response surface quadratic model

Source	Coefficient Estimate	Degree of freedom	Standard Error	t-value	p-value	95% CI Low	95% CI High
Intercept	89.93	1	0.54	235.17	< 0.0001	88.65	91.20
X_1	-8.65	1	0.52	-33.48	< 0.0001	-9.88	-7.41
X_2	-4.41	1	0.52	-3.67	< 0.0001	-5.65	-3.17
X_3	-4.26	1	0.52	2.12	< 0.0001	-5.50	-3.03
X_1X_2	-2.88	1	0.54	-18.67	0.0001	-4.15	-1.60
X_1X_3	-3.13	1	0.54	-8.91	0.0007	-4.40	-1.85
X_2X_3	-2.63	1	0.54	-5.27	0.0018	-3.90	-1.35
X_2^2	-36.11	1	3.53	-6.03	<0.0001	-44.47	-27.75

4.10.2 Statistical analysis

Statistical analysis via RSM was applied to obtain a well-fitted regression model of the efficient level of Pb removal. The experimental data was fitted into linear, interactive, quadratic and cubic models in order to gain the regression equations. The significance of the recommended regression models could be obtained via analysis of variance (ANOVA) estimation method. The excellence of the developed model was assessed according to the correlation coefficient value. The adjusted R^2 (a statistical measure of how close the experimental data are to the fitted regression line) and predicted R^2 (a statistical measure of how well the model is in the prediction of response data) should fall within 0.20 level in order to be considered as a good estimating model.

If the model fails to achieve the 0.20 threshold, it is considered as a weak model with possible problem either in the data or the model itself. The obtained R^2 value in this study was 0.9970, indicating a good agreement between the experimental and predicted values from the models (Arami-Niya et al., 2012). Figure 4.23 shows the predicted efficient removal level through utilising equation (4.2) together with the experimental values. The obtained experimental values were quite close to the predicted values, indicating that the developed model was successful and useful to describe the interaction between the variables and the level of efficient Pb removal (Arami-Niya et al., 2012).

An adequate precision compares the range of the actual values at the design points to the average prediction error. The adequate precision of this study was 54.7957, which was greater than 4 and this indicated an adequate model discrimination. In addition, the coefficient of variation (C.V. = 2.08) for the model was low, thus attaining high precision and good reliability of the experimental values. Analysis of variance (ANOVA) was used

to further justify the adequacy of the model. It is the mean square of the term divided by the mean square of the residual. The F-value generated in the study was considered as very large. In Table 4.15, X_1 (pH), X_2 (initial Pb(II) concentration), X_3 (adsorbent dosage), X_1X_2, X_1X_3, X_2X_3 (interaction term), *and* X_2^2 were all found to be significant model terms. Values which are greater than 0.1000 indicate insignificant model terms. If there are many insignificant model terms (not counting those which are required to support hierarchy), model reduction may need to be conducted to improve the model.

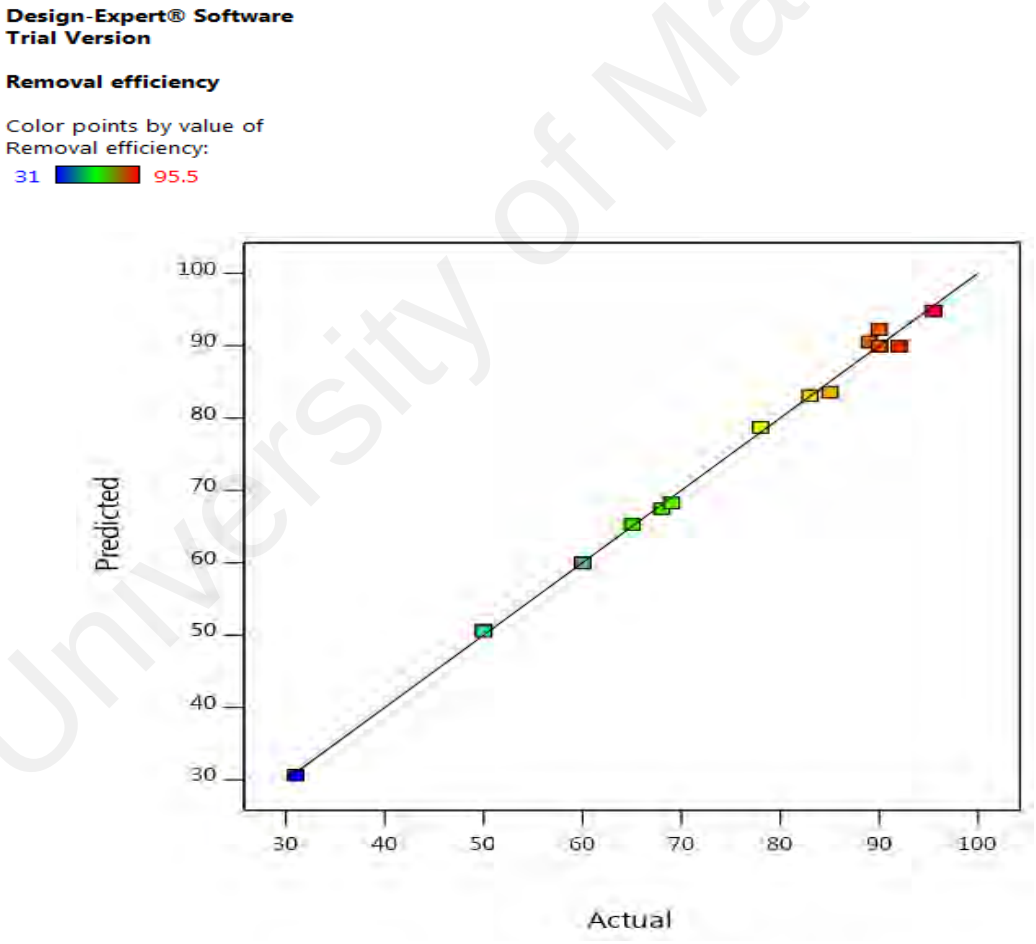

Figure 4.23: The predicted (experimental values) versus actual (measurement values by RSM) on the removal of Pb(II) by integrated system

Analysis of variance (ANOVA) was used to further justify the adequacy of the model. The ANOVA results for the quadratic model of removal efficiency of Pb are summarised in Table 4.17. It could be seen that the *F*-value of the model was 262.74, implying a significant model. *F*-value for a model is used to compare the variance which is related to a particular term of the residual variance (Arami-Niya et al., 2012). It is the mean square of the term divided by the mean square of the residual. The F-value generated in the study was considered as very large. There is only 0.01% chance that a "Model's *F*-Value" could be this large due to extraneous noise. In addition, there was also the probability value which was associated with the *F* value for the terms in this model. It is possible to obtain an *F* value of this size if the term does not have any effect on the response. In general, a term that has a probability value of less than 0.05 will be considered as significant. In this work, the value of "Prob > *F*" was less than 0.05 and this indicated significant model terms (Arami-Niya et al., 2012). In Table 4.15, X_1 (pH), X_2 (initial Pb(II) concentration), X_3 (adsorbent dosage), X_1X_2, X_1X_3, X_2X_3 (interaction term), *and* X_2^2 were all found to be significant model terms. Values which are greater than 0.1000 indicate insignificant model terms. If there are many insignificant model terms (not counting those which are required to support hierarchy), model reduction may need to be conducted to improve the model.

The "Lack of Fit F-value" is the portion of the residual sum of squares which arises due to unfit model and data. It is the weighted sum of squared deviations between the mean response at each factor level and the corresponding fitted value. The value of 13.63 for the "Lack of Fit F-value" implies that the model's Lack of Fit is not relative to the pure error. Non-significant lack of fit is good and shows that the model above is appropriate to predict the efficient level of Pb removal within the range of the variables under study. Perturbation plot helps to compare the effect of all the factors at a particular point in the

design space (Figure 4.24). The response is plotted by changing only one factor over its range while holding another factors constant. A steep slope or curvature in a factor shows that the response is sensitive to the factor. A relatively flat line shows the insensitivity of a particular factor towards any change. From the perturbation plots, it was clear that pH, initial Pb(II) concentration and adsorbent dosage played important roles in achieving the high efficient of Pb removal, in which the interactions between these factors had a significant effect on the responses.

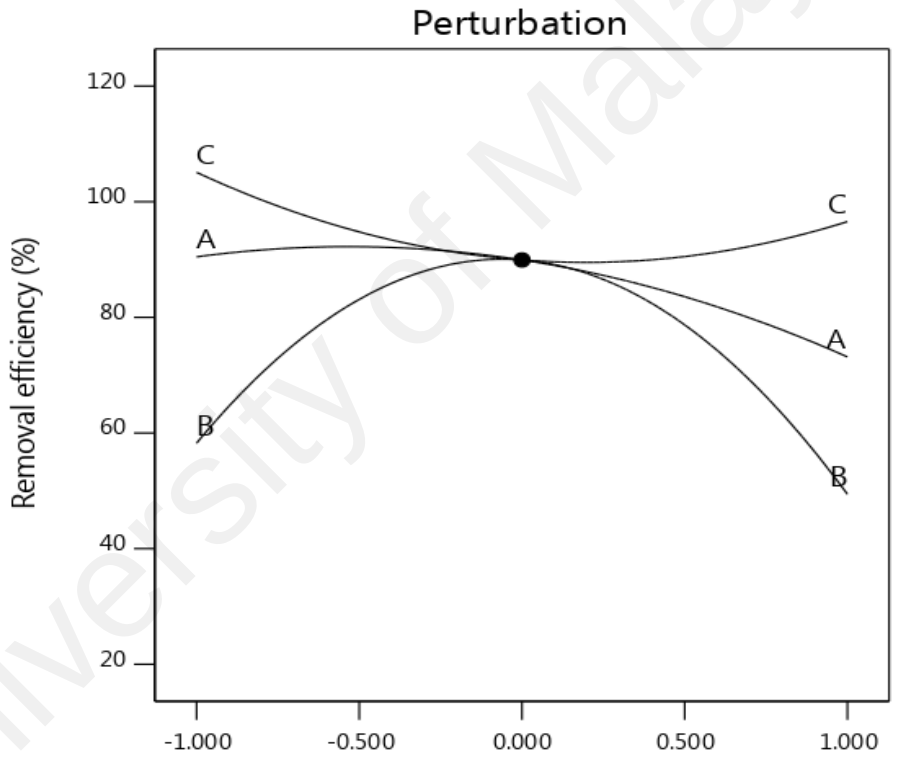

Figure 4.24: Perturbation plot at optimum condition (A: pH, B: Initial Pb(II) concentration, C: Adsorbent dosage)

Table 4.17: Analysis of variance results

Source	Sum of squares	Degree of freedom	Mean square	*F-value*	*P-value*	Suggestion
Model	5506.76	9	611.86	262.74	< 0.0001	Significant
X_1	635.56	1	635.56	272.92	< 0.0001	-
X_2	165.44	1	165.44	71.04	< 0.0001	-
X_3	154.60	1	154.60	66.39	< 0.0001	-
X_1X_2	66.13	1	66.13	28.40	0.0001	-
X_1X_3	78.13	1	78.13	33.55	0.0011	-
X_2X_3	55.13	1	55.13	23.67	0.0018	-
X_2^2	243.15	1	243.15	104.41	<0.0001	-
Residual	16.30	7	2.33			
Lack of Fit	13.63	5	2.73	2.05	0.3602	Not significant
Pure Error	2.67	2	1.33	-	-	-
Std. Dev. [a]	1.53	-	R^2	0.9970	-	-
Mean	73.26	-	Adj. R^2 [b]	0.9933	-	-
C.V. % [c]	2.08	-	Pred. R^2 [d]	0.9781	-	-
Cor Total	5523.06	-	Adeq. Prec [e]	54.7957	-	-

[a] Standard deviation. [b] Adjusted R^2. [c] Coefficient of variation. [d] Predicted R^2. [e] Adequate precision.

4.10.3 Effects of operating variables on removal efficiency of Pb

To examine the influences of the three factors on Pb removal, the RSM was applied, and 3D plots were drawn. According to the ANOVA results attained, pH and initial concentration were obtained to have significant effects on the removal of Pb and the quadratic effects are significant. The 3-D response surface graphs on the efficiency of Pb removal are shown in Figures 4.25-4.28. The CCD model analysis has indicated that the significant interaction between operating variables are A: pH and B: Initial Pb(II) concentration. The relations can be further demonstrated in the contour plot, from Figure 4.26-4.29. Response surface plots of 3-D diagram provide a method to predict the removal efficiency for dissimilar values of the evaluated operating parameters and the contours of the plots give an information to determine the type of interactions between these variables (Montgomery, 2001; Zarei et al., 2010).

It can be seen in Table 4.17 that the individual effects interaction on Pb (II) removal by pH and initial Pb(II) concentration were more superior than adsorbent dosage based on the F-values analysis of 272.92 (pH), 71.04 (initial Pb(II) concentration) and 66.39 (adsorbent dosage). Moreover, the F-value for quadratic effects of pH (5.27) and adsorbent dosage (9.50) were comparable and more pronounced than that of initial Pb(II) concentration (104.41). However, the interaction effect of pH and initial Pb(II) concentration as well as pH and adsorbent dosage was meaningful having F-value of 33.55 and 28.40. Interaction effects of adsorbent dosage and initial Pb(II) concentration show low or insignificant with F-values of 23.63 respectively. Figures 4.25 present the 3-D response surface and contour plot (Figure 4.26) as functions of pH versus initial Pb(II) concentration. As expected, the percentage removal of Pb is higher at the moderate Pb(II) concentrations. The ratio of metal ions over the adsorption surface is low at a moderate

concentration. Therefore, the metal ions quickly stick to the available adsorption sites, resulting in the higher adsorption efficiency (Abbaszadeh et al., 2016). Increment in initial concentration and pH improves the efficiency of Pb removal. However, the elimination of Pb(II) slightly decreases once the initial concentration goes beyond 30mg/L due to the slower coagulation, and settling processes hence triggers down the removal efficiency level. This could be due to the longer time needed to remove Pb at higher concentration, as explained by the theory of dilute solution. In dilute solution, formation of the diffusion layer within the vicinity of the electrode causes slower reaction.

Similarly, at low and high pH values, the elimination of Pb was very low. The highest adsorption of Pb(II) was attained at pH 6.0 (Figure 4.25). The weak adsorption of Pb(II) occurred at low pH value, would be closely related with H_3O^+ ions on active sites of activated carbon and because of repulsive forces would be limited. When increasing the pH levels, more ions with negative charge are exposed with a following rise in attraction for positively charged Pb(II) ions and the adsorption mechanism may be slowly substituted by a chelation mechanism and will increasing the adsorption capacity. The adsorption at pH>7 shows a decreasing trend due to the formation of soluble hydroxyl complexes of Pb(II) such as $Pb(OH)_2$, $PbOH^+$, aqueous $Pb(OH)_2$, and $Pb(OH)^{3-}$, and the activated carbon was declined with the buildup of Pb(II) ions. Comparable trends were investigated for adsorption of Pb(II) ions on activated carbon prepared from papaya peel (Abbaszadeh et al., 2016), maize tassel (Moyo et al., 2013), ulva lactuca (Ibrahim et al., 2016) and glutamate/sepiolite (Karaoğlu et al., 2013).

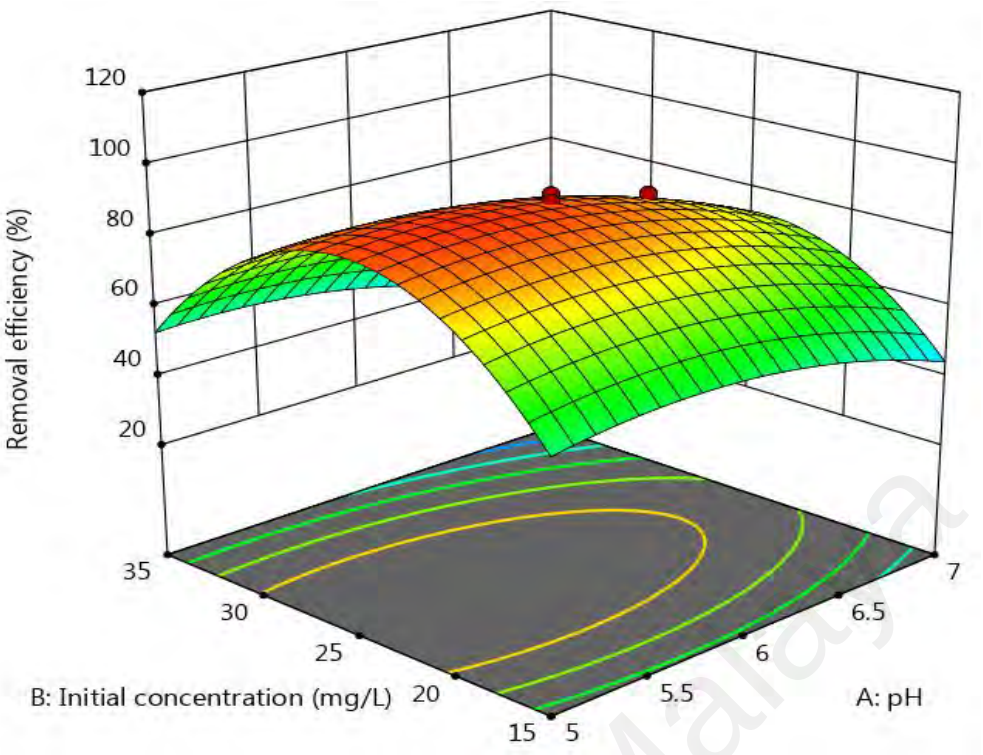

Figure 4.25: The interaction effect between initial concentration and pH at constant adsorbent dosage of 3g/L

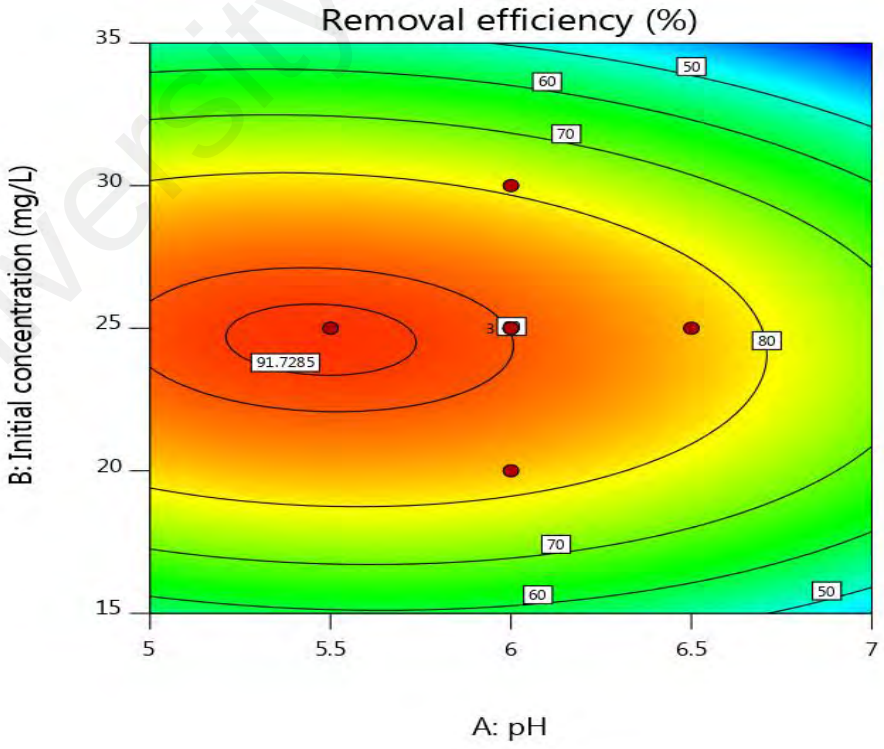

Figure 4.26: Contour plot of Pb(II) removal between pH and initial Pb(II) concentration

Figure 4.27 depicts that the effects of adsorbent dosage and pH on Pb (II) removal at constant initial concentration (25mg/L) and treatment time (20 minutes) and Figure 4.28 shows the contour plot of interaction effect. The increase in adsorbent dosage, produced significantly effect on the removal efficiency. However, the removal efficiency slightly increased when the adsorbent dosage was increased more than 3g/L. With an increase in the adsorbent dosage from 2g/L to 4g/L, the removal of Pb(II) ions increased from 60 to 90%, due to the number of binding sites would be increased. Therefore, in order to save cost of adsorbent material and reduce the cost of treatment process, low amount of adsorbent was selected.

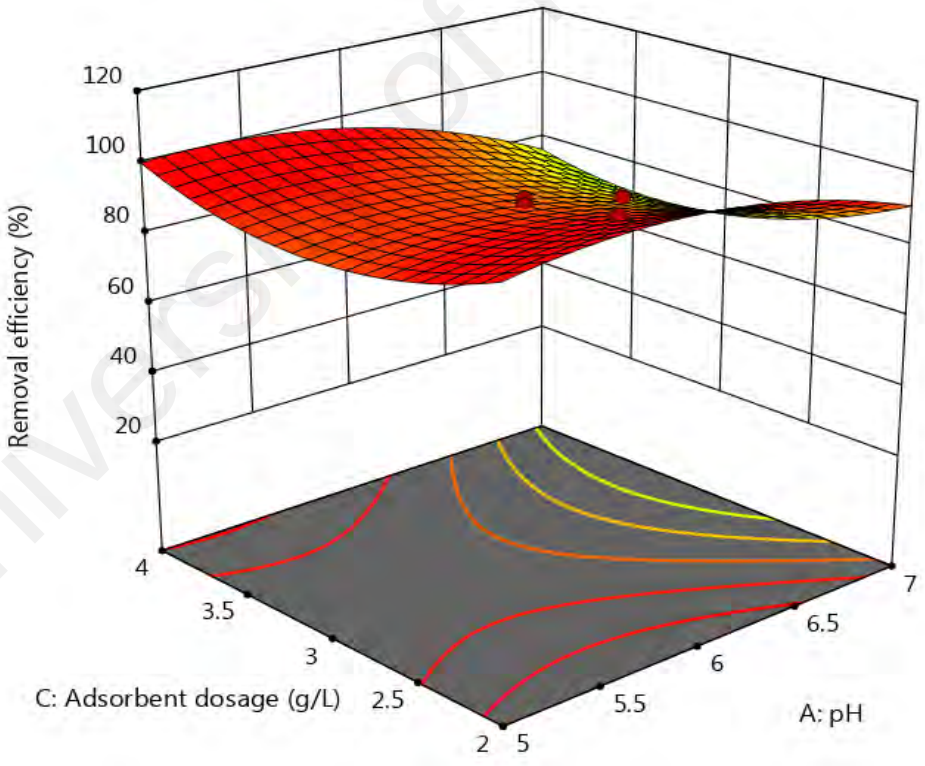

Figure 4.27: The interaction effect between pH and adsorbent dosage at constant initial concentration of 25mg/L

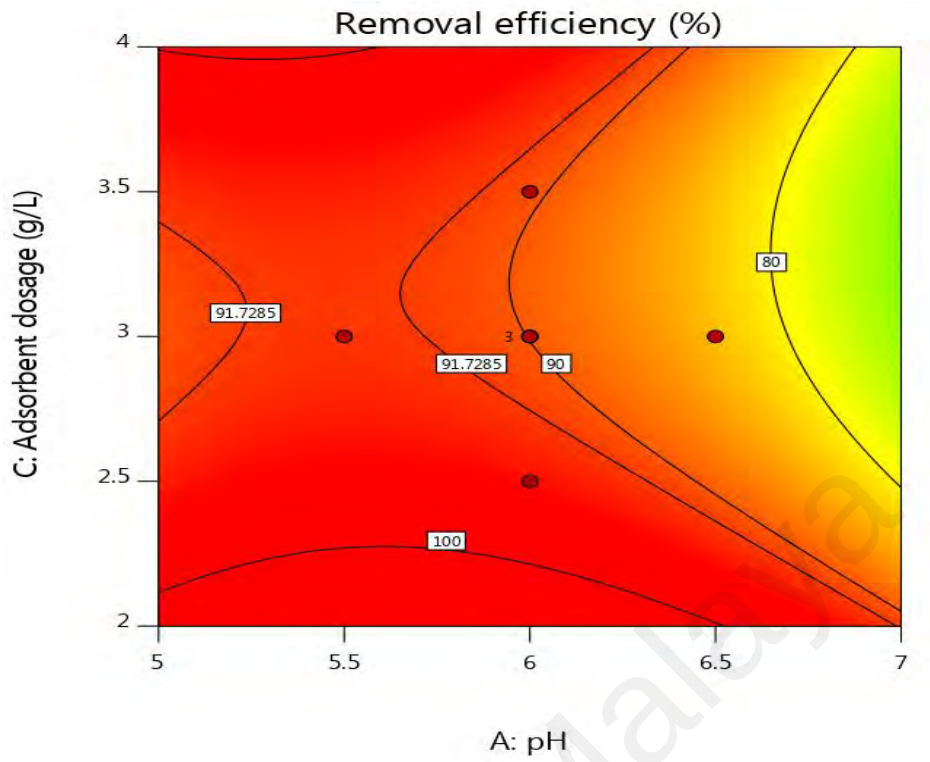

Figure 4.28: Contour plot of Pb(II) removal between pH and adsorbent dosage

The combined effect of initial Pb(II) concentration (15-35mg/L), and adsorbent dosage (2–4g/L) on the Pb(II) elimination at pH 6 is showed in Figure 4.29 and Figure 4.30. For all tested analysis, it is generally found that the adsorption efficiency indicates insignificant at the low adsorbent dosage, but at moderate initial concentration and higher adsorbent dosage indicates more substantial uptake capacity at each point of Pb(II) ion removal. This is well consistent with the hypothesis that active sites of the activated carbon can adsorb more Pb ions in the solution when higher adsorbent dosage was applied thus leading to increase in adsorption capacities (Van Thuan et al., 2017).

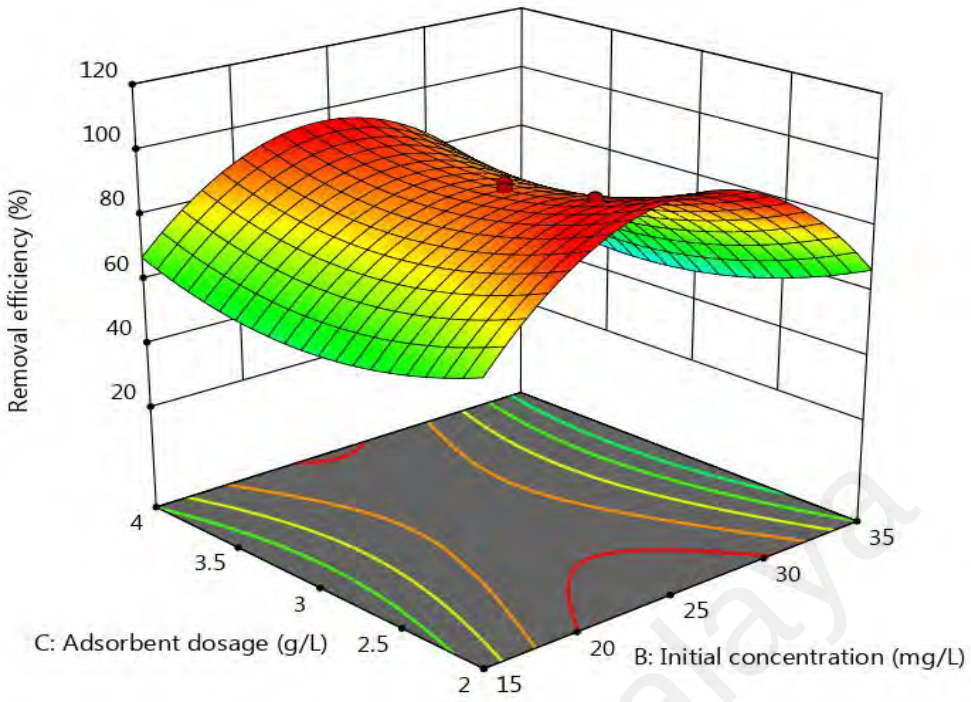

Figure 4.29: The interaction effect between initial Pb(II) concentration and adsorbent dosage at constant pH of 6

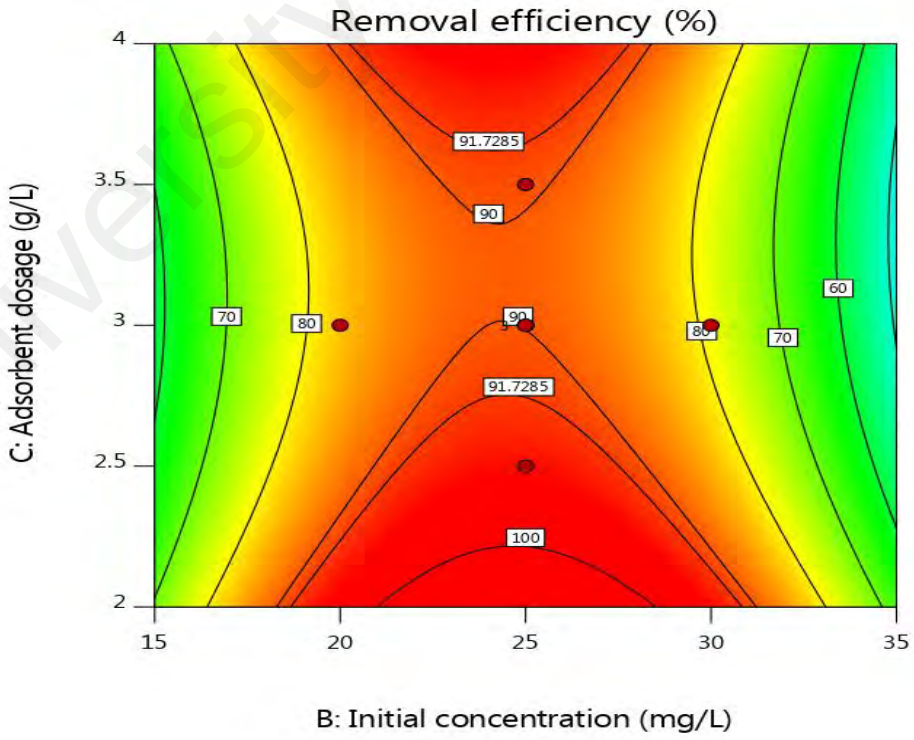

Figure 4.30: Contour plot of Pb(II) removal between initial Pb(II) concentration and adsorbent dosage

4.10.4 Model Validation

To verify the proposed model, experiment was carried out according to the optimum conditions proposed by the RSM with 0.999-1.0 desirability. The lists of optimum conditions predicted by RSM are presented in Table 4.18. From the data provided, the initial Pb(II) concentration, pH and adsorbent dosage of 25mg/L, pH 5.5 and 2.0g/L adsorbent dosage was selected as an optimum condition. The desired optimum condition suggested by RSM was 0.9997. The highest value (1.0) shows a response within the ideal intervals or that it achieves its ideal value. After rerun the experiment using an optimum condition, the amount of Pb removal under the optimum conditions was 99.5%, while the model predicted by RSM at this condition to be 99.7% of Pb removal. Error between the experimental and predicted results was less than 0.2%; thus, it was proved that the generated model was sufficient to predict the removal of Pb.

Table 4.18: Solution of optimum conditions by RSM

pH	Initial Pb(II) concentration (mg/L)	Adsorbent dosage (g/L)	Removal efficiency (%)
5.1	25	2	99.2
5.1	25.1	2.1	99.3
5.1	24	2	99.2
5.5	24.9	2	98.7
5.5	**25**	**2**	**99.7 (selected)**

4.10.5 Comparisons of this study with single and integration system

Table 4.19 shows the comparison between single process and integrated system. At optimal operating conditions of pH 5.5, initial concentration of 25mg/L and adsorbent dosage 2g/L, 99.7% removal of Pb was achieved. The obtained result shows that using integrated system gave superior performance compared to single electrocoagulation and adsorption method.

Table 4.19: Comparison optimum parameters of single electrocoagulation and activated carbon adsorption on the removal of Pb(II) at 25mg/L

Parameters	Electrocoagulation	Adsorption	Integrated system
pH	7	6	5.5
Adsorbent dosage (g/L)	-	4	2
Removal efficiency (%)	78.8	76.5	99.7

CHAPTER 5: CONCLUSIONS AND RECOMMENDATION

5.1 Conclusion

This study showed that the perforated Zn electrode has superior performance for removal of Pb(II) as compared to conventional electrode materials due to its high affinity, high current efficiency, high resistance to corrosion and low cost. The perforated Zn electrode was applied in the solar electrocoagulation process. The proposed solar PV electrocoagulation treatment system demonstrated high efficiency in Pb(II) ion removal from aqueous solutions. The evaluation of different electrodes, the effects of their geometries on Pb(II) removal, the overall energy consumption and the sludge production during electrocoagulation showed that the perforated Zn electrode is the most effective electrode. It produced the lowest amount of sludge and attained the highest Pb(II) removal efficiency of 99.9% within 10 min at 1.13 mA/cm^2 current density and pH 7.0. The solar PV electrocoagulation system has the potential to further increase energy savings. In addition, the performance of Pb(II) removal has been influenced by the natural conditions such as solar irradiation, temperature and meteorological conditions.

Palm shell based activated carbon derived from agriculture waste was used as an adsorbent to remove Pb(II) from aqueous solution. This study was carried out using palm shell activated carbon to investigate its performance and to compare it with other adsorbents reported in the literature. Variables such as contact time, pH, adsorbent dose and temperature had significant effects on Pb(II) adsorption. The pseudo-second-order model fitted well with the experimental results with high correlation coefficient and low error analysis. In addition, equilibrium data were best represented by the Langmuir isotherm model and the maximum adsorption capacity of adsorbent was 58.05 mg/g at pH 6. Pb(II) adsorption was endothermic in nature, with a high activation energy. This

research proves that, at optimal conditions, palm shell activated carbon is an environmentally friendly, economical and efficient adsorbent for Pb(II) removal from aqueous solution. The integrated system between electrocoagulation and adsorption process provides an attractive alternative over single process such as short reaction time, less sludge production, high efficiency and more effective especially for high initial concentration of heavy metals. The results from RSM proved that this integration system managed to perform better in terms of removal efficiency (99.7%) when using high Pb(II) concentration (25mg/L) and low amount of adsorbent dose (2g/L). The integrated system provides an attractive alternative over a single electrocoagulation and adsorption process as well as brings benefits such as short reaction time, less sludge production, high efficiency and more effective especially for high initial concentration of heavy metals. The results proved that this integrated system managed to perform better in terms of removal efficiency (99.7%) when using high Pb(II) concentration (25mg/L) and low amount of adsorbent dose (2g/L).

5.2 Recommendations

Electrocoagulation and adsorption methods not only have capability to remove heavy metal ions with below allowable standard discharge limit, but these technologies also provide water recycling and metal recovery in their most valuable forms. A lot of studies should be carried out to enhance the process performance from laboratory scale to pilot scale-ups for industrial applications. Therefore, the following factors should be reinforced:

1. In a combination system (electrocoagulation and adsorption) study using batch mode. It is recommended to use a continuous operation mode with the use of optimum

parameters from batch study to evaluate the Pb(II) removal performance and investigate the ability of this system to be applied in other applications.

2. In this study, the aqueous solution was used to investigate the ability of solar electrocoagulation on Pb(II) removal. It is recommended to apply this treatment system using industrial wastewater. This is because this technology provides a solution that is cost-effective for wastewater treatment.

3. High Pb(II) removal was achieved using the integrated system with solar power energy. It is recommended to apply this treatment system and their optimum parameters as guidelines to study the performance of different kinds of heavy metals such as arsenic, cadmium or mercury.

5.3 Novelty and contribution to knowledge

The wide potential window, high corrosion resistance and suitable price qualifies zinc electrode to use in many applications such as wastewater treatment, desalination and electro-generation process.

Its first time to characterize the electrochemical properties of zinc electrode. This research explores on the investigate the performance of elctrocoagulation process using solar PV. In addition, use a new approach to combine electrocoagulation and adsorption in the removal of Pb.

REFERENCES

Abadin, H., Ashizawa, A., Stevens, Y. W., Llados, F., Diamond, G., Sage, G., . . . Swarts, S. G. (2007). *Toxicological profile for lead*: Atlanta (GA): Agency for Toxic Substances and Disease Registry (US).

Abbaszadeh, S., Wan Alwi, S. R., Webb, C., Ghasemi, N., & Muhamad, I. I. (2016). Treatment of lead-contaminated water using activated carbon adsorbent from locally available papaya peel biowaste. *Journal of Cleaner Production, 118*, 210-222.

Abdel-Aty, A. M., Ammar, N. S., Abdel Ghafar, H. H., & Ali, R. K. (2013). Biosorption of cadmium and lead from aqueous solution by fresh water alga Anabaena sphaerica biomass. *Journal of Advance Research, 4*, 367-374.

Abdelhafez, A. A., & Li, J. (2016). Removal of Pb(II) from aqueous solution by using biochars derived from sugar cane bagasse and orange peel. *Journal of the Taiwan Institute of Chemical Engineers, 61*, 367-375.

Abou-Shady, A., Peng, C., Bi, J., Xu, H., & Almeria O, J. (2012). Recovery of Pb (II) and removal of NO^{3-} from aqueous solutions using integrated electrodialysis, electrolysis, and adsorption process. *Desalination, 286*, 304-315.

Acharya, J., Sahu, J. N., Mohanty, C. R., & Meikap, B. C. (2009). Removal of lead(II) from wastewater by activated carbon developed from Tamarind wood by zinc chloride activation. *Chemical Engineering Journal, 149*(1–3), 249-262.

Adams, W. G., & Day, R. E. (1877). The action of light on selenium. *Proc Roy Soc, 25*, 113-117.

Adebisi, G. A., Chowdhury, Z. Z., & Alaba, P. A. (2017). Equilibrium, kinetic, and thermodynamic studies of lead ion and zinc ion adsorption from aqueous solution onto activated carbon prepared from palm oil mill effluent. *Journal of Cleaner Production, 148*, 958-968.

Al-Alwani, M. A. M., Mohamad, A. B., Ludin, N. A., Kadhum, A. A. H., & Sopian, K. (2016). Dye-sensitised solar cells: development, structure, operation principles, electron kinetics, characterisation, synthesis materials and natural photosensitisers. *Renewable and Sustainable Energy Reviews, 65*, 183-213.

Al-Rashdi, B., Somerfield, C., & Hilal, N. (2011). Heavy metals removal using adsorption and nanofiltration techniques. *Separation and Purification Reviews, 40*, 209-259.

Al-Shannag, M., Al-Qodah, Z., Bani-Melhem, K., Qtaishat, M. R., & Alkasrawi, M. (2015). Heavy metal ions removal from metal plating wastewater using electrocoagulation: Kinetic study and process performance. *Chemical Engineering Journal, 260*, 749-756.

Alam, K. (2005). Waste Management Centre, waste Evaluation Guidelines, from http://www.kualitialam.com/web/services/weg.htm

Ali, M. M. E., & Salih, S. K. (2013). A visual basic-based tool for design of stand-alone solar power systems. *Energy Procedia, 36*, 1255-1264.

Alim, M. A., Lee, J. H., Akoh, C. C., Choi, M. S., Jeon, M. S., Shin, J. A., & Lee, K. T. (2008). Enzymatic transesterification of fractionated rice bran oil with conjugated linoleic acid: Optimization by response surface methodology. *LWT - Food Science and Technology, 41*(5), 764-770.

Alloway, B. J. (1995). *Heavy metals in soils*: Blackie Academic & Professional.

Alvarez-Guerra, E., Dominguez-Ramos, A., & Irabien, A. (2011). Photovoltaic solar electro-oxidation (PSEO) process for wastewater treatment. *Chemical Engineering Journal, 170*(1), 7-13.

An, C., Huang, G., Yao, Y., & Zhao, S. (2017). Emerging usage of electrocoagulation technology for oil removal from wastewater: A review. *Science of The Total Environment, 579*, 537-556.

Anwar, J., Shafique, U., Waheed uz, Z., Salman, M., Dar, A., & Anwar, S. (2010). Removal of Pb(II) and Cd(II) from water by adsorption on peels of banana. *Bioresource Technology, 101*, 1752-1755.

Arami-Niya, A., Wan Daud, W. M. A., S. Mjalli, F., Abnisa, F., & Shafeeyan, M. S. (2012). Production of microporous palm shell based activated carbon for methane adsorption: Modeling and optimization using response surface methodology. *Chemical Engineering Research and Design, 90*(6), 776-784.

Ardani, K., & Margolis, R. (2010). Solar technologies market report. Retrieved from U.S. Department of Energy website:

Ariffin, N., Abdullah, M. M. A. B., Zainol, M. R. R. M. A., Murshed, M. F., Zain, H., Faris, M. A., & Bayuaji, R. (2017). *Review on adsorption of heavy metal in wastewater by using geopolymer*. Paper presented at the MATEC Web of Conferences

Asaithambi, P., Aziz, A. R. A., & Daud, W. M. A. B. W. (2016). Integrated ozone—electrocoagulation process for the removal of pollutant from industrial effluent: optimization through response surface methodology. *Chemical Engineering and Processing: Process Intensification, 105*, 92-102.

Asfaram, A., Ghaedi, M., Hajati, S., Goudarzi, A., & Bazrafshan, A. A. (2015). Simultaneous ultrasound-assisted ternary adsorption of dyes onto copper-doped zinc sulfide nanoparticles loaded on activated carbon: Optimization by response surface methodology. *Spectrochimica Acta Part A: Molecular and Biomolecular Spectroscopy, 145*, 203-212.

Asgari, G., Roshani, B., & Ghanizadeh, G. (2012). The investigation of kinetic and isotherm of fluoride adsorption onto functionalize pumice stone. *Journal of Hazardous Materials, 217–218*, 123-132.

Assadi, A., Fazli, M. M., Emamjomeh, M. M., & Ghasemi, M. (2015). Optimization of lead removal by electrocoagulation from aqueous solution using response surface methodology. *Desalination and Water Treatment*, 1-8.

Asuquo, E., Martin, A., Nzerem, P., Siperstein, F., & Fan, X. (2017). Adsorption of Cd(II) and Pb(II) ions from aqueous solutions using mesoporous activated carbon adsorbent: Equilibrium, kinetics and characterisation studies. *Journal of Environmental Chemical Engineering, 5*(1), 679-698.

ATSDR. (2014). The priority list of hazardous substances from http://www.atsdr.cdc.gov/

Ay, Ç., Özcan, A. S., Erdoğan, Y., & Özcan, A. (2017). Characterization and lead(II) ions removal of modified Punica granatum L. peels. *International Journal of Phytoremediation, 19*(4), 327-339. doi: 10.1080/15226514.2016.1225285

Aziz, A. R. A., Asaithambi, P., & Daud, W. A. W. (2016). Combination of electrocoagulation with advanced oxidation processes for the treatment of distillery industrial effluent. *Process Safety and Environmental Protection, 99*, 227-235.

Baghban, E., Mehrabani-Zeinabad, A., & Moheb, A. (2014). The effects of operational parameters on the electrochemical removal of cadmium ion from dilute aqueous solutions. *Hydrometallurgy, 149*, 97-105.

Balaria, A., & Schiewer, S. (2008). Assessment of biosorption mechanism for Pb binding by citrus pectin. *Separation and Purification Technology, 63*, 577-581.

Bartczak, P., Norman, M., Klapiszewski, Ł., Karwańska, N., Kawalec, M., Baczyńska, M., . . . Jesionowski, T. (2013). Removal of nickel(II) and lead(II) ions from aqueous solution using peat as a low-cost adsorbent: A kinetic and equilibrium study. *Arabian Journal of Chemistry*.

Basha, C. A., Somasundaram, M., Kannadasan, T., & Lee, C. W. (2011). Heavy metals removal from copper smelting effluent using electrochemical filter press cells. *Chemical Engineering Journal, 171*(2), 563-571.

Basu, M., Guha, A. K., & Ray, L. (2017). Adsorption of lead on cucumber peel. *Journal of Cleaner Production, 151*, 603-615.

Bayramoglu, M., Kobya, M., Can, O. T., & Sozbir, M. (2004). Operating cost analysis of electrocoagulation of textile dye wastewater. *Separation and Purification Technology, 37*(2), 117-125.

Bazrafshan, E., Alipour, M. R., & Mahvi, A. H. (2016). Textile wastewater treatment by application of combined chemical coagulation, electrocoagulation, and adsorption processes. *Desalination and Water Treatment, 57*(20), 9203-9215.

Bazrafshan, E., Ownagh, K. A., & Mahvi, A. H. (2012). Application of electrocoagulation process using iron and aluminum electrodes for fluoride removal from aqueous environment. *E-Journal of Chemistry, 9*(4), 2297-2308.

Bebelis, S., Bouzek, K., Cornell, A., Ferreira, M., Kelsall, G., Lapicque, F., . . . Walsh, F. (2013). Highlights during the development of electrochemical engineering. *Chemical Engineering Research and Design, 91*, 1998-2020.

Belhout, D., Ghernaout, D., Djezzar-Douakh, S., & Kellil, A. (2010). Electrocoagulation of a raw water of Ghrib Dam (Algeria) in batch using aluminium and iron electrodes. *Desalination and Water Treatment, 16*(1-3), 1-9.

Bellinger, D. C. (2004). Lead. *Pediatrics, 113*, 1016-1022

Beyazit, N. (2014). Copper(II), chromium(VI) and nickel(II) removal from metal plating effluent by electrocoagulation. *International Journal of Electrochemical Sciences, 92014*, 4315-4330.

Bhattacharjee, S., Chakrabarty, S., Maity, S., Kar, S., Thakur, P., & Bhattacharyya, G. (2003). Removal of lead from contaminated water bodies using sea nodule as an adsorbent. *Water Research, 37*, 3954-3966.

Bilton, A. M., Wiesman, R., Arif, A. F. M., Zubair, S. M., & Dubowsky, S. (2011). On the feasibility of community-scale photovoltaic-powered reverse osmosis desalination systems for remote locations. *Renewable Energy, 36*, 3246-3256.

Bouchelkia, N., Mouni, L., Belkhiri, L., Bouzaza, A., Bollinger, J.-C., Madani, K., & Dahmoune, F. (2016). Removal of lead(II) from water using activated carbon developed from jujube stones, a low-cost sorbent. *Separation Science and Technology, 51*(10), 1645-1653.

Bouguerra, W., Barhoumi, A., Ibrahim, N., Brahmi, K., Aloui, L., & Hamrouni, B. (2015). Optimization of the electrocoagulation process for the removal of lead from water using aluminium as electrode material. *Desalination and Water Treatment*, 1-10.

Box, G. E. P., & Wilson, K. B. (1951). On the experimental attainment of optimum conditions. *Journal of the Royal Statistical Society B, 13*, 1-45.

Brudey, T., Largitte, L., Jean-Marius, C., Tant, T., Dumesnil, P. C., & Lodewyckx, P. (2016). Adsorption of lead by chemically activated carbons from three lignocellulosic precursors. *Journal of Analytical and Applied Pyrolysis, 120*, 450-463.

Bulut, Y., & Tez, Z. (2007). Adsorption studies on ground shells of hazelnut and almond. *Journal of Hazardous Materials, 149*(1), 35-41.

Can, B. Z., Boncukcuoglu, R., Yilmaz, A. E., & Fil, B. A. (2014). Effect of some operational parameters on the arsenic removal by electrocoagulation using iron electrodes. *Journal of Environmental Health Science and Engineering, 12*, 95-95.

Can, O. T., Bayramoglu, M., & Kobya, M. (2003). Decolorization of reactive dye olutions by electrocoagulation using aluminum electrodes. *Industrial & Engineering Chemistry Research, 42*(14), 3391-3396.

Castañeda-Díaz, J., Pavón-Silva, T., Gutiérrez-Segura, E., & Colín-Cruz, A. (2017). Electrocoagulation-adsorption to remove anionic and cationic dyes from aqueous solution by pv-energy. *Journal of Chemistry, 2017*, 14.

Cataldo, S., Gianguzza, A., Milea, D., Muratore, N., & Pettignano, A. (2016). Pb(II) adsorption by a novel activated carbon alginate composite material. A kinetic and equilibrium study. *International Journal of Biological Macromolecules, 92*, 769-778.

Cechinel, M. A. P., Ulson de Souza, S. M. A. G., & Ulson de Souza, A. A. (2014). Study of lead (II) adsorption onto activated carbon originating from cow bone. *Journal of Cleaner Production, 65*, 342-349.

Ceskaa. (2015). Global activated carbon market: 2014-2019 Retrieved 20/9/2016, 2016, from https://www.ceskaa.com/shop/advanced-materials/global-activated-carbon-market/

Cestari, A. R., Vieira, E. F. S., Pinto, A. A., & Lopes, E. C. N. (2005). Multistep adsorption of anionic dyes on silica/chitosan hybrid: 1. Comparative kinetic data from liquid- and solid-phase models. *Journal of Colloid and Interface Science, 292*(2), 363-372.

Chakchouk, I., Elloumi, N., Belaid, C., Mseddi, S., Chaari, L., & Kallel, M. (2017). A combined electrocoagulation-electrooxidation treatment for dairy wastewater. *Brazilian Journal of Chemical Engineering, 34*, 109-117.

Chan, J. (2013). Report: global BIPV and BAPV market to reach 2.25GW by 2017. Retrieved from pvtech website: http://www.pvtech.org/news/report_global_bipv_and_bapv_market_to_reach_2.25gw_by_2017

Chaturvedi, S. (2013). Electrocoagulation: a novel waste water treatment method. *International Journal of Moden Engineering and Reserach Technology, 3*, 93-100.

Chen, G. (2008). *Electrochemical technologies in wastewater treatment.* . Paper presented at the The Hong Kong University of Science and Technology Eco Asia Conference, Hong Kong.

Chen, J. P., Chang, S.-Y., & Hung, Y.-T. (2005). Electrolysis. In L. K. Wang, Y.-T. Hung & N. K. Shammas (Eds.), *Physicochemical Treatment Processes* (pp. 359-378). Totowa, NJ: Humana Press.

Chen, X., Chen, G., & Yue, P. (2000). Separation of pollutants from restaurant wastewater by electrocoagulation. *Separation and Purification Technology, 19*(1–2), 65-76.

Chen, X., Chen, G., & Yue, P. L. (2002). Investigation on the electrolysis voltage of electrocoagulation. *Chemical Engineering Science, 57*, 2449-2455.

Chen, X., & Deng, H. (2012). Removal of humic acids from water by hybrid titanium-based electrocoagulation with ultrafiltration membrane processes. *Desalination, 300*, 51-57.

Choong, C. E., Ibrahim, S., Yoon, Y., & Jang, M. (2018). Removal of lead and bisphenol A using magnesium silicate impregnated palm-shell waste powdered activated carbon: Comparative studies on single and binary pollutant adsorption. *Ecotoxicology and Environmental Safety, 148*, 142-151.

Cicek, V. (2017). *Corrosion engineering and cathodic protection handbook: with an extensive question and answer section*: Wiley.

Coelho, G. F., Gonçalves Jr, A. C., Tarley, C. R. T., Casarin, J., Nacke, H., & Francziskowski, M. A. (2014). Removal of metal ions Cd (II), Pb (II), and Cr (III) from water by the cashew nut shell Anacardium occidentale L. *Ecological Engineering, 73*, 514-525.

Comninellis, C., & Chen, G. (Eds.). (2009). *Electrochemistry for the environment*: Springer New York.

Costa, J. M., Brillas, E., & Cabot, P.-L. (2004). *Trends in electrochemistry and corrosion at the beginning of the 21st century : dedicated to professor Dr. Josep M. Costa on the occasion of his 70th birthday*. Barcelona: Publicacions Universitat de Barcelona.

CRS. (2017). Electrocoagulation Retrieved 24 september, 2017, from http://www.crs-reprocessing.com/en/crs-solutions/electrocoagulation/

Dalvand, A., Gholami, M., Joneidi, A., & Mahmoodi, N. M. (2011). Dye removal, energy consumption and operating cost of electrocoagulation of textile wastewater as a clean process. *CLEAN – Soil, Air, Water, 39*(7), 665-672.

Daneshvar, N., Oladegaragoze, A., & Djafarzadeh, N. (2006). Decolorization of basic dye solutions by electrocoagulation: An investigation of the effect of operational parameters. *Journal of Hazardous Materials, 129*, 116-122.

Daous, M., & El-Shazly, A. (2012). Enhancing the performance of a batch electrocoagulation reactor for chromium reduction using gas sparging. *International Journal od Electrochemical Science, 7*, 3513-3526.

de Mello Ferreira, A., Marchesiello, M., & Thivel, P. X. (2013). Removal of copper, zinc and nickel present in natural water containing Ca^{2+} and HCO^{3-} ions by electrocoagulation. *Separation and Purification Technology, 107*, 109-117.

de Oliveira da Mota, I., de Castro, J. A., de Góes Casqueira, R., & de Oliveira Junior, A. G. (2015). Study of electroflotation method for treatment of wastewater from washing soil contaminated by heavy metals. *Journal of Materials Research and Technology, 4*, 109-113.

Deiana, A. C., Gimenez, M. G., Rómoli, S., Sardella, M. F., & Sapag, K. (2014). Batch and column studies for the removal of ead from aqueous solutions using activated carbons from viticultural industry wastes. *Adsorption Science & Technology, 32*.

Dermentzis, K., Christoforidis, A., Valsamidou, E., Lazaridou, A., & Kokkinos, N. (2011). Removal of hexavalent chromium from electroplating wastewater by electrocoagulation with iron electrodes. *Global NEST Journal, 13*(4), 412-418.

Dermentzis, K., Marmanis, D., Christoforidis, A., & Moumtzakis, A. (2015). Photovoltaic electrocoagulation process for remediation of chromium plating wastewaters. *Desalination and Water Treatment, 56*(5), 1413-1418.

Dominguez-Ramos, A., Aldaco, R., & Irabien, A. (2010). Photovoltaic solar electrochemical oxidation (PSEO) for treatment of lignosulfonate wastewater. *Journal of Chemical Technology & Biotechnology, 85*(6), 821-830.

Eiband, M. M. S. G., de A. Trindade, K. C., Gama, K., Melo, J. V. D., Martínez-Huitle, C. A., & Ferro, S. (2014). Elimination of Pb^{2+} through electrocoagulation: Applicability of adsorptive stripping voltammetry for monitoring the lead concentration during its elimination. *Journal of Electroanalytical Chemistry, 717*, 213-218.

El-Ashtoukhy, E. S. Z., Amin, N. K., & Abdelwahab, O. (2008). Removal of lead (II) and copper (II) from aqueous solution using pomegranate peel as a new adsorbent. *Desalination, 223*(1), 162-173.

El-Korashy, S. A., Elwakeel, K. Z., & El-Hafeiz, A. A. (2016). Fabrication of bentonite/thiourea-formaldehyde composite material for Pb(II), Mn(VII) and Cr(VI) sorption: A combined basic study and industrial application. *Journal of Cleaner Production, 137*, 40-50.

El-Sayed, M., & Nada, A. A. (2017). Polyethylenimine −functionalized amorphous carbon fabricated from oil palm leaves as a novel adsorbent for Cr(VI) and Pb(II) from aqueous solution. *Journal of Water Process Engineering, 16*, 296-308.

El Chaar, L., lamont, L. A., & El Zein, N. (2011). Review of photovoltaic technologies. *Renewable and Sustainable Energy Reviews, 15*(5), 2165-2175.

Emamjomeh, M. M., & Sivakumar, M. (2009). Review of pollutants removed by electrocoagulation and electrocoagulation/flotation processes. *Journal of Environmental Management, 90*, 1663-1679.

Energy, S. (2012). How photovoltaic cell works Retrieved July, 13th, 2013, from http://www.solarenergy.net/Articles/how-photovoltaic-cells-work.aspx

Erdem, E., Karapinar, N., & Donat, R. (2004). The removal of heavy metal cations by natural zeolites. *Journal of Colloid and Interface Science, 280*(2), 309-314.

Escobar, C., Soto-Salazar, C., & Inés, T. M. (2006). Optimization of the electrocoagulation process for the removal of copper, lead and cadmium in natural waters and simulated wastewater. *Journal of Environmental Management, 81*, 384-391.

Essadki, A. H. (2012). Electrochemical cells - new advances in fundamental researches and applications Y. Shao (Ed.) *Electrochemical probe for frictional force and*

bubble measurements in gas-liquid-solid contactors and innovative electrochemical reactors for electrocoagulation

Fales, A. L. (1948). A plating waste disposal problem. *Sewage Works Journal, 20*, 857-860.

Farghali, A. A., Bahgat, M., Enaiet Allah, A., & Khedr, M. H. (2013). Adsorption of Pb(II) ions from aqueous solutions using copper oxide nanostructures. *Beni-Suef University Journal of Basic and Applied Sciences, 2*(2), 61-71.

Ferniza-García, F., Amaya-Chávez, A., Roa-Morales, G., & Barrera-Díaz, C. E. (2017). Removal of pb, cu, cd, and zn present in aqueous solution using coupled electrocoagulation-phytoremediation treatment. *International Journal of Electrochemistry, 2017*, 11.

Flora, G., Gupta, D., & Tiwari, A. (2012). Toxicity of lead: A review with recent updates. *Interdisciplinary Toxicology, 5*(2), 47-58.

Flora, S. J. S., Flora, G., & Saxena, G. (Eds.). (2006). *Environmental occurrence, health effects and management of lead poisoning*. Amsterdam: Amsterdam: Elsevier Science B.V.

Fraas, L. M. (2014). *Low-cost solar electric power*: Springer International Publishing.

Fraile, D., Latour, M., Gammal, A. E., & Annett, M. (2009). Photovoltaic energy electricity from the sun. Retrieved from European Photovoltaic Industry Association (EPIA)

website:

Garba, Z. N., Bello, I., Galadima, A., & Lawal, A. Y. (2016). Optimization of adsorption conditions using central composite design for the removal of copper (II) and lead (II) by defatted papaya seed. *Karbala International Journal of Modern Science, 2*, 20-28.

García-García, A., Martínez-Miranda, V., Martínez-Cienfuegos, I. G., Almazán-Sánchez, P. T., Castañeda-Juárez, M., & Linares-Hernández, I. (2015). Industrial wastewater treatment by electrocoagulation–electrooxidation processes powered by solar cells. *Fuel, 149*, 46-54.

Garcia-Segura, S., Eiband, M. M. S. G., de Melo, J. V., & Martínez-Huitle, C. A. (2017). Electrocoagulation and advanced electrocoagulation processes: A general review about the fundamentals, emerging applications and its association with other technologies. *Journal of Electroanalytical Chemistry, 801*, 267-299.

Gautam, R. K., & Chattopadhyaya, M. C. (2016). *Advanced nanomaterials for wastewater remediation*: CRC Press.

Gaya, U. I., Otene, E., & Abdullah, A. H. (2015). Adsorption of aqueous Cd(II) and Pb(II) on activated carbon nanopores prepared by chemical activation of doum palm shell. [journal article]. *SpringerPlus, 4*(1), 458.

Ghaedi, M., Mazaheri, H., Khodadoust, S., Hajati, S., & Purkait, M. K. (2015). Application of central composite design for simultaneous removal of methylene blue and Pb^{2+} ions by walnut wood activated carbon. *Spectrochimica Acta Part A: Molecular and Biomolecular Spectroscopy, 135*, 479-490.

Ghosh, D., Medhi, C. R., & Purkait, M. K. (2008). Treatment of fluoride containing drinking water by electrocoagulation using monopolar and bipolar electrode connections. *Chemosphere, 73*(9), 1393-1400.

Goel, J., Kadirvelu, K., Rajagopal, C., & Garg, V. K. (2005). Removal of lead(II) from aqueous solution by adsorption on carbon aerogel using a response surface methodological approach. *Industrial & Engineering Chemistry Research, 44*(7), 1987-1994.

Gonzalez, M. A., Trocoli, R., Pavlovic, I., Barriga, C., & La Mantia, F. (2016). Capturing cd(II) and pb(II) from contaminated water sources by electro-deposition on hydrotalcite-like compounds. [10.1039/C5CP05235A]. *Physical Chemistry Chemical Physics, 18*(3), 1838-1845.

Grossiord, N., Kroon, J. M., Andriessen, R., & Blom, P. W. M. (2012). Degradation mechanisms in organic photovoltaic devices. *Organic Electronics, 13*(3), 432-456.

Gueu, S., Yao, B., Adouby, K., & Ado, G. (2006). Heavy metals removal in aqueous solution by activated carbons prepared from coconut shell and seed shell of the palm tree. *Journal of Applied Sciences, 6*, 2789-2793.

Gunaraj, V., & Murugan, N. (1999). Application of response surface methodologies for predicting weld base quality in submerged arc welding of pipes. *Journal of Materials Processing Technology, 8*, 266-275.

Günay, A., Arslankaya, E., & Tosun, İ. (2007). Lead removal from aqueous solution by natural and pretreated clinoptilolite: adsorption equilibrium and kinetics. *Journal of Hazardous Materials, 146*, 362-371.

Hakizimana, J. N., Gourich, B., Chafi, M., Stiriba, Y., Vial, C., Drogui, P., & Naja, J. (2017). Electrocoagulation process in water treatment: A review of electrocoagulation modeling approaches. *Desalination, 404*, 1-21.

Hamane, D., Arous, O., Kaouah, F., Trari, M., Kerdjoudj, H., & Bendjama, Z. (2015). Adsorption/photo-electrodialysis combination system for Pb^{2+} removal using bentonite/membrane/semiconductor. *Journal of Environmental Chemical Engineering, 3*, 60-69.

Hamdan, S. S., & El-Naas, M. H. (2014). Characterization of the removal of chromium(VI) from groundwater by electrocoagulation. *Journal of Industrial and Engineering Chemistry, 20*(5), 2775-2781.

Hameed, B. H., Lai, L. F., & Chin, L. H. (2009). Production of biodiesel from palm oil (Elaeis guineensis) using heterogeneous catalyst: An optimized process. *Fuel Processing Technology, 90*(4), 606-610.

Hansen, H. K., Nuñez, P., Raboy, D., Schippacasse, I., & Grandon, R. (2007). Electrocoagulation in wastewater containing arsenic: Comparing different process designs. *Electrochimica Acta, 52*(10), 3464-3470.

Hasnain, S. M., & Alajlan, S. A. (1998). Coupling of PV-powered RO brackish water desalination plant with solar stills. *Desalination, 116*, 57-64.

Heidmann, I., & Calmano, W. (2008). Removal of Zn(II), Cu(II), Ni(II), Ag(I) and Cr(VI) present in aqueous solutions by aluminium electrocoagulation. *Journal of Hazardous Materials, 152*(3), 934-941.

Hernández-Morales, V., Nava, R., Acosta-Silva, Y. J., Macías-Sánchez, S. A., Pérez-Bueno, J. J., & Pawelec, B. (2012). Adsorption of lead (II) on SBA-15 mesoporous molecular sieve functionalized with $-NH_2$ groups. *Microporous and Mesoporous Materials, 160*, 133-142.

Ho, Y.-S. (2004). Selection of optimum sorption isotherm. *Carbon, 42*(10), 2115-2116.

Ho, Y. S., & McKay, G. (1998). A comparison of chemisorption kinetic models applied to pollutant removal on various sorbents. *Process Safety and Environmental Protection, 76*, 332-340.

Hu, Z.-P., Gao, Z.-M., Liu, X., & Yuan, Z.-Y. (2017). High surface area activated red mud for efficient removal of methylene blue from wastewater. *Adsorption Science & Technology*, 1-18.

Hussin, F., Abnisa, F., Issabayeva, G., & Aroua, M. K. (2017). Removal of lead by solar-photovoltaic electrocoagulation using novel perforated zinc electrode. *Journal of Cleaner Production, 147*, 206-216.

Ibrahim, W. M., Hassan, A. F., & Azab, Y. A. (2016). Biosorption of toxic heavy metals from aqueous solution by Ulva lactuca activated carbon. *Egyptian Journal of Basic and Applied Sciences, 3*(3), 241-249.

IRENA. (2012). Renewable energy technologies: cost analysis series Retrieved 10 January, 2017, from http://www.limza.cl/p53/modulo4/RE_Technologies_Cost_Analysis-SOLAR_PV.pdf

Ismaiel, A. A., Aroua, M. K., & Yusoff, R. (2013). Palm shell activated carbon impregnated with task-specific ionic-liquids as a novel adsorbent for the removal of mercury from contaminated water. *Chemical Engineering Journal, 225*, 306-314.

IWK. (2016). Effluent standards Retrieved January, 15, 2016, from https://www.iwk.com.my/do-you-know/effluent-standards

Jayaram, K., Murthy, I. Y. L. N., Lalhruaitluanga, H., & Prasad, M. N. V. (2009). Biosorption of lead from aqueous solution by seed powder of Strychnos potatorum L. *Colloids and Surfaces B: Biointerfaces, 71*(2), 248-254.

Jegede, D. (2016). Top 10 largest solar photovoltaic plants in the world. Instituition of mechanical engineers. Retrieved 2 February, 2017, from http://www.imeche.org/news/news-article/top-10-solar-photovoltaic-plants-in-the-world

Jelle, B. P., & Breivik, C. (2012). State-of-the-art Building Integrated Photovoltaics. *Energy Procedia, 20*, 68-77. doi: http://dx.doi.org/10.1016/j.egypro.2012.03.009

Jiang, J.-Q., Graham, N., André, C., Kelsall, G. H., & Brandon, N. (2002). Laboratory study of electro-coagulation–flotation for water treatment. *Water Research, 36*(16), 4064-4078. doi: http://dx.doi.org/10.1016/S0043-1354(02)00118-5

Kabdaşlı, I., Arslan-Alaton, I., Ölmez-Hancı, T., & Tünay, O. (2012). Electrocoagulation applications for industrial wastewaters: a critical review. *Environmental Technology Reviews, 1*(1), 2-45.

Kamaraj, R., Ganesan, P., & Vasudevan, S. (2015). Removal of lead from aqueous solutions by electrocoagulation: isotherm, kinetics and thermodynamic studies. *International Journal of Environmental Science and Technology, 12*, 683-692.

Kara, S., Gürbulak, E., Eyvaz, M., & Yüksel, E. (2013). Treatment of winery wastewater by electrocoagulation process. *Desalination and Water Treatment, 51*(28-30), 5421-5429.

Karaoğlu, M. H., Kula, İ., & Uğurlu, M. (2013). Adsorption kinetic and equilibrium studies on removal of lead(II) onto glutamic acid/sepiolite. *CLEAN – Soil, Air, Water, 41*(6), 548-556.

Katal, R., & Pahlavanzadeh, H. (2011). Influence of different combinations of aluminum and iron electrode on electrocoagulation efficiency: Application to the treatment of paper mill wastewater. *Desalination, 265*(1), 199-205.

Kaundinya, D. P., Balachandra, P., & Ravindranath, N. H. (2009). Grid-connected versus stand-alone energy systems for decentralized power—A review of literature. *Renewable and Sustainable Energy Reviews, 13*(8), 2041-2050.

Kavak, D. (2013). Removal of lead from aqueous solutions by precipitation: statistical analysis and modeling. *Desalination and Water Treatment, 51*, 1720-1726.

Kershman, S. A., Rheinländer, J., & Gabler, H. (2003). Seawater reverse osmosis powered from renewable energy sources - hybrid wind/photovoltaic/grid power supply for small-scale desalination in Libya. *Desalination, 153*, 17-23.

Khalaf, A. M., Mubarak, A. A., & Nosier, S. A. (2016). Removal of Cr(VI) by electrocoagulation using vertical and horizontal rough cylinder anodes. *International Journal of Electrochemistry Science, 11* 1601-1610.

Khaled, B., Wided, B., Béchir, H., Elimame, E., Mouna, L., & Zied, T. (2015). Investigation of electrocoagulation reactor design parameters effect on the removal of cadmium from synthetic and phosphate industrial wastewater. *Arabian Journal of Chemistry*.

Khandegar, V., & Saroha, A. K. (2013). Electrocoagulation for the treatment of textile industry effluent – A review. *Journal of Environmental Management, 128*, 949-963.

Khuri, A. I., & Mukhopadhyay, S. (2010). Response surface methodology. *Wiley Interdisciplinary Reviews: Computational Statistics, 2*(2), 128-149.

Kobya, M., Can, O. T., & Bayramoglu, M. (2003). Treatment of textile wastewaters by electrocoagulation using iron and aluminum electrodes. *Journal of Hazardous Materials, 100*(1), 163-178.

Kobya, M., Demirbas, E., Senturk, E., & Ince, M. (2005). Adsorption of heavy metal ions from aqueous solutions by activated carbon prepared from apricot stone. *Bioresource Technology, 96*(13), 1518-1521.

Kobya, M., Hiz, H., Senturk, E., Aydiner, C., & Demirbas, E. (2006). Treatment of potato chips manufacturing wastewater by electrocoagulation. *Desalination, 190*(1–3), 201-211.

Kreith, F., & Goswami, D. Y. (2007). Handbook of energy efficiency and renewable energy, from http://www.crcnetbase.com/isbn/9780849317309

Kumar, A., Richhariya, G., & Sharma, A. (2015). Solar photovoltaic technology and its sustainability. In A. Sharma & S. K. Kar (Eds.), *Energy Sustainability Through Green Energy* (pp. 3-25). New Delhi: Springer India.

Kuroda, Y., Kawada, Y., Takahashi, T., Ehara, Y., Ito, T., Zukeran, A., . . . Yasumoto, K. (2003). Effect of electrode shape on discharge current and performance with barrier discharge type electrostatic precipitator. *Journal of Electrostatics, 57*(3–4), 407-415.

Kurtz, S., & Wilson, G. (2016). Research cell efficiency records (latest chart). Retrieved from www.nrel.gov/ncpv/

Lara, M. A. M., Rico, I. L. R., Vicete, G. B., Garcia, G. B., & Hoces, M. C. (2010). Modification of sportive characteristics of sugarcane bagasse for removing lead from aqueous solutions. *Desalination, 256*, 58-63.

Largitte, L., Brudey, T., Tant, T., Dumesnil, P. C., & Lodewyckx, P. (2016). Comparison of the adsorption of lead by activated carbons from three lignocellulosic precursors. *Microporous and Mesoporous Materials, 219*, 265-275.

Lee, K., & Hamid, S. (2015). Simple response surface methodology: investigation on advance photocatalytic oxidation of 4-chlorophenoxyacetic acid using UV-active ZnO photocatalyst. *Materials, 8*(1), 339.

Lee, S. Y., & Gagnon, G. A. (2016). Comparing the growth and structure of flocs from electrocoagulation and chemical coagulation. *Journal of Water Process Engineering, 10*, 20-29.

Levy, E. (1992). Water filter: Google Patents.

Li, X., Li, H., Xu, X., Guo, N., Yuan, L., & Yu, H. (2017). Preparation of a reduced graphene oxide @ stainless steel net electrode and its application of electrochemical removal Pb(II). *Journal of the Electrochemical Society, 164*, 71-77.

Lingfang, Y., Zhou, S., & Wenhao, Y. (2014). Enhanced capacitive deionization of lead ions using air-plasma treated carbon nanotube electrode. *Surface and Coatings Technology, 251*, 122-127.

Liu, Y. X., Yan, J. M., Yuan, D. X., Li, Q. L., & Wu, X. Y. (2013). The study of lead removal from aqueous solution using an electrochemical method with a stainless steel net electrode coated with single wall carbon nanotubes. *Chemical Engineering Journal, 218*, 81-88.

Maarof, H., Daud, W., & Aroua, M. K. (2017). Recent trends in removal and recovery of heavy metals from wastewater by electrochemical technologies. *Reviews in Chemical Engineering, 33*, 359.

Mah, O. (1998). Fundamentals of photovoltaic materials. Retrieved from National Solar Power Reasearch Institute website:

Maher, A., Sadeghi, M., & Moheb, A. (2014). Heavy metal elimination from drinking water using nanofiltration membrane technology and process optimization using response surface methodology. *Desalination, 352*, 166-173.

Mahvi, A. H., Ebrahimi. S.J.A.D., Mesdaghinia, A., Gharibi, H., & Sowlat, M. H. (2011). Performance evaluation of a continuous bipolar electrocoagulation/electrooxidation-electroflotation (ECEO-EF) reactor designed for simultaneous removal of ammonia and phosphate from wastewater effluent. *Journal of Hazardous Material, 192*, 1267-1274.

Makrides, G., Zinsser, B., Norton, M., Georghiou, G. E., Schubert, M., & Werner, J. H. (2010). Potential of photovoltaic systems in countries with high solar irradiation. *Renewable and Sustainable Energy Reviews, 14*, 754-762.

Mansoorian, H. J., Mahvi, A. H., & Jafari, A. J. (2014). Removal of lead and zinc from battery industry wastewater using electrocoagulation process: Influence of direct and alternating current by using iron and stainless steel rod electrodes. *Separation and Purification Technology, 135*, 165-175.

Marmanis, D., Dermentzis, K., Christoforidis, A., Ouzounis, K., & Moumtzakis, A. (2015). Electrochemical treatment of actual dye house effluents using electrocoagulation process directly powered by photovoltaic energy. *Desalination and Water Treatment, 56*, 2988-2993.

Matlock, M. M., Howerton, B. S., & Atwood, D. A. (2002). Chemical precipitation of lead from lead battery recycling plant wastewater. *Industrial and Engineering Chemistry Research, 41*, 1579-1582.

McAlister, J., Smith, B., Neto, J., & Simpson, J. (2005). Geochemical distribution and bioavailability of heavy metals and oxalate in street sediments from Rio de

Janeiro, Brazil: A preliminary investigation. *Environmental Geochemistry and Health, 27*(5-6), 429-441.

Mints, P. (2016). 2015 top ten PV cell manufacturers, from http://www.renewableenergyworld.com/articles/2016/04/2015-top-ten-pv-cell-manufacturers.html

Misolar. (2016). It's here : a simple know how on solar farm Retrieved 2 February, 2017, from http://www.misolar.in/solar-farm/

Mohammadi, S. Z., Karimi, M. A., Yazdy, S. N., Shamspur, T., & Hamidian, H. (2014). Removal of Pb(II) ions and malachite green dye from wastewater by activated carbon produced from lemon peel. *Química Nova, 37*, 804-809.

Mohammed, A. A., & Al-Mureeb, M. D. F. (2010). Removal of lead from simulated wastewater by electrocoagulation method *Journal of Engineering, 16*, 5811-5821.

Mollah, M. Y. A., Morkovsky, P., Gomes, J. A. G., Kesmez, M., Parga, J., & Cocke, D. L. (2004). Fundamentals, present and future perspectives of electrocoagulation. *Journal of Hazardous Materials, 114*, 199-210.

Mollah, M. Y. A., Pathak, S. R., Patil, P. K., Vayuvegula, M., Agrawal, T. S., Gomes, J. A. G., . . . Cocke, D. L. (2004). Treatment of orange II azo-dye by electrocoagulation (EC) technique in a continuous flow cell using sacrificial iron electrodes. *Journal of Hazardous Materials, 109*(1–3), 165-171.

Mollah, M. Y. A., Schennach, R., Parga, J. R., & Cocke, D. L. (2001). Electrocoagulation (EC) — science and applications. *Journal of Hazardous Materials, 84*(1), 29-41.

Momčilović, M., Purenović, M., Bojić, A., Zarubica, A., & Ranđelović, M. (2011). Removal of lead(II) ions from aqueous solutions by adsorption onto pine cone activated carbon. *Desalination, 276*, 53-59.

Montgomery, D. C. (2001). Design and analysis of experiments

Mook, W. T., Aroua, M. K., Chakrabarti, M. H., Low, C. T. J., Aravind, P. V., & Brandon, N. P. (2013). The application of nano-crystalline PbO_2 as an anode for the simultaneous bio-electrochemical denitrification and organic matter removal in an up-flow undivided reactor. *Electrochimica Acta, 94*, 327-335.

Mook, W. T., Aroua, M. K., & Issabayeva, G. (2014). Prospective applications of renewable energy based electrochemical systems in wastewater treatment: A review. *Renewable and Sustainable Energy Reviews, 38*, 36-46.

Moreno-Barbosa, J. J., López-Velandia, C., Maldonado, A. d. P., Giraldo, L., & Moreno-Piraján, J. C. (2013). Removal of lead(II) and zinc(II) ions from aqueous solutions by adsorption onto activated carbon synthesized from watermelon shell and walnut shell. [journal article]. *Adsorption, 19*(2), 675-685.

Mousavi, H. Z., Hosseynifar, A., Jahed, V., & Dehghani, S. A. M. (2010). Removal of lead from aqueous solution using waste tire rubber ash as an adsorbent. *Brazilian Journal of Chemical Engineering, 27*, 79-87.

Moussa, D. T., El-Naas, M. H., Nasser, M., & Al-Marri, M. J. (2017). A comprehensive review of electrocoagulation for water treatment: Potentials and challenges. *Journal of Environmental Management, 186*, 24-41.

Moyo, M., Chikazaza, L., Nyamunda, B. C., & Guyo, U. (2013). Adsorption batch studies on the removal of pb(II) using maize tassel based activated carbon. *Journal of Chemistry, 2013*, 8.

Myers, R. H., & Montgomery, D. C. (2002). *Response surface methodology: process and product optimization using designed experiments*: Wiley.

Najafi, N. M., Eidizadeh, M., Seidi, S., Ghasemi, E., & Alizadeh, R. (2009). Developing electrodeposition techniques for preconcentration of ultra-traces of ni, cr and pb prior to arc-atomic emission spectrometry determination. *Microchemical Journal, 93*, 159-163.

Naje, A., Chelliapan, S., Zakaria, Z., Ajeel, M., & Alaba, P. (2017). A review of electrocoagulation technology for the treatment of textile wastewater *Reviews in Chemical Engineering* (Vol. 33, pp. 263).

Nandi, B. K., & Patel, S. (2017). Effects of operational parameters on the removal of brilliant green dye from aqueous solutions by electrocoagulation. *Arabian Journal of Chemistry, 10*, 2961-2968.

Narayanan, N. V., & M., G. (2009). Use of adsorption using granular activated carbon (GAC) for the enhancement of removal of chromium from synthetic wastewater by electrocoagulation. *Journal of Hazardous Material, 161*, 575-580.

Nasrullah, M., Islam Siddique, M. N., & Zularisam, A. W. (2014). Effect of high current density in electrocoagulation process for sewage treatment. [Article]. *Asian Journal of Chemistry, 26*(14), 4281-4285.

Needleman, H. (2004). Lead poisoning. *Annual Review of Medicine, 55*, 209-222.

Nwachukwu, O. I., Odoemelam, L. E., & Muoneke, C. O. (2015). Contaminants in selected industrial effluents and their effect on groundwater quality near factories in two cities of South East Nigeria. *International Journal of Advanced Research, 3*(9), 326-333.

Orescanin, V., Kollar, R., & Nad, K. (2011). The application of the ozonation/electrocoagulation treatment process of the boat pressure washing wastewater. *Journal of Environment Science Health A Toxic Hazard Substance Environmental Engineering, 46*(12), 1338-1345.

Ortiz, J. M., Exposito, E., Gallud, F., Garcia-Garcia, V., Montiel, V., & Aldaz, A. (2008). Desalination of underground brackish waters using an electrodialysis system powered directly by photovoltaic energy. *Solar Energy Materials and Solar Cells, 92*, 1677-1688.

Pal, A. M., Das, S., & Raju, N. B. (2015). Designing of a standalone photovoltaic system for a residential building in Gurgaon, India. *Sustainable Energy, 3*(1), 14-24.

Palahouane, B., Drouiche, N., Aoudj, S., & Bensadok, K. (2015). Cost-effective electrocoagulation process for the remediation of fluoride from pretreated photovoltaic wastewater. *Journal of Industrial and Engineering Chemistry, 22*, 127-131.

Pang, F., Teng, S., Teng, T., & Omar, A. K. M. (2009). Heavy metals removal by hydroxide precipitation and coagulation-flocculation methods from aqueous solutions. *Water Quality Research Journal of Canada, 44*(2), 174-182.

Pang, F. M., Kumar, P., Teng, T. T., Mohd Omar, A. K., & Wasewar, K. L. (2011). Removal of lead, zinc and iron by coagulation–flocculation. *Journal of the Taiwan Institute of Chemical Engineers, 42*(5), 809-815.

Parga, J. R., Cocke, D. L., Valverde, V., Gomes, J. A., Kesmez, M., Moreno, H., . . . Mencer., D. (2005). Characterization of electrocoagulation for removal of chromium and arsenic. *Chemical Engineering and Technology, 28*, 605-612.

Park, S.-M., Shin, S.-Y., Yang, J.-S., Ji, S.-W., & Baek, K. (2015). Selective recovery of dissolved metals from mine drainage using electrochemical reactions. *Electrochimica Acta, 181*, 248-254.

Pillai, G. G., Putrus, G. A., Georgitsioti, T., & Pearsall, N. M. (2014). Near-term economic benefits from grid-connected residential PV (photovoltaic) systems. *Energy, 68*, 832-843.

Pociecha, M., & Lestan, D. (2010). Using electrocoagulation for metal and chelant separation from washing solution after EDTA leaching of Pb, Zn and Cd contaminated soil. *Journal of Hazardous Materials, 174*(1), 670-678.

Putra, W. P., Kamari, A., Yusoff, M. S. N., Ishak, C. F., Mohamed, A., Hashim, N., & Isa, I. M. (2014). Biosorption of cu(II), pb(II) and zn(II) ions from aqueous solutions using selected waste materials: adsorption and characterisation studies. *Journal of Encapsulation and Adsorption Sciences, 4*, 25-35.

Rahman, N., Haseen, U., & Rashid, M. (2017). Synthesis and characterization of polyacrylamide zirconium (IV) iodate ion-exchanger: Its application for selective removal of lead (II) from wastewater. *Arabian Journal of Chemistry, 10*, 1765-1773.

Rajeshwar, K., & Ibanez, J. G. (1997). *Environmental electrochemistry: Fundamentals and applications in pollution sensors and abatement*: Elsevier Science.

Rama Raju, D. S. S., Ravi Kiran, G. A., & Rao, V. N. (2013). Comparison studies on biosorption of lead (II) from an aqueous solution using anacardium occidentale and carica papaya leaves powder. *International Journal of Emerging Trends in Engineering and Development, 1*(3), 273-283.

Ramavandi, B., Asgari, G., Faradmal, J., Sahebi, S., & Roshani, B. (2014). Abatement of Cr (VI) from wastewater using a new adsorbent, cantaloupe peel: Taguchi L16 orthogonal array optimization. *Korean Journal of Chemical Engineering, 4*, 1-8.

Rebane, K. L., & Barham, B. L. (2011). Knowledge and adoption of solar home systems in rural Nicaragua. *Energy Policy, 39*(6), 3064-3075.

Reddy, D. H. K., Seshaiah, K., Reddy, A. V. R., Rao, M. M., & Wang, M. C. (2010). Biosorption of Pb^{2+} from aqueous solutions by moringa oleifera bark: equilibrium and kinetic studies. *Journal of Hazardous Materials, 174*, 831-838.

Ren, H., Gao, Z., Wu, D., Jiang, J., Sun, Y., & Luo, C. (2016). Efficient Pb(II) removal using sodium alginate–carboxymethyl cellulose gel beads: Preparation, characterization, and adsorption mechanism. *Carbohydrate Polymers, 137*, 402-409.

Romano, A. P., & Olivier, M. G. (2015). Investigation by electrochemical impedance spectroscopy of filiform corrosion of electrocoated steel substrates. *Progress in Organic Coatings, 89*, 1-7.

Sahu, O., Mazumdar, B., & Chaudhari, P. K. (2014a). Treatment of wastewater by electrocoagulation: a review. [journal article]. *Environmental Science and Pollution Research, 21*(4), 2397-2413. doi: 10.1007/s11356-013-2208-6

Sahu, O., Mazumdar, B., & Chaudhari, P. K. (2014b). Treatment of wastewater by electrocoagulation: a review. [journal article]. *Environmental Science and Pollution Research, 21*, 2397-2413.

Salihi, I. U., Kutty, S. R. M., & Isa, M. H. (2017). Adsorption of Lead ions onto Activated Carbon derived from Sugarcane bagasse. *IOP Conference Series: Materials Science and Engineering, 201*(1), 012034.

Secula, M. S., Cagnon, B., DeOliveira, T. F., Chedeville, O., & Fauduet, H. (2012). Removal of acid dye from aqueous solutions by electrocoagulation/GAC adsorption coupling: kinetics and electrical operating costs. *Journal of Taiwan Institute Chemical Engineering, 43*, 767-775.

Segundo, J. E. D. V., Salazar-Banda, G. R., Feitoza, A. C. O., Vilar, E. O., & Cavalcanti, E. B. (2012). Cadmium and lead removal from aqueous synthetic wastes utilizing chemelec electrochemical reactor: Study of the operating conditions. *Separation and Purification Technology, 88*, 107-115.

Shakir, I. K., & Husein, B. I. (2009). Lead removal from industrial wastewater by electrocoagulation process. *Iraqi Journal Of Chemical And Petroleum Engineering, 10*(2), 35-42.

Sharma, A., Sharma, V., & Kansal, L. (2010). Amelioration of lead-induced hepatotoxicity by Allium sativum extracts in Swiss albino mice. *The Libyan Journal of Medicine, 5*. doi: 10.4176/091107

Sharma, G., Choi, J., Shon, H. K., & Phuntsho, S. (2011). Solar-powered electrocoagulation system for water and wastewater treatment. *Desalination and Water Treatment, 32*, 381-388.

Shekinah, P., Kadirvelu, K., Kanmani, P., Senthilkumar P., & Subburam, V. (2002). Adsorption of lead(II) from aqueous solution by activated carbon prepared from Eichhornia. *Journal of Chemical Technology & Biotechnology, 77*, 458-464.

Shen, F., Chen, X., Gao, P., & Chen, G. (2003). Electrochemical removal of fluoride ions from industrial wastewater. *Chemical Engineering Science, 58*, 987-993.

Siahkamari, M., Jamali, A., Sabzevari, A., & Shakeri, A. (2017). Removal of lead(II) ions from aqueous solutions using biocompatible polymeric nano-adsorbents: A comparative study. *Carbohydrate Polymers, 157*, 1180-1189.

Şık, E., Demirbas, E., Goren, A. Y., Oncel, M. S., & Kobya, M. (2017). Arsenite and arsenate removals from groundwater by electrocoagulation using iron ball anodes: Influence of operating parameters. *Journal of Water Process Engineering, 18*, 83-91.

Simbolotti, G., & Taylor, M. (2013). Photovoltaic solar power insights for policy makers. Retrieved from IRENA International Renewable Energy Agency website:

Singh, C. K., Sahu, J. N., Mahalik, K. K., Mohanty, C. R., Mohan, B. R., & Meikap, B. C. (2008a). Studies on the removal of Pb(II) from wastewater by activated carbon developed from Tamarind wood activated with sulphuric acid. *Journal of Hazardous Materials, 153*(1), 221-228.

Singh, C. K., Sahu, J. N., Mahalik, K. K., Mohanty, C. R., Mohan, B. R., & Meikap, B. C. (2008b). Studies on the removal of Pb(II) from wastewater by activated carbon developed from Tamarind wood activated with sulphuric acid. *Journal of Hazardous Materials, 153*, 221-228.

Singh, S., Jain, D. V. S., & Meena, V. K. (2017). Organic-inorganic hybrid matrix for electrochemical biosensing of tyrosine. *Materials Research Bulletin, 94*, 520-527.

Solanki, C. S. (2013). *Solar photovoltaic technology and systems: A manual for technicians, trainers and engineers*: PHI Learning.

Soliman, A. M., Elwy, H. M., Thiemann, T., Majedi, Y., Labata, F. T., & Al-Rawashdeh, N. A. F. (2016). Removal of Pb(II) ions from aqueous solutions by sulphuric acid-treated palm tree leaves. *Journal of the Taiwan Institute of Chemical Engineers, 58*, 264-273.

Subramaniam, R., & Kumar Ponnusamy, S. (2015). Novel adsorbent from agricultural waste (cashew NUT shell) for methylene blue dye removal: Optimization by response surface methodology. *Water Resources and Industry, 11*, 64-70.

Szlachta, M., & Chubar, N. (2013). The application of Fe–Mn hydrous oxides based adsorbent for removing selenium species from water. *Chemical Engineering Journal, 217* 159-168.

Tang, C., Shu, Y., Zhang, R., Li, X., Song, J., Li, B., . . . Ou, D. (2017). Comparison of the removal and adsorption mechanisms of cadmium and lead from aqueous solution by activated carbons prepared from Typha angustifolia and Salix matsudana. [10.1039/C6RA28035H]. *RSC Advances, 7*(26), 16092-16103.

Tezcan Un, U., Koparal, A. S., & Bakir Ogutveren, U. (2013). Fluoride removal from water and wastewater with a bach cylindrical electrode using electrocoagulation. *Chemical Engineering Journal, 223*, 110-115.

Thitame, P. V., & Shukla, S. R. (2017). Removal of lead (II) from synthetic solution and industry wastewater using almond shell activated carbon. *Environmental Progress & Sustainable Energy, 36*(6), 1628-1633.

Tiwari, G. N., & Dubey, S. (2010). *Fundamentals of photovoltaic modules and their applications*: Royal Society of Chemistry.

Toor, M., & Jin, B. (2012). Adsorption characteristics, isotherm, kinetics, and diffusion of modified natural bentonite for removing diazo dye. *Chemical Engineering Journal, 187*, 79-88.

Uğurlu, M., Gürses, A., Doğar, Ç., & Yalçın, M. (2008). The removal of lignin and phenol from paper mill effluents by electrocoagulation. *Journal of Environmental Management, 87*, 420-428.

Valero, D., García-García, V., Expósito, E., Aldaz, A., & Montiel, V. (2014). Electrochemical treatment of wastewater from almond industry using DSA-type anodes: Direct connection to a PV generator. *Separation and Purification Technology, 123*, 15-22.

Valero, D., Ortiz, J. M., Expósito, E., Montiel, V., & Aldaz, A. (2008). Electrocoagulation of a synthetic textile effluent powered by photovoltaic energy without batteries: Direct connection behaviour. *Solar Energy Materials and Solar Cells, 92*(3), 291-297.

Valero, D., Ortiz, J. M., Expósito, E., Montiel, V., & Aldaz, A. (2010). Electrochemical wastewater treatment directly powered by photovoltaic panels: electrooxidation of a dye-containing wastewater. *Environmental Science & Technology, 44*, 5182-5187.

Van Thuan, T., Quynh, B. T. P., Nguyen, T. D., Ho, V. T. T., & Bach, L. G. (2017). Response surface methodology approach for optimization of Cu^{2+}, Ni^{2+} and Pb^{2+} adsorption using KOH-activated carbon from banana peel. *Surfaces and Interfaces, 6*, 209-217.

Vasudevan, S., & Lakshmi, J. (2011a). Effects of alternating and direct current in electrocoagulation process on the removal of cadmium from water – A novel approach. *Separation and Purification Technology, 80*, 643-651.

Vasudevan, S., & Lakshmi, J. (2011b). Studies relating to an electrochemically assisted coagulation for the removal of chromium from water using zinc anode. *Water Science and Technology: Water Supply, 11*(2), 142-150.

Vasudevan, S., & Oturan, M. A. (2014). Electrochemistry: As cause and cure in water pollution—an overview. *Environmental Chemistry Letters, 12*, 97-108.

Vergili, I., Gönder, Z. B., Kaya, Y., Gürdağ, G., & Çavuş, S. (2017). Sorption of Pb (II) from battery industry wastewater using a weak acid cation exchange resin. *Process Safety and Environmental Protection, 107*, 498-507.

Wako, T. (2012). Industrial wastewater management in Japan Retrieved 2 september, 2017, from https://www.env.go.jp/en/focus/docs/files/20120801-51.pdf

Wang, C. T., Chou, W. L., & Kuo, Y. M. (2009). Removal of COD from laundry wastewater by electrocoagulation/electroflotation. *Journal of Hazardous Material, 164*, 81-86.

Wang, L. K., Hung, Y.-T., & Shammas, N. K. (2010). Handbook of advanced industrial and hazardous wastes treatment (pp. 71-151).

Weber, W. J., & Morris, J. C. (1963). Kinetics of adsorption carbon from solutions. *Journal Sanitary Engeering Division Proceedings. American Society of Civil Engineers, 89*, 31-60.

Wei, Y., Gao, C., Meng, F. L., Li, H. H., Wang, L., Liu, J. H., & Huang, X. J. (2012). SnO_2/reduced graphene oxide nanocomposite for the simultaneous electrochemical detection of cadmium(II), lead(II), copper(II), and mercury(II): an interesting favorable mutual interference. *The Journal of Physical Chemistry C, 116*, 1034-1041.

Wei, Y., Xu, L., Tao, Y., Yao, C., Xue, H., & Kong, Y. (2016). Electrosorption of lead ions by nitrogen-doped graphene aerogels via one-pot hydrothermal route. *Industrial and Engineering Chemistry Research, 55*, 1912-1920.

WHO. (2016). Lead poisoning and health Retrieved January, 15, 2016, from http://www.who.int/mediacentre/factsheets/fs379/en/

Wippermann, K., Schultze, J. W., Kessel, R., & Penninger, J. (1991). The inhibition of zinc corrosion by bisaminotriazole and other triazole derivatives. *Corrosion Science, 32*(2), 205-230.

Xia, D.-H., Ma, C., Song, S., Ma, L., Wang, J., Gao, Z., . . . Hu, W. (2017). Assessing atmospheric corrosion of metals by a novel electrochemical sensor combining with a thin insulating net using electrochemical noise technique. *Sensors and Actuators B: Chemical, 252*, 353-358.

Xu, W., Zhao, Q., Wang, R., Jiang, Z., Zhang, Z., Gao, X., & Ye, Z. (2017). Optimization of organic pollutants removal from soil eluent by activated carbon derived from peanut shells using response surface methodology. *Vacuum, 141*, 307-315.

Yang, J. K., Park, H. J., Lee, H. D., & Lee, S. M. (2009). Removal of Cu(II) by activated carbon impregnated with iron(III). *Colloids and Surfaces A: Physicochemical and Engineering Aspects, 337*, 154-158.

Yang, L., & Shi, Z. (2015). Enhanced electrosorption capacity for lead ion removal with polypyrrole and air-plasma activated carbon nanotube composite electrode. *Journal of Applied Polymer Science, 132*(14).

Yanine, F. F., & Sauma, E. E. (2013). Review of grid-tie micro-generation systems without energy storage: Towards a new approach to sustainable hybrid energy systems linked to energy efficiency. *Renewable and Sustainable Energy Reviews, 26*, 60-95.

Zarei, M., Niaei, A., Salari, D., & Khataee, A. (2010). Application of response surface methodology for optimization of peroxi-coagulation of textile dye solution using carbon nanotube–PTFE cathode. *Journal of Hazardous Materials, 173*(1), 544-551.

Zewail, T. M., & Yousef, N. S. (2014). Chromium ions (Cr^{6+} & Cr^{3+}) removal from synthetic wastewater by electrocoagulation using vertical expanded Fe anode. *Journal of Electroanalytical Chemistry, 735*, 123-128.

Zhang, C., Jiang, Y., Li, Y., Hu, Z., Zhou, L., & Zhou, M. (2013). Three-dimensional electrochemical process for wastewater treatment: A general review. *Chemical Engineering Journal, 228*, 455-467.

Zhang, S., Zhang, J., Cheng, X., Mei, Y., Hu, C., Wang, M., & Li, J. F. (2014). Electrokinetic remediation of soil containing Cr(VI) by photovoltaic solar panels and a DC-DC converter. *Journal of Chemical Technology and Biotechnology, 90*, 693-700.

Zhang, S., Zhang, J., Wang, W., Li, F., & Cheng, X. (2013). Removal of phosphate from landscape water using an electrocoagulation process powered directly by photovoltaic solar modules. *Solar Energy Materials and Solar Cells, 117*, 73-80.

Zhao, X., Zhang, B., Liu, H., & Qu, J. (2011). Simultaneous removal of arsenite and fluoride via an integrated electro-oxidation and electrocoagulation process. *Chemosphere, 83*, 726-729.

Zhi, X., Yang, H., Berthold, S., Doetsch, C., & Shen, J. (2010). Potential improvement to a citric wastewater treatment plant using bio-hydrogen and a hybrid energy system. *Journal of Power Sources, 195*, 6945-6953.

Zhou, Y. (2015). *Waste discharge into the marine environment: principles and guidelines for the Mediterranean action plan*: Elsevier Science.

Zolgharnein, J., Shahmoradi, A., & Ghasemi, J. B. (2013). Comparative study of box–behnken, central composite, and doehlert matrix for multivariate optimization of Pb (II) adsorption onto Robinia tree leaves. *Journal of Chemometrics, 27*(1-2), 12-20.

LIST OF PUBLICATIONS AND PAPERS PRESENTED

Paper publications

1. Farihahusnah Hussin, Gulnaziya Issabayeva & Mohamed Kheireddine Aroua (2017). Solar Photovoltaic Application: Opportunities and Challenges. Reviews in Chemical Engineering. (ISI-cited, Impact factor: 3.173)

2. Farihahusnah Hussin, Faisal Abnisa, Gulnaziya Issabayeva & Mohamed Kheireddine Aroua (2017). Removal of Lead by Solar-Photovoltaic Electrocoagulation Using Novel Perforated Zinc Electrode. Cleaner Production Journal, 147, 206-216. (ISI-cited, Impact factor: 5.715)

3. Farihahusnah Hussin & Mohamed Kheireddine Aroua (2017). A low sludge generated anode by hybrid solar electrocoagulation for the removal of lead. (Conference Publication: IOP Conference Series: Materials Science and Engineering)

4. Hussin, F., Maarof, H.I., Szlachta, M., & Aroua, M.K. (2017). Removal of Pb(II) ions from aqueous solutions using oil palm shell activated carbon: operating parameters and batch studies. Water Science and Technology (submitted).

List of seminars

1. **Farihahusnah Hussin** & Mohamed Kheireddine Aroua
Removal of lead from synthetic wastewater powered by solar photovoltaic
Higher Degree Seminar, Faculty of Engineering
(21 April 2016)

List of conferences

1. Farihahusnah Hussin, Mohamed Kheireddine Aroua

The Effects of pH of Lead Removal by Electrochemical Processes

4th International Congress on Green Process Engineering

(7-10 October 2014, Sevilla Spain)

2. Farihahusnah Hussin, Mohamed Kheireddine Aroua

The Effects of Electrode Material and pH on Lead Removal by Electrochemical Processes

IWA Regional Conference on Water Reuse and Energy 2015

(21-24 October 2015, Daegu Korea)

3. Farihahusnah Hussin, Mohamed Kheireddine Aroua

A Low Sludge Generated Anode by Hybrid Solar Electrocoagulation for the Removal of Lead

International Technical Postgraduate Conference

(5-6 April 2017, Kuala Lumpur)